Topological Deep Learning: Going Beyond Graph Data

Mustafa Hajij   *mhajij@usfca.edu*

Ghada Zamzmi[*]   *ghadh@mail.usf.edu*

Theodore Papamarkou[*]   *theo.papamarkou@manchester.ac.uk*

Nina Miolane   *ninamiolane@ucsb.edu*

Aldo Guzmán-Sáenz   *aldo.guzman.saenz@ibm.com*

Karthikeyan Natesan Ramamurthy   *knatesa@us.ibm.com*

Tolga Birdal   *tbirdal@imperial.ac.uk*

Tamal K. Dey   *tamaldey@purdue.edu*

Soham Mukherjee   *mukher26@purdue.edu*

Shreyas N. Samaga   *ssamaga@purdue.edu*

Neal Livesay   *n.livesay@northeastern.edu*

Robin Walters   *r.walters@northeastern.edu*

Paul Rosen   *prosen@sci.utah.edu*

Michael T. Schaub   *schaub@cs.rwth-aachen.de*

Contents

---

[*]These authors contributed equally to this work.

Abstract

Topological deep learning is a rapidly growing field that pertains to the development of deep learning models for data supported on topological domains such as simplicial complexes, cell complexes, and hypergraphs, which generalize many domains encountered in scientific computations. In this paper, we present a unifying deep learning framework built upon a richer data structure that includes widely adopted topological domains.

Specifically, we first introduce *combinatorial complexes*, a novel type of topological domain. Combinatorial complexes can be seen as generalizations of graphs that maintain certain desirable properties. Similar to hypergraphs, combinatorial complexes impose no constraints on the set of relations. In addition, combinatorial complexes permit the construction of hierarchical higher-order relations, analogous to those found in simplicial and cell complexes. Thus, combinatorial complexes generalize and combine useful traits of both hypergraphs and cell complexes, which have emerged as two promising abstractions that facilitate the generalization of graph neural networks to topological spaces.

Second, building upon combinatorial complexes and their rich combinatorial and algebraic structure, we develop a general class of message-passing *combinatorial complex neural networks (CCNNs)*, focusing primarily on attention-based CCNNs. We characterize permutation and orientation equivariances of CCNNs, and discuss pooling and unpooling operations within CCNNs in detail.

Third, we evaluate the performance of CCNNs on tasks related to mesh shape analysis and graph learning. Our experiments demonstrate that CCNNs have competitive performance as compared to state-of-the-art deep learning models specifically tailored to the same tasks. Our findings demonstrate the advantages of incorporating higher-order relations into deep learning models in different applications.

1   Introduction

In recent years, there has been an exponential growth in the amount of data available for computational analysis, including scientific data as well as common data types such as text, images, and audio. This abundance of data has empowered various fields, including physics, chemistry, computational social sciences, and biology, to make significant progress using machine learning techniques, primarily deep neural networks. As deep neural networks can effectively summarize and extract patterns from large data sets, they are suitable for many complex tasks. Initially, deep neural networks have been developed to learn from data supported on regular (Euclidean) domains, such as grids in images, sequences of text and time-series. These models, including convolutional neural networks (CNNs) [166, 173, 257], recurrent neural networks (RNNs) [263, 14] and transformers [271], have proven highly effective in processing such Euclidean data [122], resulting in unprecedented performance in various applications, most recently in chat-bots (e.g., ChatGPT [3]) and text-controlled image synthesis [237].

However, scientific data in various fields are often structured differently and are not supported on regular Euclidean domains. As a result, adapting deep neural networks to process this type of data has been a challenge. Against this backdrop, geometric deep learning (GDL) [52, 301, 284] has emerged as an extension of deep learning models to non-Euclidean domains. To achieve this, GDL restricts the performed computations via principles of geometric regularity, such as symmetries, invariances, and equivariances. The GDL perspective allows for appropriate inductive biases to be imposed when working with arbitrary data domains, including sets [227, 229, 86, 300, 147], grids [47, 198, 48, 164, 256, 283, 207], manifolds [47, 198, 48, 164, 256, 283, 207], and graphs [246, 106, 301, 284, 48, 207, 51, 160]. Graphs, in particular, have garnered interest due to their applicability in numerous scientific studies and their ability to generalize conventional grids. Accordingly, the development of graph neural networks (GNNs) [51, 160] has remarkably enhanced our ability to model and analyze several types of data in which graphs naturally appear.
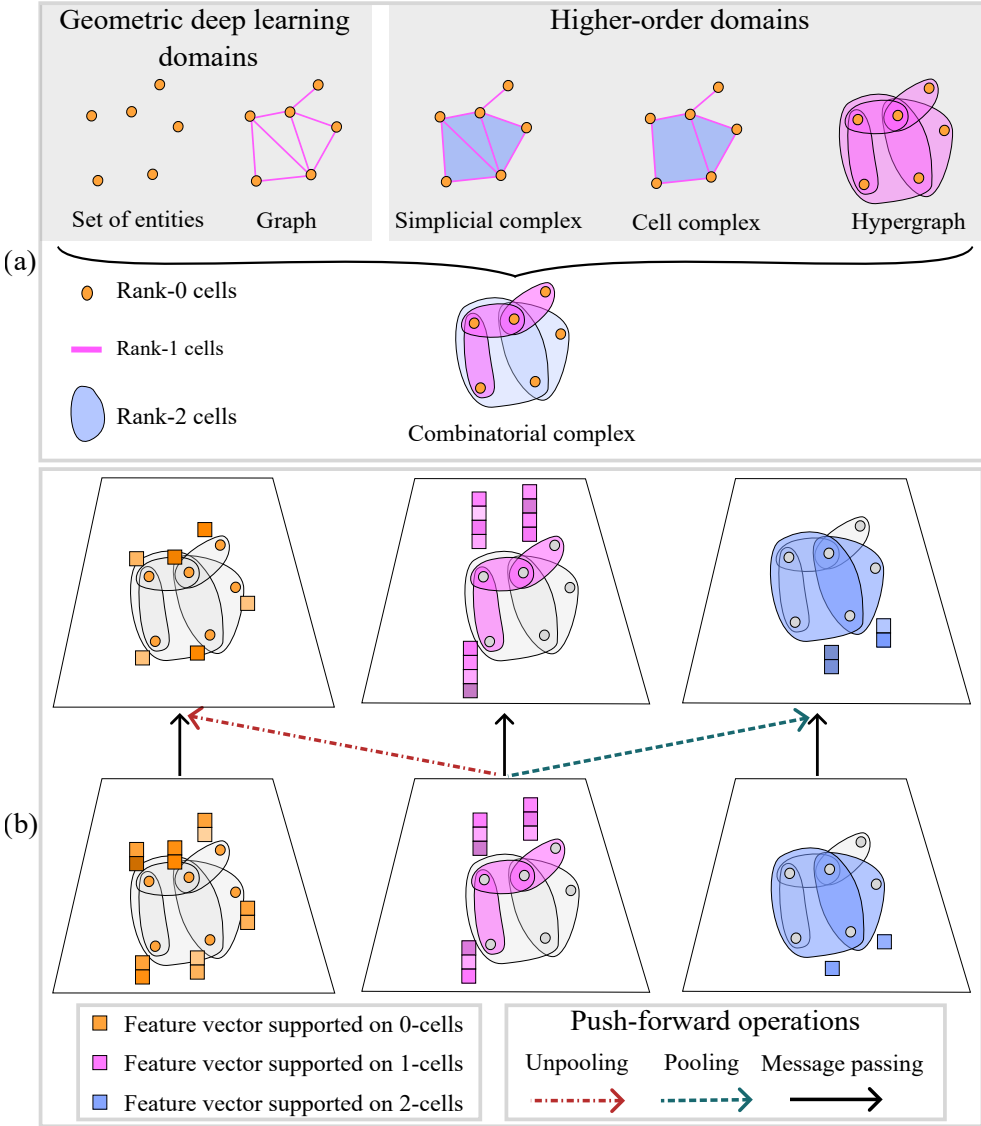
Figure 1: A graphical abstract that visualizes our main contributions. (a): Different mathematical structures can be used to represent relations between abstract entities. Sets have entities with no connections, graphs encode binary relations between vertices, simplicial and cell complexes model hierarchical higher-order relations, and hypergraphs accommodate arbitrary set-type relations with no hierarchy. We introduce combinatorial complexes (CCs), which generalize graphs, simplicial and cell complexes, and hypergraphs. CCs are equipped with set-type relations as well as with a hierarchy of these relations. (b): By utilizing the hierarchical and topological structure of CCs, we introduce the push-forward operation, a fundamental building block for higher-order message-passing protocols and for (un)pooling operations on CCs. Our push-forward operations on CCs enable us to construct combinatorial complex neural networks (CCNNs), which provide a general conceptual framework for topological deep learning on higher-order domains.

Despite the success of GDL and GNNs, seeing graphs through a purely geometric viewpoint yields a solely local abstraction and falls short of capturing non-local properties and dependencies in data. *Topological data*, including interactions of edges (in graphs), triangles (in meshes) or cliques, arise naturally in an array of novel applications in complex physical systems [31, 172], traffic forecasting [153], social influence [302], protein interaction [212], molecular design [251], visual enhancement [100], recommendation systems [171], and epidemiology [87]. To natively and effectively model such data, we are bound to go beyond graphs and

consider qualitative spatial properties remaining unchanged under some geometric transformations. In other words, we need to consider the *topology of data* [61] to formulate neural network architectures capable of extracting semantic meaning from complex data.

One approach to extract more global information from data is to go beyond graph-based abstractions and consider extensions of graphs, such as simplicial complexes, cell complexes, and hypergraphs, generalizing most data domains encountered in scientific computations [43, 30, 33, 267]. The development of machine learning models to learn from data supported on these topological domains [102, 56, 236, 248, 44, 126, 128, 96, 249, 235, 117, 288] is a rapidly growing new frontier, to which we refer hereafter as *topological deep learning (TDL)*. TDL intertwines several research areas, including topological data analysis (TDA) [98, 61, 91, 189, 113], topological signal processing [247, 289, 250, 236, 22, 233, 243], network science [259, 172, 21, 30, 43, 41, 34, 85, 20, 215], and geometric deep learning [295, 59, 104, 188, 28, 209, 27].

Despite the growing interest in TDL, a broader synthesis of the foundational principles of these ideas has not been established so far. We argue that this is a deficiency that inhibits progress in TDL, as it makes it challenging to draw connections between different concepts, impedes comparisons, and makes it difficult for researchers of other fields to find an entry point to TDL. Hence, in this paper, we aim to provide a foundational overview over the principles of TDL, serving not only as a unifying framework for the many exciting ideas that have emerged in the literature over recent years, but also as a conceptual starting point to promote the exploration of new ideas. Ultimately, we hope that this work will contribute to the accelerated growth in TDL, which we believe would be a key enabler of transferring deep learning successes to an enlarged range of application scenarios.

By drawing inspiration from traditional topological notions in algebraic topology [113, 138] and recent advancements in higher-order networks [30, 267, 43, 31], we first introduce *combinatorial complexes (CCs)* as the major building blocks of our TDL framework. CCs constitute a novel topological domain that unifies graphs, simplicial and cell complexes, and hypergraphs as special cases, as illustrated in Figure 1[1]. Similar to hypergraphs, CCs can encode arbitrary set-like relations between collections of abstract entities. Moreover, CCs permit the construction of hierarchical higher-order relations, analogous to those found in simplicial and cell complexes. Hence, CCs generalize and combine the desirable traits of hypergraphs and cell complexes.

In addition, we introduce the necessary operators to construct deep neural networks for learning features and abstract summaries of input anchored on CCs. Such operators provide convolutions, attention mechanisms, message-passing schemes as well as the means for incorporating invariances, equivariances, or other geometric regularities. Specifically, our novel *push-forward operation* allows pushing data across different dimensions, thus forming an elementary building block upon which *higher-order message-passing protocols* and *(un)pooling operations* are defined on CCs. The resulting learning machines, which we call *combinatorial complex neural networks (CCNNs)*, are capable of learning abstract higher-order data structures, as clearly demonstrated in our experimental evaluation.

We envisage our contributions to be a platform encouraging researchers and practitioners to extend our CCNNs, and invite the community to build upon our work to expand TDL on higher-order domains. Our contributions, which are also visually summarized in Figure 1, are the following:

- First, we introduce CCs as domains for TDL. We characterize CCs and their properties, and explain how they generalize major existing domains, such as graphs, hypergraphs, simplicial and cell complexes. CCs can thus serve as a unifying starting point that enables the learning of expressive representations of topological data.
- Second, using CCs as domains, we construct CCNNs, an abstract class of higher-order message-passing neural networks that provide a unifying blueprint for TDL models based on hypergraphs and cell complexes.
  - Based upon a push-forward operator defined on CCs, we introduce convolution, attention, pooling and unpooling operators for CCNNs.
  - We formalize and investigate *permutation and orientation equivariance* of CCNNs, paving the way to future work on geometrization of CCNNs.

---

[1]All figures in this paper should be displayed in color, as different colors communicate different pieces of information.

- – We show how CCNNs can be intuitively constructed via graphical notation.
- Third, we evaluate our ideas in practical scenarios.
  - – We release the source code of our framework as three supporting Python libraries: *TopoNetX*, *TopoEmbedX* and *TopoModelX*.
  - – We show that CCNNs attain competing predictive performance against state-of-the-art task-specific neural networks in various applications, including shape analysis and graph learning.
  - – We establish connections between our work and classical constructions in TDA, such as the *mapper* [258]. Particularly, we realize the mapper construction in terms of our TDL framework and demonstrate how it can be utilized in higher-order (un)pooling on CCs.
  - – We demonstrate the reducibility of any CC to a special graph called the *Hasse graph*. This enables the characterization of certain aspects of CCNNs in terms of graph-based models, allowing us to reduce higher-order representation learning to graph representation learning (using an enlarged computational graph).

Glossary.   Prior to delving into more details, we present the elementary terminologies of already established concepts used throughout the paper. Some of these terms are revisited formally in Section 3. Appendix A provides notation and terminology glossaries for novel ideas put forward by the paper.

Cell complex: a topological space obtained as a disjoint union of topological disks (cells), with each of these cells being homeomorphic to the interior of a Euclidean ball. These cells are attached together via attaching maps in a locally reasonable manner.

Domain: the underlying space where data is typically supported.

Entity or **vertex**: an abstract point; it can be thought as an element of a set.

Graph or **network**: a set of entities (vertices) together with a set of edges representing binary relations between the vertices.

Hierarchical structure on a topological domain: an integer-valued function that assigns a positive integer (rank) to every relation in the domain such that higher-order relations are assigned higher rank values. For instance, a simplicial complex admits a hierarchical structure induced by the cardinality of its simplices.

Higher-order network/topological domain: generalization of a graph that captures (binary and) higher-order relations between entities. Simplicial/cell complexes and hypergraphs are examples of higher-order networks.

Hypergraph: a set of entities (vertices) and a set of hyperedges representing binary or higher-order relations between the vertices.

Message passing: a computational framework that involves passing data, 'messages', among neighbor entities in a domain to update the representation of each entity based on the messages received from its neighbors.

Relation or **cell**: a subset of a set of entities (vertices). A relation is called **binary** if its cardinality is equal to two. A relation is called **higher-order** if its cardinality is greater than two.

Set-type relation: a higher-order network is said to have set-type relations if the existence of a relation is not implied by another relation in the network; e.g., hypergraphs admit set-type relations.

Simplex: a generalization of a triangle or tetrahedron to arbitrary dimensions; e.g., a simplex of dimension zero, one, two, or three is a point, line segment, triangle, or tetrahedron, respectively.

Simplicial complex: a collection of simplices such that every face of each simplex in the collection is also in the collection, and the intersection of any two simplices in the collection is either empty or a face of both simplices.

Topological data: feature vectors supported on relations in a topological domain.

Topological deep learning: the study of topological domains using deep learning techniques, and the use of topological domains to represent data in deep learning models.
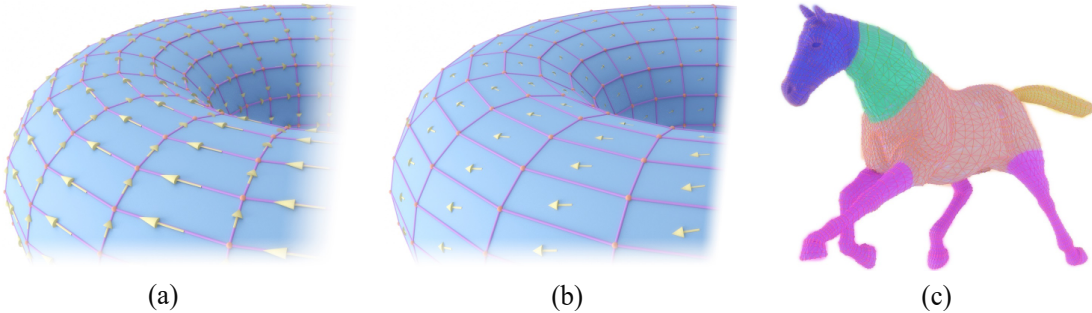

Figure 2: Data might be supported naturally on higher-order relations. (a): An edge-based vector field. (b): A face-based vector field. Both vector fields in (a) and (b) are defined on a cell complex torus. An interactive visualization of (a–b) is provided here. (c): Class-labeled topological data might naturally be supported on higher-order relations. For instance, mesh segmentation labels for 2-faces are depicted by different colors (blue, green, turquoise, pink, brown) to represent different parts (head, neck, body, legs, tail) of the horse.

2 Motivation: what does topology offer to machine learning?

Combinatorial complex neural networks (CCNNs), as presented in this work, generalize graph neural networks (GNNs) and their higher-order analogues via topological constructions. In this section, we provide the motivation for the use of topological constructions in machine learning, and specifically in deep learning from three angles. First, *data modeling*: how topological abstraction can help us to reason and compute with various data types supported on topological spaces. Second, *utility*: how accounting for topology improves performance. Third, *unification*: how topology can be used to synthesize and abstract disparate concepts.

2.1 Modeling and learning from data on topological spaces

In the context of machine learning, the domain on which the data is supported is typically a (linear) vector space. This underlying vector space facilitates many computations and is often implicitly assumed. However, as has been recognized within geometric deep learning, it is often essential to consider data supported on different domains. Indeed, explicitly considering and modeling the domain on which the data is supported can be crucial for various reasons.

First, different domains can have distinct characteristics and properties that require different types of deep learning models to effectively process and analyze the data. For example, a graph domain may require a graph convolutional network [160] to account for the non-Euclidean structure, while a point cloud domain may require a PointNet-like architecture [227, 292] to handle unordered sets of points.

Second, the specific data within each domain can vary widely in terms of size, complexity and noise. By understanding specific data properties within a given domain, researchers can develop models that are tailored to those particular properties. For example, a model designed for point clouds with high levels of noise may incorporate techniques such as outlier removal or local feature aggregation.

Third, accurately distinguishing between domain and data is important for developing models that generalize well to new, unseen data. By identifying the underlying structure of the domain, researchers can develop models that are robust to variations in the data while still being able to capture relevant geometric features. To summarize, by considering both the domain and data together, researchers can develop models that are better suited to handle the specific challenges and complexities of different geometric learning tasks.

Different perspectives on data: domains and relations. When referring to topological data or topological data analysis in the literature, there are different views on what the actual data consists of and what it is supposed to model. Here, we follow [43] and distinguish between different types of data and goals of our learning procedures, even though the distinction between these different types of data can sometimes be more blurry than what is presented here.

(a)   (b)

Figure 3: Examples of processing data supported on graphs or on higher-order networks. (a): Graphs can be used to model particle interactions in fluid dynamics. Vertices represent particles, whereas particle-to-particle interactions are modeled via message passing among vertices [240, 255]. (b): When modeling springs and self-collision, it is natural to work with edges rather than vertices. This is because the behavior of the cloth is determined by the tension and compression forces acting along the edges, and not only by the position of individual particles. To model the interactions among multiple edges, polygonal faces can be used to represent the local geometry of the cloth. The polygonal faces provide a way to compute higher-order message passing among the edges.

Relational data. Relational data describes the relations between different entities or objects. This fundamental concept can manifest in various ways, such as connections between users in social networks, where friend relationships or follower-ship serve as examples of such relations. Traditionally, these relations are understood through graphs, with vertices and edges representing entities and their *pairwise connections*, respectively. Stated differently, the edges within the graph are considered to be units of measurement; i.e., every piece of relational data involves two vertices.

However, many real-world phenomena naturally involve complex, multi-party interactions, where more than two entities interact with each other in intricate ways. For instance, groups of individuals within a society, sets of co-authors, and genes or proteins that interact with each other are all examples of such higher-order relations. Such dependencies, which go beyond pairwise interactions, can be modeled by *higher-order relations* and aptly abstracted as hypergraphs, cell complexes, or CCs. Clearly, topological ideas can play an important role for understanding this data, and crucially enable us to move from graphs modeling pairwise relations to richer representations.

Data as an instance of a domain. A related conceptualization of what our observed data is supposed to represent is adopted in TDA. Namely, all of observed data is supposed to correspond to a noisy instance of a topological object itself; i.e., we aim to learn the 'topological shape' of the data. Note that in this context, we typically do not directly observe relational data, but instead we *construct relations from observed data*, which we then use to classify the observed dataset. Persistent homology performed on point cloud data is a mainstream example for this viewpoint.

Data supported on a topological domain. Topological ideas also play an important role when considering data that is defined on top of a domain such as a graph. This could be particular dynamics, such as epidemic spreading, or it could be any type of other data or signals supported on the vertices (cases of edge-signals on a graph are not considered often, though exceptions exist [247, 249]). In the language of *graph signal processing*, a variety of functions or signals can be defined on a graph *domain*, and these are said to be *supported by the domain.* Crucially, the graph itself can be arbitrarily complex but is typically considered to be fixed; the observed data is not relational, but supported on the vertices of a graph.

Moving beyond graphs, more general topological constructions, such as CCs, can support data not just on vertices and edges, but also on other 'higher-order' entities, as demonstrated in Figure 2(a–b). For example, vector fields defined on meshes in computer graphics are often data supported on edges and faces, and can be conveniently modeled as data supported on a higher-order domain [119]. Similarly, class-labeled data can be provided on the edges and faces of a given mesh; see Figure 2(c) for an example. To process such data it is again relevant to take into account the structure of the underlying topological domain.
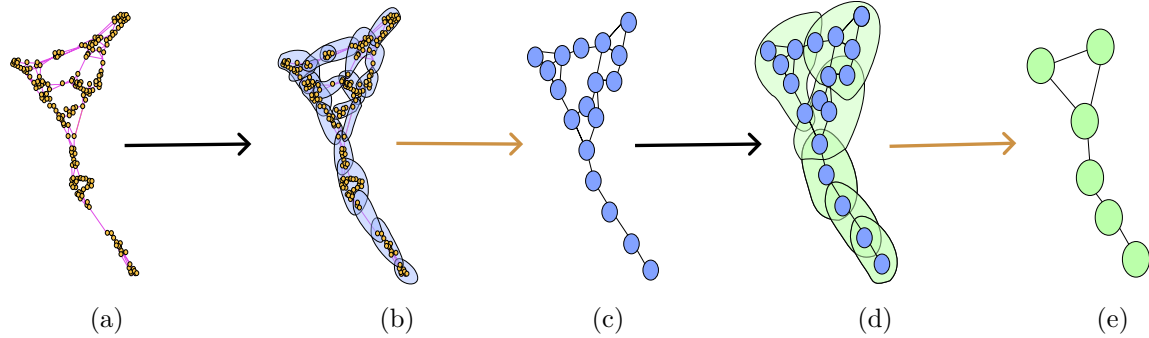
Figure 4: An illustration of representing hierarchical data via higher-order networks. Black arrows indicate graph augmentation by higher-order relations, whereas orange arrows indicate coarsened graph extraction. (a): A graph encodes binary relations (pink edges) among abstract entities (yellow vertices). (b): Higher-order relations, represented by blue cells, can be thought as relations among vertices or edges of the original graph. (c): Extraction of a coarsened version of the original graph. In the coarsened graph, vertices represent the higher-order relations (blue cells) of the original graph, and edges represent the intersections of these blue cells. (d–e): The same process repeats to obtain a more coarsened version of the original graph. The entire process corresponds to hierarchical higher-order relations, that is relations among relations, which extract meaning and content (including the 'shape of data'), a common task in topological data analysis [61, 91].

Modeling and processing data beyond graphs: illustrative examples.   Graphs are well-suited for modeling systems that exhibit pairwise interactions. For instance, particle-based fluid simulations can be effectively represented using graphs as shown in Figure 3(a), with message passing used to update the physical state of fluid molecules. In this approach, each molecule is represented as a vertex containing its physical state, and the edges connecting them are utilized to calculate their interactions [240, 255].

Graphs may not be adequate for modeling more complex systems such as cloth simulation, where state variables are associated with relations like edges or triangular faces rather than vertices. In such cases, higher-order message passing is required to compute and update physical states, as depicted in Figure 3(b). A similar challenge arises in natural language processing, where language exhibits multiple layers of syntax, semantics and context. Although GNNs may capture basic syntactic and semantic relations between words, more complex relations such as negation, irony or sarcasm may be difficult to represent [115]. Including higher-order and hierarchical relations can provide a better model for these relations, and can enable a more nuanced and accurate understanding of language.

2.2   The utility of topology

In addition to providing a versatile framework for modeling complex systems, TDL models have broad utility: they can induce meaningful inductive biases for learning, facilitate efficient message propagation over longer ranges in the underlying domain, enhance the expressive power of existing graph-based models, and have the potential to unveil crucial characteristics of deep networks themselves, as described next.

Building hierarchical representations of data.   While leveraging higher-order information is important for learning representations, it is also crucial to preserve the complex higher-order relations between entities for achieving powerful and versatile representations. For instance, humans can form abstractions and analogies by building relations among relations hierarchically. However, graph-based models, which are commonly used for building relational reasoning among various entities [241, 295, 74, 252], are limited in their ability to build higher-order relations among these entities.

The need for hierarchical relational reasoning [285] demands methods that can capture deeper abstract relations among relations, beyond modeling relations between raw entities. Higher-order network models provide a promising solution for addressing the challenge of higher-order relational reasoning, as depicted in Figure 4.
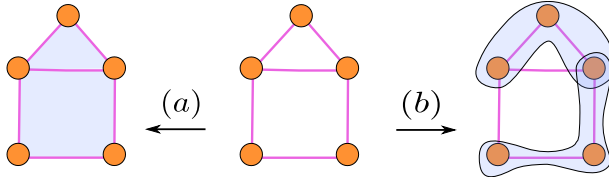
Figure 5: The graph in the middle can be augmented with higher-order relations to improve a learning task. In (a), cells have been added to the missing faces; a similar inductive bias has been considered in [46] to improve classification on molecular data. In (b), one-hop neighborhoods have been added to some of the vertices in the graph; [102] use such an inductive bias, based on lifting a graph to its corresponding one-hop neighborhood hypergraph, to improve performance on vertex-based tasks.
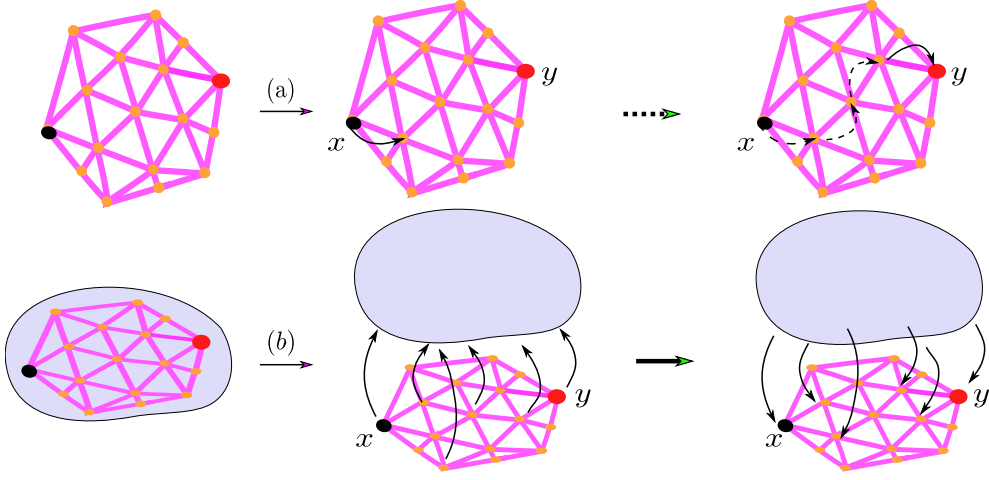
Figure 6: Illustration of message-passing among binary or higher-order cells. (a): Using a graph-based message-passing scheme, some information that starts at vertex x needs to travel a long distance, that is a long edge path, before reaching vertex y. (b): Using a higher-order cell structure, indicated by the the blue cell, the signal can be lifted from the vertices to a higher-order cell and thus propagates back and forth between vertices x and y in fewer steps. This shortcut allows to share information efficiently, in fewer computational steps, among all vertices that belong to the blue cell [131].

Improving performance through inductive bias.   A topological deep learning model can be leveraged to enhance the predictive performance on graph-based learning tasks by providing a well-defined procedure to lift a graph to a given higher-order network. The incorporation of multi-vertex relations via this approach can be viewed as an inductive bias, and is utilized to improve predictive performance. Inductive bias allows a learning algorithm to prioritize one solution over another, based on factors beyond the observed data [205]. Figure 5 illustrates two forms of augmentation on graphs using higher-order cells.

Construction of efficient graph-based message passing over long-range.   The hierarchical structure of TDL networks facilitates the construction of long-range interactions in an efficient manner. By leveraging such structures, signals defined on the vertices of a domain can propagate efficiently distant dependencies among vertices connected by long edge paths. Figure 6 illustrates the process of lifting a signal defined on graph vertices by augmenting the graph with additional topological relations and unpooling the signal back to the vertices. [131] employ such pooling and unpooling operations to construct models capable of capturing distant dependencies, leading to more effective and adaptive learning of both the local and global structure of the underlying domain. For related work on graph-based pooling, we refer the reader to [150, 261].

Improved expressive power.   TDL can capture intricate and subtle dependencies that elude traditional graph-based models. By allowing richer higher-order interactions, higher-order networks can have improved expressive power and lead to superior performance in numerous tasks [46, 209].
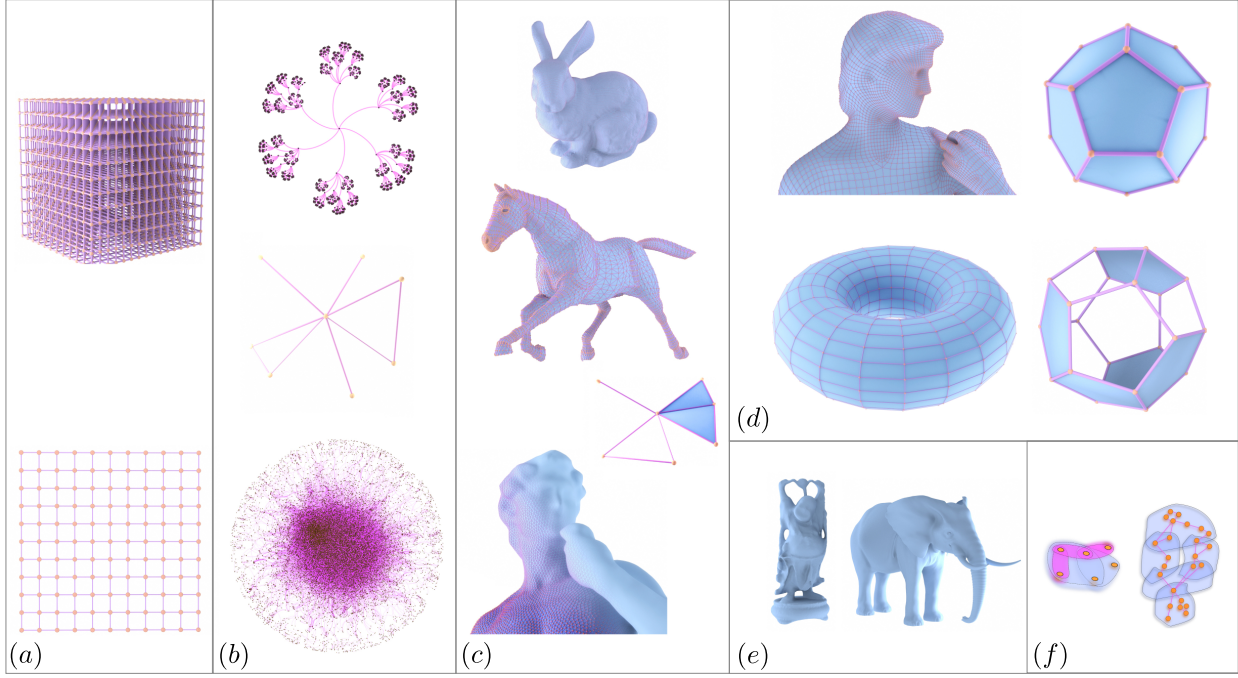
Figure 7: This work introduces combinatorial complexes, which are higher-order networks that generalize most discrete domains typically encountered in scientific computing, including (a) sequences and images, (b) graphs, (c) 3D shapes and simplicial complexes, (d) cubical and cellular complexes, (e) discrete manifolds, and (f) hypergraphs.

2.3 A unifying perspective on deep learning and structured computations

Topology provides a framework to generalize numerous discrete domains that are typically encountered in scientific computations. Examples of these domains include graphs, simplicial complexes, and cell complexes (see Figure 7). Computational models supported on such domains can be seen as a generalization of various deep learning architectures; i.e., can provide a unifying framework to compare and design TDL architectures. Further, understanding the connections between different types of TDL via a unifying theory can provide valuable insights into the underlying structure and behavior of complex systems, where higher-order relations naturally occur [128, 137, 43, 193].

Understanding why deep networks work.   A remarkable aspect of contemporary deep neural networks is their capacity to generalize very well to unseen data, even though they have an enormous number of parameters. This contradicts our previous understanding of statistical learning theory, prompting researchers to seek novel approaches in comprehending the underlying workings of deep neural networks [213]. Recent studies have revealed that the topology of graphs induced by deep neural networks or their corresponding training trajectories, modeled as Markov chains, exhibit strong correlations with generalization performance [45, 95]. An open question is how far such correlations between topological structure, computational function and generalization properties can be found in learning architectures supported on higher-order domains. We believe that by studying these questions using our novel topological constructs, such as CCs and CCNNs, we can gain deeper insights not only into TDL but also into deep learning more generally.

3 Preliminaries: from graphs to higher-order networks

The notion of proximity among entities in a set S holds significant relevance in various machine learning applications as it facilitates the comprehension of inter-entity relationships in S. For example, clustering algorithms aim to group points that are proximal to each other. In recommendation systems, the objective is
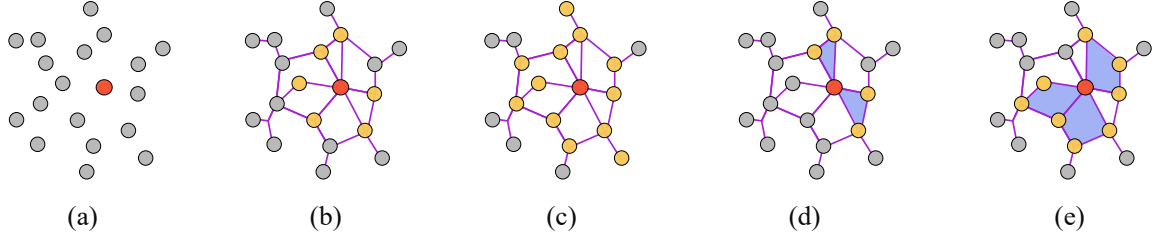
Figure 8: Demonstration of the notion of proximity among the entities of a set S. (a): A finite set S of abstract entities. (b): A neighborhood (in yellow) of an entity x (in red) in S. The neighborhood is defined to be the set of entities in S that are adjacent to x via an edge. (c): A neighborhood of x consisting of all yellow entities in S that have distance at most two from red entity x. (d): A neighborhood of x consisting of all yellow entities in S that form triangles (in blue) incident to red entity x. (d): A neighborhood of x consisting of all yellow entities in S that form trapezoids (in blue) incident to red entity x.

to suggest items that exhibit similarity to those for which a user has already expressed interest. However, the question is how do we precisely quantify the notion of proximity?

Consider a set S consisting of a collection of abstract entities, as depicted in Figure 8(a). Consider the red entity (vertex) x in the same figure. We wish to identify the entities (vertices) in S that are 'closely related' or 'in close proximity' to x. However, a set has no inherent notion of proximity or relations between its entities.

Defining binary relations (edges) among the entities of set S provides one way of introducing the concept of proximity, which results in a graph whose vertex set is S, as shown in Figure 8(b). Using this 'auxiliary structure' of edges defined on top of set S, one may declare the 'local neighborhood' of x, denoted by $\mathcal{N}(x)$, to be the subset of S consisting of all entities that are adjacent to x via an edge. In Figure 8(b), the neighborhood of vertex x (in red) in S consists of all vertices colored in yellow.

The choice of neighborhood $\mathcal{N}(x)$ in Figure 8(b) is arbitrary. For example, an alternative valid notion of neighborhood is given by defining $\mathcal{N}(x)$ to contain all vertices whose distance from the red vertex x is at most two, represented by all vertices colored in yellow in Figure 8(c). In Figure 8(d), the neighborhood $\mathcal{N}(x)$ is chosen to consist of all yellow vertices that form triangles incident to red vertex x. In Figure 8(e), the neighborhood $\mathcal{N}(x)$ is chosen to consist of all yellow vertices that form trapezoids incident to the red vertex x. It becomes clear from Figures 8(d) and (e) that additional auxiliary structures, such as triangles and trapezoids, can be used to define the notion of neighborhood. In practice, the choice of neighborhood typically depends on the application. Recent research has explored using graph geometry to obtain richer neighborhood notions, as seen in [209, 299, 128]. However, the fundamental concept remains the same: one starts by introducing an auxiliary structure defined on a vertex set, and then utilizes the auxiliary structure to induce a well-defined notion of proximity.

Upon generalizing graphs to higher-order networks, it is natural to also generalize the notion of neighborhood for graphs to higher-order networks. The precise notion of neighborhood or proximity among entities of a set S has been studied in topology [211]. A topology defined on S allows us to meaningfully describe the proximity of the elements in S to each other. This section introduces topological notions and definitions with the aim of generalizing graphs to higher-order networks.

3.1 Neighborhood functions and topological spaces

There are several equivalent ways to define a topological space. For example, topological spaces are commonly defined in terms of 'open' or 'closed' sets (e.g., [211]). In this work, we opt to define topological spaces in terms of 'neighborhoods'. This definition is more compatible with the message-passing paradigm that is usually defined on graphs [114], and it can be generalized to higher-order networks. We refer the reader to [53, Section 2.2] for an explanation of why the definition in terms of neighborhoods is equivalent to the definition in terms of open sets.

> **Definition 1** (Neighborhood function)**.** *Let S be a nonempty set. A **neighborhood function** on S is a function $\mathcal{N}\colon S \to \mathcal{P}(\mathcal{P}(S))$ that assigns to each point x in S a nonempty collection $\mathcal{N}(x)$ of subsets of S. The elements of $\mathcal{N}(x)$ are called **neighborhoods** of x with respect to $\mathcal{N}$.*

> **Definition 2** (Neighborhood topology)**.** *Let $\mathcal{N}$ be a neighborhood function on a set S. $\mathcal{N}$ is called a **neighborhood topology** on S if it satisfies the following axioms:*
>
>   *1. If N is a neighborhood of x, then $x \in N$.*
>
>   *2. If N is a subset of S containing a neighborhood of x, then N is a neighborhood of x.*
>
>   *3. The intersection of two neighborhoods of a point x in S is a neighborhood of x.*
>
>   *4. Any neighborhood N of a point x in S contains a neighborhood M of x such that N is a neighborhood of each point of M.*

> **Definition 3** (Topological space)**.** *A pair $(S, \mathcal{N})$ consisting of a nonempty set S and a neighborhood topology $\mathcal{N}$ on S is called a **topological space**.*

Hence, a topological space is a set S equipped with a neighborhood function $\mathcal{N}$, which satisfies the properties specified in Definition 2. In Section 4.4, we introduce a similar notion of proximity in the context of higher-order networks. Further, the choice of neighborhood function $\mathcal{N}$ is the first and most fundamental step in the construction of a deep learning model supported on a higher-order domain (see Section 5).

3.2   Bridging the gap among higher-order networks

Given a finite set S of abstract entities, a neighborhood function $\mathcal{N}$ on S can be induced by equipping S with an auxiliary structure, such as edges, as demonstrated in Figure 8(b). Edges provide one way of defining relations among the entities of S[2]. Specifically, each edge defines a binary relation (i.e., a relation between two entities) in S. In many applications, it is desirable to permit relations that incorporate more than two entities. The idea of using relations that involve more than two entities is central to higher-order networks. Such higher-order relations allow for a broader range of neighborhood functions to be defined on S to capture multi-way interactions among entities of S.

To describe more intricate multi-way interactions, it is necessary to employ more intricate neighborhood functions and topologies. With an eye towards defining a general higher-order network in Section 4 (as motivated in Section 2), this section reviews the definitions, advantages, and disadvantages of some commonly studied higher-order networks, including (abstract) simplicial complexes, regular cell complexes, and hypergraphs. In Section 4, we introduce combinatorial complexes, which generalize and bridge the gaps between all of these commonly studied topological domains.

Simplicial complexes are one of the simplest higher-order domains with many desirable properties, extending the corresponding properties of graphs. For instance, Hodge theory is naturally defined on simplicial complexes, extending similar notions on graphs [248, 22, 249].

> **Definition 4** (Simplicial complex)**.** *An **abstract simplicial complex** on a nonempty set S is a pair $(S, \mathcal{X})$, where $\mathcal{X}$ is a subset of $\mathcal{P}(S) \setminus \{\emptyset\}$ such that $x \in \mathcal{X}$ and $y \subseteq x$ imply $y \in \mathcal{X}$. Elements of $\mathcal{X}$ are called **simplices**.*

Figure 7(c) displays examples of triangular meshes, which are special cases of simplicial complexes with many applications in computer graphics. We refer the reader to [249, 80] for a relevant introduction to simplicial

---

[2]Recall that a relation on S is a nonempty subset of S.

complexes. As it is evident from Definition 4, each relation x on S must contain all relations y with $y \subseteq x$. Hence, a simplicial complex may encode a relatively large amount of data, taking up a lot of memory [236]. Further, real-world higher-order data (e.g., traffic-flows on a rectangular street network) may not admit a meaningful simplicial complex structure due to the inherent lack of available simplices on the underlying data space. To address this limitation, cell complexes [138, 137] can generalize simplicial complexes, and overcome many of their drawbacks.

Definition 5 (Regular cell complex). *A **regular cell complex** is a topological space S with a partition into subspaces (**cells**) $\{x_\alpha\}_{\alpha \in P_S}$, where P_S is an index set, satisfying the following conditions:*

1. *$S = \cup_{\alpha \in P_S} \mathrm{int}(x_\alpha)$, where $\mathrm{int}(x)$ denotes the interior of cell x.*

2. *For each $\alpha \in P_S$, there exists a homeomorphism ψ_α, called an **attaching map**, from x_α to $\mathbb{R}^{n_\alpha}$ for some $n_\alpha \in \mathbb{N}$, called the **dimension** n_α of cell x_α.*

3. *For each cell x_α, the boundary ∂x_α is a union of finitely many cells, each having dimension less than the dimension of x_α.*

For the sake of brevity, we henceforth refer to a 'regular cell complex' as a 'cell complex'. Cell complexes encompass a wide range of higher-order networks. Several types of higher-order networks can be viewed as instances of cell complexes. For instance, cell complexes are a natural generalization of graphs, simplicial complexes, and cubical complexes [128]. Figure 7(d) shows examples of cell complexes. Intuitively, a cell complex is a disjoint union of cells, with each of these cells being homeomorphic to the interior of a k-dimensional Euclidean ball for some k. These cells are attached together via attaching maps in a locally suitable manner. The information of attaching maps of a regular cell-complex can be stored combinatorially in a sequence of matrices, called the *incidence matrices* [138]. We describe these matrices in detail in Section 4.4.1.

Condition 3 in Definition 5 is known as the *regularity condition* for regular cell complexes. The regularity condition implies that the topological information of a cell complex can be realized combinatorially by equipping the index set P_S with a poset structure given by $\alpha \leq \beta$ if and only if $x_\alpha \subseteq \overline{x_\beta}$, where $\overline{x}$ denotes the closure of a cell x. This poset structure is typically called the *face poset* [137]. It can be shown that the topological information encoded in a cell complex is completely determined by the face poset structure [137], which allows cell complexes to be represented combinatorially in practice via a poset [9, 26, 245, 162].

Definition 5 implies that the boundary cells of each cell in a cell complex are also cells in the cell complex. Hence, one may think about a cell complex as a collection of cells of varying dimensions, which are related via their boundaries. In terms of relations, this implies that the boundary of a cell in a cell complex must also be a cell in the cell complex. While cell complexes form a general class of higher-order networks, this property sets a constraint on the relations of a cell complex. Such a constraint may not be desirable in certain applications if the data do not satisfy it. To remove all constraints on the relations among entities of a set, hypergraphs are typically considered.

Definition 6 (Hypergraph). *A **hypergraph** on a nonempty set S is a pair $(S, \mathcal{X})$, where $\mathcal{X}$ is a subset of $\mathcal{P}(S) \setminus \{\emptyset\}$. Elements of $\mathcal{X}$ are called **hyperedges**.*

A hyperedge of cardinality two is called an *edge*. Hypergraphs can be considered as a generalization of simplicial and cell complexes. However, hypergraphs do not directly entail the notion of the dimension of a cell (or of a relation), which is explicitly encoded in the definition of cell complex and is also indicated by the cardinality of a relation in a simplicial complex. As we demonstrate in Section 4.3, the dimensionality of cells and relations in simplicial and cell complexes can be used to endow these complexes with hierarchical structures, which can be utilized for (un)pooling type computations on these structures.
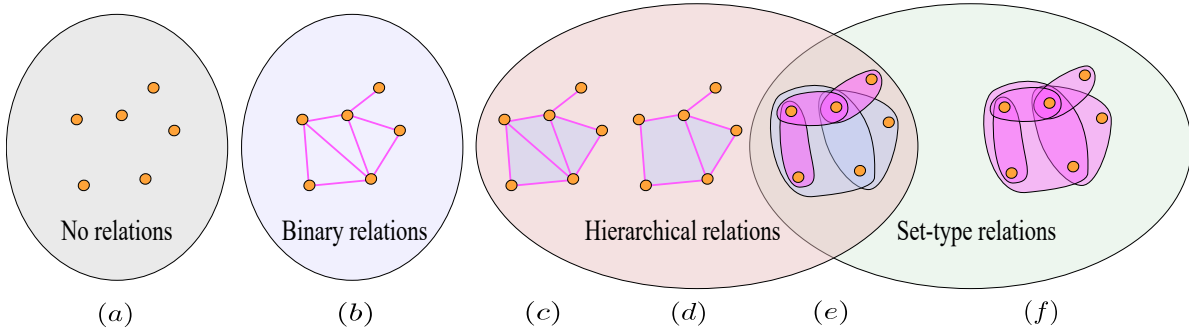
Figure 9: Illustration of how CCs generalize various domains. (a): A set S consists of abstract entities (vertices) with no relations. (b): A graph models binary relations between its vertices (i.e., elements of S). (c): A simplicial complex models a hierarchy of higher-order relations (i.e., relations between the relations) but with rigid constraints on the 'shape' of its relations. (d): Similar to simplicial complexes, a cell complex models a hierarchy of higher-order relations, but with more flexibility in the shape of the relations (i.e., 'cells'). (f): A hypergraph models arbitrary set-type relations between elements of S, but these relations do not have a hierarchy among them. (e): A CC combines features of cell complexes (hierarchy among its relations) and of hypergraphs (arbitrary set-type relations), generalizing both domains.

3.3 Hierarchical structure and set-type relations

The properties of simplicial complexes, cell complexes and hypergraphs, as outlined in Section 3.2, give rise to two main features of relations on higher-order domains, namely hierarchies of relations and set-type relations. In the present subsection, we formalize these two features.

Definition 7 (Rank function). *A **rank function** on a higher-order domain $\mathcal{X}$ is an order-preserving function* $\mathrm{rk}\colon \mathcal{X} \to \mathbb{Z}_{\geq 0}$*; i.e., $x \subseteq y$ implies $\mathrm{rk}(x) \leq \mathrm{rk}(y)$ for all $x, y \in \mathcal{X}$.*

Intuitively, a rank function rk on a higher-order domain $\mathcal{X}$ attaches a ranking, represented by a non-negative integer value, to every relation in $\mathcal{X}$ such that set inclusion in $\mathcal{X}$ is preserved via rk. Effectively, a rank function induces a *hierarchical structure* on $\mathcal{X}$. Cell and simplicial complexes are common examples of higher-order domains equipped with rank functions and therefore with hierarchies of relations.

Definition 8 (Set-type relations). *Relations in a higher-order domain are called **set-type relations** if the existence of a relation is not implied by another relation in the domain.*

Hypergraphs constitute examples of higher-order domains equipped with set-type relations. Given the modeling limitations of simplicial complexes, cell complexes, and hypergraphs, we develop the combinatorial complex in Section 4, a higher-order domain that features both hierarchies of relations and set-type relations.

4 Combinatorial complexes (CCs)

This section introduces combinatorial complexes (CCs), a novel class of higher-order domains that generalizes graphs, simplicial complexes, cell complexes, and hypergraphs. Figure 9 shows a first illustration of the generalization that CCs provide over such domains. Moreover, Table 1 enlists the relation-related features of higher-order domains and graphs, thus summarizing the relation-related generalization attained by CCs.

In Section 4.1, we introduce the definition of CC and provide examples of CCs. In Section 4.2, we define the notion of CC-homomorphism and present relevant examples. In Section 4.3, we present the motivation behind the CC structure from a practical point of view. In Section 4.4, we demonstrate the computational

Relation-related features	Topological domains				Graph
	CC	Hypergraph	Cell complex	Simplicial complex	
Hierarchy of relations	✓		✓	✓	
Set-type relations	✓	✓			
Multi-relation coupling	✓		✓	✓	
Rank $\not\Rightarrow$ cardinality	✓	✓	✓		

Table 1: Tabular summary of relation-related features of topological domains and of graphs. Recall that a relation is an element of a domain. A domain is specified via its relations and via the way these relations are related to each other. Desirable relation-related features are indicated in the first column. A *hierarchy of relations* implies that relations of the higher-order domain can have different rankings. *Set-type relations* are free from constraints among relations or their lengths. *Multi-relation coupling* implies that each relation can have other neighboring relations via multiple neighborhood functions defined on the higher-order domain. '*Rank $\not\Rightarrow$ cardinality*' indicates that relations with the same ranking in a given hierarchy on the higher-order domain do not need to have the same cardinality.

version of neighborhood functions on neighborhood matrices. Finally, in Section 4.5, we introduce the notion of CC-cochain.

4.1   CC definition

We seek to define a structure that bridges the gap between simplicial/cell complexes and hypergraphs, as discussed in Section 3.3. To this end, we introduce the combinatorial complex (CC), a higher-order domain that can be viewed from three perspectives: as a simplicial complex whose cells and simplices are allowed to be missing; as a generalized cell complex with relaxed structure; or as a hypergraph enriched through the inclusion of a rank function.

> **Definition 9** (CC). *A **combinatorial complex (CC)** is a triple* $(S, \mathcal{X}, \mathrm{rk})$ *consisting of a set S, a subset $\mathcal{X}$ of $\mathcal{P}(S) \setminus \{\emptyset\}$, and a function* $\mathrm{rk} \colon \mathcal{X} \to \mathbb{Z}_{\geq 0}$ *with the following properties:*
>
> *1. for all $s \in S$, $\{s\} \in \mathcal{X}$, and*
>
> *2. the function rk is order-preserving, which means that if $x, y \in \mathcal{X}$ satisfy $x \subseteq y$, then $\mathrm{rk}(x) \leq \mathrm{rk}(y)$.*
>
> *Elements of S are called **entities** or **vertices**, elements of $\mathcal{X}$ are called **relations** or **cells**, and rk is called the **rank function** of the CC.*

For brevity, $\mathcal{X}$ is used as shorthand notation for a CC $(S, \mathcal{X}, \mathrm{rk})$. Definition 9 sets up a framework to construct higher-order networks upon which we can define general purpose higher-order deep learning architectures. Observe that CCs exhibit both hierarchical and set-type relations. Particularly, the rank function rk of a CC induces a hierarchy of relations in the CC. Further, CCs encompass set-type relations as there are no relation constraints in Definition 9. Thus, CCs subsume cell complexes and hypergraphs in the sense that they combine the relation-related features of both. Table 1 provides a comparative summary of relation-related features among CCs and common higher-order networks and graphs.

Remark 4.1. *We typically require that* $\mathrm{rk}(\{s\}) = 0$ *for each singleton cell $\{s\}$ in a CC. Such a convention aligns CCs naturally with simplicial and cellular complexes.*

The rank of a cell $x \in \mathcal{X}$ is the value $\mathrm{rk}(x)$ of the rank function rk at x. The *dimension* $\dim(\mathcal{X})$ of a CC $\mathcal{X}$ is the maximal rank among its cells. A cell of rank k is called a *k-cell* and is denoted by x^k. The *k-skeleton* of a CC $\mathcal{X}$, denoted $\mathcal{X}^{(k)}$, is the set of cells of rank at most k in $\mathcal{X}$. The set of cells of rank exactly k is denoted by $\mathcal{X}^k$. Note that this set corresponds to $\mathcal{X}^k = \mathrm{rk}^{-1}(\{k\})$. The 1-cells are called the *edges* of $\mathcal{X}$. In general, an edge of a CC may contain more than two nodes. CCs whose edges have exactly two nodes are called *graph-based* CCs. In this paper, we primarily work with graph-based CCs.
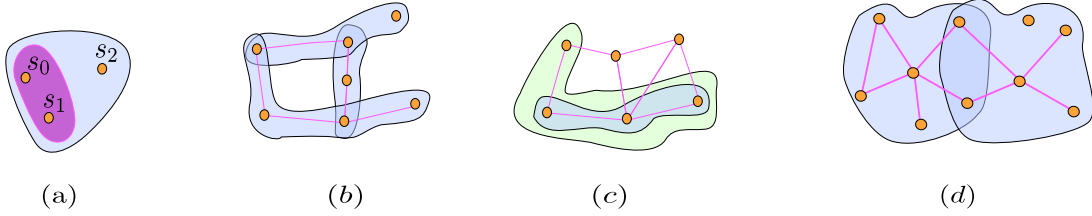
Figure 10: Examples of CCs. Orange circles represent vertices. Pink, blue, and green colors represent cells of rank one, two, and three, respectively. Each of the CCs in (a), (b), and (d) has dimension equal to two, whereas the CC in (c) has dimension equal to three.

Example 4.2 (CCs of dimension two and three). *Figure 10 shows four examples of CCs. For instance, Figure 10(a) shows a 2-dimensional CC on a vertex set $S = \{s_0, s_1, s_2\}$, consisting of 0-cells $\{s_0\}$, $\{s_1\}$, and $\{s_2\}$ (shown in orange), 1-cell $\{s_0, s_1\}$ (purple), and 2-cell $\{s_0, s_1, s_2\} = S$ (blue).*

4.2   CC-homomorphisms and sub-CCs

CC-homomorphisms are maps relating CCs to one another. CC-homomorphisms play an important role in delineating the process of lifting graphs or other higher-order domains to CCs. Intuitively, a lifting map is a well-defined procedure that converts a domain of certain type, such as a graph, to a domain of another type, such as a CC. The usefulness of lifting maps lie in their ability to enable the application of deep learning models defined on CCs to more common domains, such as graphs, cell complexes or simplicial complexes. We study lifting maps in detail and provide examples of them in Appendix B. Definition 10 formalizes the notion of CC-homomorphism.

Definition 10 (CC-homomorphism). *A homomorphism from a CC $(S_1, \mathcal{X}_1, \mathrm{rk}_1)$ to a CC $(S_2, \mathcal{X}_2, \mathrm{rk}_2)$, also called a **CC-homomorphism**, is a function $f \colon \mathcal{X}_1 \to \mathcal{X}_2$ that satisfies the following conditions:*

1. If $x, y \in \mathcal{X}_1$ satisfy $x \subseteq y$, then $f(x) \subseteq f(y)$.

2. If $x \in \mathcal{X}_1$, then $\mathrm{rk}_1(x) \geq \mathrm{rk}_2(f(x))$.

The second condition in Definition 10 assures that a CC-homomorphism may only map a k-cell in $\mathcal{X}_1$ to a cell in $\mathcal{X}_2$ with rank no greater than k. When $\mathrm{rk}_1(x) = \mathrm{rk}_2(f(x))$ for all $x \in \mathcal{X}_1$ and f is injective, then we call the homomorphism f a *CC-embedding*. CC-embeddings are useful in practice as they can be used to 'lift' a domain, such as a graph, to a CC by augmenting that domain with higher-order cells. Example 4.3 displays three CC-embeddings, while Example 4.4 presents a CC-homomorphism that is not a CC-embedding.

Example 4.3 (CC-embeddings). *Figures 11(a) and (b) show two CC-embeddings. In Figure 11(a), each cell in the graph on the left-hand side is sent to its corresponding cell in the CC on the right-hand side. Similarly, in Figure 11(b), each cell in the cell complex on the left is sent to its corresponding cell in the CC on the right. It is easy to verify that each of these two maps is a CC-embedding.*

Example 4.4 (A CC-homomorphism). *We present an example of a CC-homomorphism that is not a CC-embedding. Consider the sets $S_1 = \{1, 2, 3, 4\}$ and $S_2 = \{a, b, c\}$. Let $\mathcal{X}_1$ denote the CC on S_1 consisting of one 3-cell $\{1, 2, 3, 4\}$, one 2-cell $\{1, 2, 3\}$, and four 0-cells corresponding to the elements of S_1. Likewise, let $\mathcal{X}_2$ denote the CC on S_2 consisting of one 3-cell $\{a, b, c\}$, one 2-cell $\{a, b\}$, and three 0-cells corresponding to the elements of S_2. CCs $\mathcal{X}_1$ and $\mathcal{X}_2$ are visualized in Figure 11(c). Consider the function $f \colon S_1 \to S_2$ defined as $f(1) = f(2) = a$, $f(3) = b$ and $f(4) = c$. It is easy to verify that f induces a CC-homomorphism from $\mathcal{X}_1$ to $\mathcal{X}_2$.*

(a)   (b)   (c)
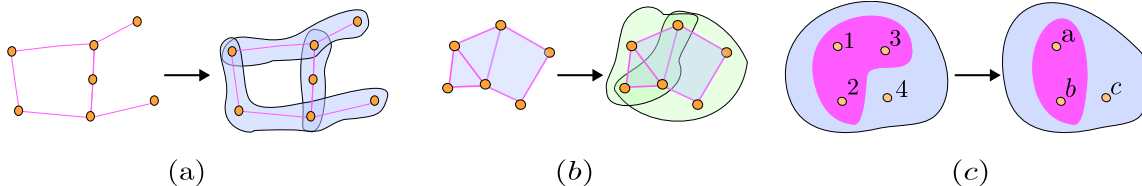
Figure 11: Examples of CC-homomorphisms. Pink, blue, and green colors represent cells of rank one, two, and three, respectively. (a): An embedding of a 1-dimensional CC into a 2-dimensional CC. (b): An embedding of a 2-dimensional CC into a 3-dimensional CC. (c) An example of a CC-homomorphism, as defined in Example 4.4. The CC $\mathcal{X}_1$ is on the left, $\mathcal{X}_2$ is on the right, and the homomorphism f is represented by the black arrow. Intuitively, the CC-homomorphism f can be viewed as a combinatorial analogue to a continuous function between $S_1 = \{1, 2, 3, 4\}$ and $S_2 = \{a, b, c\}$ that 'collapses' the cell $\{1, 2, 3\}$ to the cell $\{a, b\}$, and the cell $\{1, 2, 3, 4\}$ to the cell $\{a, b, c\}$. Observe that CC-homomorphisms generalize simplicial maps [210] from this perspective.

Definition 11 (Sub-CC). *Let $(S, \mathcal{X}, \mathrm{rk})$ be a CC. A **sub-combinatorial complex (sub-CC)** of a CC $(S, \mathcal{X}, \mathrm{rk})$ is a CC $(A, \mathcal{Y}, \mathrm{rk}')$ such that $A \subseteq S$, $\mathcal{Y} \subseteq \mathcal{X}$ and $\mathrm{rk}' = \mathrm{rk}\,|_{\mathcal{Y}}$ is the restriction of rk on $\mathcal{Y}$.*

For brevity, we refer to the sub-CC $(A, \mathcal{Y}, \mathrm{rk}')$ as $\mathcal{Y}$. Any subset of $A \subseteq S$ can be used to induce a sub-CC as follows. Consider the set $\mathcal{X}_A = \{x \in \mathcal{X} \mid x \subseteq A\}$ together with the restriction $\mathrm{rk}\,|_{\mathcal{X}_A}$. It is easy to see that the triple $(A, \mathcal{X}_A, \mathrm{rk}\,|_{\mathcal{X}_A})$ constitutes a CC, which we call the *sub-CC of $\mathcal{X}$ induced by A*. Note that any cell in the set $\mathcal{X}$ induces a sub-CC obtained by considering all the cells that are contained in it. Finally, for any k, it is easy to see that the skeleton $\mathcal{X}^k$ of a CC $\mathcal{X}$ is a sub-CC.

Example 4.5 (Sub-CC). *Recall the CC $\mathcal{X} = \{\{s_0\}, \{s_1\}, \{s_2\}, \{s_0, s_1\}, \{s_0, s_1, s_2\}\}$ displayed in Figure 10(a). The set $A = \{s_0, s_1\}$ induces the sub-CC $\mathcal{X}_A = \{\{s_0\}, \{s_1\}, \{s_0, s_1\}\}$ of $\mathcal{X}$.*

4.3   Motivation for CCs

Definition 9 for CCs aims to fulfill all motivational aspects of higher-order modeling, as outlined in Section 2. To further motivate Definition 9, we consider the pooling operations on CCs along with several structural advantages of CCs.

4.3.1   Pooling operations on CCs

We first consider the general characteristics of pooling on graphs, and then demonstrate how graph-based pooling can be realized in a unified manner via CCs. A general pooling function on a graph $\mathcal{G}$ is a function $\mathcal{POOL} \colon \mathcal{G} \to \mathcal{G}'$, where $\mathcal{G}'$ is a pooled graph that represents a coarsened version of $\mathcal{G}$. A vertex of $\mathcal{G}'$ corresponds to a cluster of vertices (a super-vertex) in the original graph $\mathcal{G}$, while edges in $\mathcal{G}'$ indicate the presence or absence of a connection among such clusters. See Figure 12 for an example.

The formalism proposed via CCs encompasses graph-based pooling as a special case. Specifically, the super-vertices (cluster of vertices in $\mathcal{G}$) defined by the vertices in $\mathcal{G}'$ can be realized as higher-order ranked cells in a CC obtained by augmenting $\mathcal{G}$ with the cells representing these super-vertices. The hierarchical structure consisting of the original graph $\mathcal{G}$ as well as augmented higher-order cells induces a CC. This realization of graph-based pooling in terms of CC-based higher-ranked cells is hierarchical because the new cells can be grouped together in a recursive manner to obtain a coarser version of the underlying space. Given such a notion of higher-order pooling operations on CCs, we demonstrate how to express graph/mesh pooling and image-based pooling in Sections 7.2.1 and 7.2.2, respectively. From this perspective, CCs provide a general framework for defining pooling operations on higher-order networks, which include graphs and images as special cases.
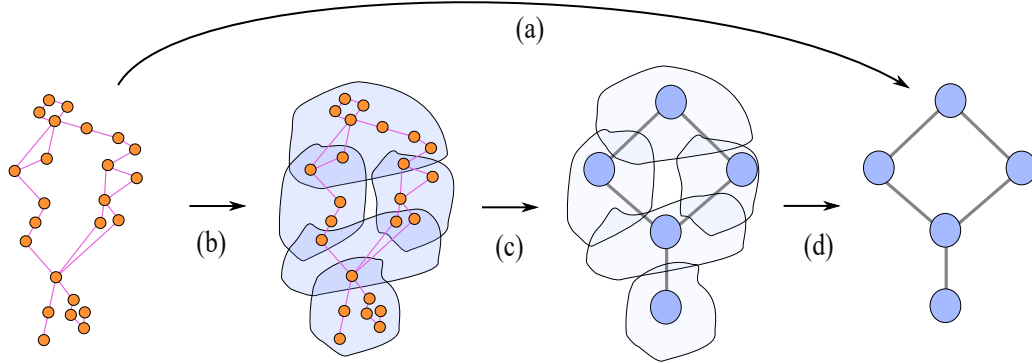
Figure 12: Graph-based pooling formulated via CCs. (a): Pooling on graphs is expressed here in terms of a pooling function that maps a graph along with the data defined on it to a coarser version of the graph. The super-vertices in the pooled graph on the right correspond to a clustering of vertices in the original graph on the left, whereas edges in the graph on the right indicate the presence or absence of a connection among these clusters. (b-d): The super-vertices in the pooled graph on the right can be realized as augmented higher-order cells (blue cells) in a CC obtained from the original graph. The edges in the pooled graph on the right can be realized in terms of an incidence matrix of the CC between the vertices and the higher-order augmented cells.

In addition, two main features of CCs are exploited via higher-order pooling operations. First, the ability of CCs to model set-type cells provides flexibility in the shape of the clusters that define the pooling operation. This flexibility is needed to realize novel user-defined pooling operations, in which the shape of the clusters might be task-specific. Second, higher-order ranked cells in a CC correspond to a coarser version of the underlying space. The type of higher-order pooling proposed here enables the construction of coarser representations. See Figure 12 for an example. Note that less general structures, such as hypergraphs and cell complexes, do not accommodate simultaneous flexibility in cluster shaping and generation of coarser representations of the underlying space.

4.3.2   Structural advantages of CCs

In addition to the realization of graph-based pooling, CCs offer several structural advantages. Specifically, CCs unify numerous commonly used higher-order networks, enable fine-grained analysis of topological properties, facilitate message passing of topological features in deep learning, and accommodate flexible modeling of relations among relations.

Flexible higher-order structure and fine-grained message passing. Message-passing graph models pass messages between vertices in a graph to learn the representations of the graph, with messages computed based on the vertex and edge features. These messages update the vertex and edge features, and gather information from the graph's local neighborhood. The rank functions of CCs render CCs more versatile than other higher-order networks and than graphs in two fronts. First, rank functions make CCs more flexible in terms of higher-order structure representation. Second, in the context of deep learning, rank functions equip CCs with more fine-grained message-passing capabilities. For instance, each hyperedge in a hypergraph is treated as a set without any notion of a rank, and consequently all hyperedges are treated uniformly without any distinction. Further details are provided in Section 5.

Flexible modeling of relations among relations. In the process of populating a topological domain with topological data, constructing meaningful relations can be challenging due to the inherent lack of data that can be naturally supported on all cells in the domain. This is particularly true when working with simplicial or cell complexes. For instance, any relation between k entities of a simplicial complex must be built from the relations of all corresponding subsets of $k-1$ entities. Real-world data may contain a subset of these relations, and not all of them. While cell complexes offer more flexibility in modeling relations, the boundary conditions that cell complexes must satisfy constraints the types of permissible relations. In order
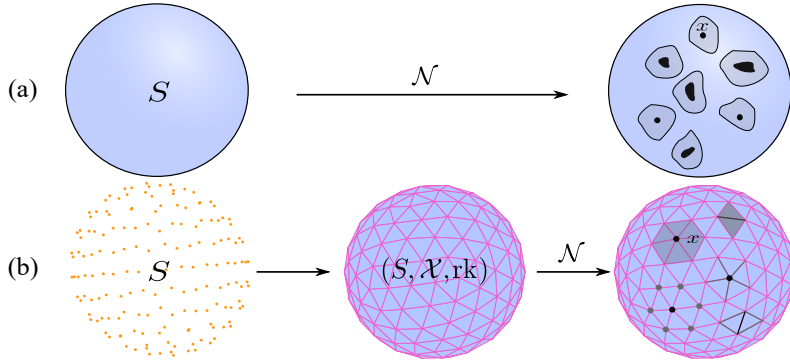
Figure 13: A visual comparison between neighborhood functions with continuous domains and CC-neighborhood functions, adhering to Definitions 1 and 12, respectively. (a): A neighborhood function with a continuous domain S assigns to $x \in S$ a set $\mathcal{N}(x)$ of subsets of S that are in the local vicinity of x. (b): Similarly, a CC-neighborhood function on a CC $(S, \mathcal{X}, \mathrm{rk})$ assigns to $x \in S$ a set $\mathcal{N}(x)$ of subsets of $\mathcal{X}$ that are in the local vicinity of x.

to remove all restrictions among relations, hypergraphs come to aid as they allow arbitrary set-type relations. However, hypergraphs do not offer hierarchical features, which can be disadvantageous in applications that require considering local and global features simultaneously.

4.4   Neighborhood functions on CCs

We introduce the notion of a CC-neighborhood function on a CC as a mechanism of exploiting the topological information stored in the CC. In practice, crafting a neighborhood function is usually a part of the learning task. For our purposes, we restrict the discussion to two types of generalized neighborhood functions, namely those specifying adjacency and incidence. From a deep learning perspective, CC-neighborhood functions set the foundations to extend the general message-passing schemes of deep learning models, thus subsuming several state-of-the-art GNNs [104, 188, 28, 209, 27, 160].

Given a CC, we aim to describe cells in the local proximity of a sub-CC of the CC. To this end, we define the CC-neighborhood function, an analogue of Definition 1 in the context of CCs.

> **Definition 12** (CC-neighborhood function)**.** *A **CC-neighborhood function** on a CC $(S, \mathcal{X}, \mathrm{rk})$ is a function $\mathcal{N}$ that assigns to every sub-CC $(A, \mathcal{Y}, \mathrm{rk}')$ of the CC a nonempty collection $\mathcal{N}(\mathcal{Y})$ of subsets of S.*

Without loss of generality, we assume that the elements of the neighborhood $\mathcal{N}(\mathcal{Y})$ are cells or sub-CCs of $\mathcal{X}$. Intuitively, the neighborhood $\mathcal{N}(\mathcal{Y})$ of the sub-CC $\mathcal{Y}$ is a set of subsets of S that are in the 'local vicinity' of $\mathcal{Y}$. The term 'local vicinity' is generally stated here, since it is typically context-specific.

Definition 12 is a discrete analogue of the well-known Definition 1. The correspondence between these two definitions is demonstrated in Figure 13. For the rest of the paper, CC-neighborhood functions are succinctly called neighborhood functions. In practice, the information encoded in CC-neighborhood functions is represented in terms of matrices as described next.

Neighborhood matrix induced by a neighborhood function.   For the purposes of computation, it is convenient to represent neighborhood functions as matrices. Incidence, adjacency, and coadjacency matrices are well-known examples of matrices that encode respective neighborhood functions. In Definition 13, we introduce a generalization of these matrices called the 'neighborhood matrix'. In this definition and henceforth, we denote the cardinality of a set S by $|S|$.

Definition 13 (Neighborhood matrix)**.** *Let $\mathcal{N}$ be a neighborhood function defined on a CC $\mathcal{X}$. Moreover, let $\mathcal{Y} = \{y_1, \ldots, y_n\}$ and $\mathcal{Z} = \{z_1, \ldots, z_m\}$ be two collections of cells in $\mathcal{X}$ such that $\mathcal{N}(y_i) \subseteq \mathcal{Z}$ for all $1 \le i \le n$. The **neighborhood matrix of $\mathcal{N}$ with respect to $\mathcal{Y}$ and $\mathcal{Z}$** is the $|\mathcal{Z}| \times |\mathcal{Y}|$ binary matrix G whose (i,j)-th entry $[G]_{ij}$ has value 1 if $z_i \in \mathcal{N}(y_j)$ and 0 otherwise.*

Remark 4.6. *In Definition 13, $\mathcal{N}(y_j)$ is stored in the j-th column of the associated neighborhood matrix G. For this reason, we denote by $\mathcal{N}_G(j)$ the neighborhood function of the cell y_j when we work with the neighborhood matrix G.*

There are many ways to define useful neighborhood functions on a CC. In this work, we constrain ourselves to the most immediate neighborhood functions: the incidence and adjacency neighborhood functions.

4.4.1   Incidence in a CC

We define three notions of incidence to capture different facets of incidence structures of cells in a CC. First, in Definition 14, we introduce the down-incidence and up-incidence neighborhood functions to describe the incidence structure of a cell via cells of arbitrary rank. Second, in Definition 15, we introduce the k-down and k-up incidence neighborhood functions to describe the incidence structure of a cell via cells of a particular rank k. Third, in Definition 16, we introduce (r, k)-incidence matrices to describe the incidence structures of cells of particular ranks r and k. In what follows, we assume that the cells in the set $\mathcal{X}$ of a CC $(S, \mathcal{X}, \mathrm{rk})$ are given a fixed order.

Definition 14 (Down/up-incidence neighborhood functions)**.**   *Let $(S, \mathcal{X}, \mathrm{rk})$ be a CC. Two cells $x, y \in \mathcal{X}$ of the CC are called **incident** if either $x \subsetneq y$ or $y \subsetneq x$. In particular, the **down-incidence neighborhood function** $\mathcal{N}_{\searrow}(x)$ of a cell $x \in \mathcal{X}$ is defined to be the set $\{y \in \mathcal{X} \mid y \subsetneq x\}$, while the **up-incidence neighborhood function** $\mathcal{N}_{\nearrow}(x)$ of x is defined to be the set $\{y \in \mathcal{X} \mid x \subsetneq y\}$.*

Definition 15 provides a more granular specification of incidence than Definition 14. In particular, Definitions 15 and 14 describe the incidence structure of a cell with respect to cells of a particular rank or of arbitrary rank, respectively.

Definition 15 (k-down/up incidence neighborhood functions)**.** *Let $(S, \mathcal{X}, \mathrm{rk})$ be a CC. For any $k \in \mathbb{N}$, the k-**down incidence neighborhood function** $\mathcal{N}_{\searrow,k}(x)$ of a cell $x \in \mathcal{X}$ is defined to be the set $\{y \in \mathcal{X} \mid y \subsetneq x, \mathrm{rk}(y) = \mathrm{rk}(x) - k\}$. The k-**up incidence neighborhood function** $\mathcal{N}_{\nearrow,k}(x)$ of x is defined to be the set $\{y \in \mathcal{X} \mid y \subsetneq x, \mathrm{rk}(y) = \mathrm{rk}(x) + k\}$.*

Clearly, $\mathcal{N}_{\searrow}(x) = \bigcup_{k \in \mathbb{N}} \mathcal{N}_{\searrow,k}(x)$ and $\mathcal{N}_{\nearrow}(x) = \bigcup_{k \in \mathbb{N}} \mathcal{N}_{\nearrow,k}(x)$. Immediate incidence is particularly important. To this end, the set of *faces* of a cell $x \in \mathcal{X}$ is defined to be $\mathcal{N}_{\searrow,1}(x)$, and the set of *cofaces* of a cell x is defined to be $\mathcal{N}_{\nearrow,1}(x)$. An illustration of k-down and k-up incidence neighborhood functions is given in Figure 14.

Definition 16 (Incidence matrix)**.** *Let $(S, \mathcal{X}, \mathrm{rk})$ be a CC. For any $r, k \in \mathbb{Z}_{\ge 0}$ with $0 \le r < k \le \dim(\mathcal{X})$, the (r, k)-**incidence matrix** $B_{r,k}$ between $\mathcal{X}^r$ and $\mathcal{X}^k$ is defined to be the $|\mathcal{X}^r| \times |\mathcal{X}^k|$ binary matrix whose (i,j)-th entry $[B_{r,k}]_{ij}$ equals one if x_i^r is incident to x_j^k and zero otherwise.*

The incidence matrices $B_{r,k}$ of Definition 16 determine a neighborhood function on the underlying CC. Neighborhood functions induced by incidence matrices are utilized to construct a higher-order message passing scheme on CCs, as described in Section 5.
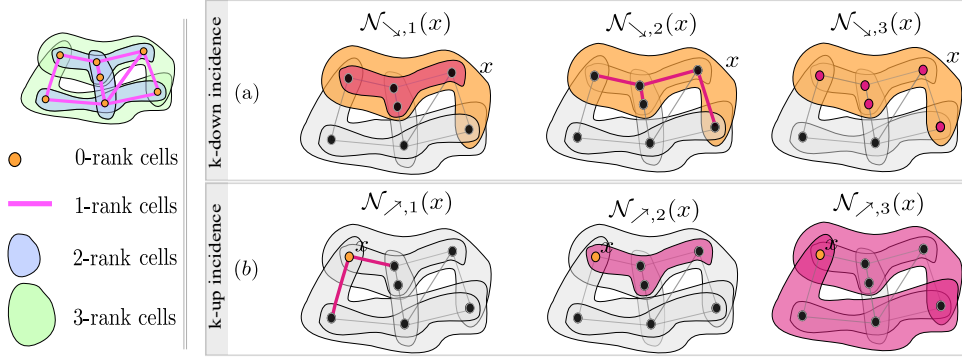
Figure 14: Illustration of k-down and k-up incidence neighborhood functions on a CC of dimension three. (a): Illustration of k-down incidence neighborhood functions. The target orange cell x has rank three. From left to right, the red cells represent $\mathcal{N}_{\searrow,1}(x)$, $\mathcal{N}_{\searrow,2}(x)$ and $\mathcal{N}_{\searrow,3}(x)$. (b): Illustration of k-up incidence neighborhood functions. The target orange cell x has rank zero. From left to right, the red cells represent $\mathcal{N}_{\nearrow,1}(x)$, $\mathcal{N}_{\nearrow,2}(x)$ and $\mathcal{N}_{\nearrow,3}(x)$.

4.4.2   Adjacency in a CC

CCs admit incidence as well as other neighborhood functions. For instance, for a CC that is reduced to a graph, a more natural neighborhood function is based on the notion of adjacency relation. Incidence defines relations among cells of different ranks, while adjacency defines relations among cells of similar ranks. Definitions 17, 18 and 19/20 introduce the (co)adjacency analogues of the respective incidence-related Definitions 14, 15, and 16.

Definition 17 ((Co)adjacency neighborhood functions). *Let $(S, \mathcal{X}, \mathrm{rk})$ be a CC. The **adjacency neighborhood function** $\mathcal{N}_a(x)$ of a cell $x \in \mathcal{X}$ is defined to be the set*

$$\{y \in \mathcal{X} \mid \mathrm{rk}(y) = \mathrm{rk}(x), \exists z \in \mathcal{X} \text{ with } \mathrm{rk}(z) > \mathrm{rk}(x) \text{ such that } x, y \subsetneq z\}.$$

*The **coadjacency neighborhood function** $\mathcal{N}_{co}(x)$ of x is defined to be the set*

$$\{y \in \mathcal{X} \mid \mathrm{rk}(y) = \mathrm{rk}(x), \exists z \in \mathcal{X} \text{ with } \mathrm{rk}(z) < \mathrm{rk}(x) \text{ such that } z \subsetneq y \text{ and } z \subsetneq x\}.$$

*A cell z satisfying the conditions of either $\mathcal{N}_a(x)$ or $\mathcal{N}_{co}(x)$ is called a **bridge cell**.*

Definition 18 (k-(co)adjacency neighborhood functions). *Let $(S, \mathcal{X}, \mathrm{rk})$ be a CC. For any $k \in \mathbb{N}$, The k-**adjacency neighborhood function** $\mathcal{N}_{a,k}(x)$ of a cell $x \in \mathcal{X}$ is defined to be the set*

$$\{y \in \mathcal{X} \mid \mathrm{rk}(y) = \mathrm{rk}(x), \exists z \in \mathcal{X} \text{ with } \mathrm{rk}(z) = \mathrm{rk}(x) + k \text{ such that } x, y \subsetneq z\}.$$

*The k-**coadjacency neighborhood function** $\mathcal{N}_{co,k}(x)$ of x is defined to be the set*

$$\{y \in \mathcal{X} \mid \mathrm{rk}(y) = \mathrm{rk}(x), \exists z \in \mathcal{X} \text{ with } \mathrm{rk}(z) = \mathrm{rk}(x) - k \text{ such that } z \subsetneq y \text{ and } z \subsetneq x\}.$$

Definition 19 (Adjacency matrix). *For any $r \in \mathbb{Z}_{\geq 0}$ and $k \in \mathbb{Z}_{>0}$ with $0 \leq r < r + k \leq \dim(\mathcal{X})$, the (r, k)-**adjacency matrix** $A_{r,k}$ among the cells of $\mathcal{X}^r$ with respect to the cells of $\mathcal{X}^k$ is defined to be the $|\mathcal{X}^r| \times |\mathcal{X}^r|$ binary matrix whose (i, j)-th entry $[A_{r,k}]_{ij}$ equals one if x_i^r is k-adjacent to x_j^r and zero otherwise.*

Definition 20 (Coadjacency matrix). *For any $r \in \mathbb{Z}_{\geq 0}$ and $k \in \mathbb{N}$ with $0 \leq r - k < r \leq \dim(\mathcal{X})$, the (r, k)-**coadjacency matrix** $coA_{r,k}$ among the cells of $\mathcal{X}^r$ with respect to the cells of $\mathcal{X}^k$ is defined to be the $|\mathcal{X}^r| \times |\mathcal{X}^r|$ binary matrix whose (i, j)-th entry $[coA_{r,k}]_{ij}$ has value 1 if x_i^r is k-coadjacent to x_j^r and 0 otherwise.*

Clearly, $\mathcal{N}_a(x) = \cup_{k \in \mathbb{N}} \mathcal{N}_{a,k}(x)$ and $\mathcal{N}_{co}(x) = \cup_{k \in \mathbb{N}} \mathcal{N}_{co,k}(x)$. An illustration of k-adjacency and k-coadjacency neighborhood functions is given in Figure 15.

4.5   Data on CCs: cochain spaces and maps

As we are interested in processing the data defined over a CC $(S, \mathcal{X}, \mathrm{rk})$, we introduce k-cochain spaces, k-cochains and cochain maps.

Definition 21 (k-cochain spaces). *Let $\mathcal{C}^k(\mathcal{X}, \mathbb{R}^d)$ be the $\mathbb{R}$-vector space of functions $\mathbf{H}_k \colon \mathcal{X}^k \to \mathbb{R}^d$ for a rank $k \in \mathbb{Z}_{\geq 0}$ and dimension d. d is called the **data dimension**. $\mathcal{C}^k(\mathcal{X}, \mathbb{R}^d)$ is called the k-**cochain space**. Elements $\mathbf{H}_k$ in $\mathcal{C}^k(\mathcal{X}, \mathbb{R}^d)$ are called k-**cochains** or k-**signals**.*

We use the notation $\mathcal{C}^k(\mathcal{X})$ or $\mathcal{C}^k$ when the underlying CC is clear. Moreover, we say that a k-cochain space $\mathcal{C}^k(\mathcal{X})$ is defined on $\mathcal{X}$. Intuitively, a k-cochain can be interpreted as a signal defined on the k-cells of $\mathcal{X}$ [124]. Figure 16(a) shows an example of a cochain supported on 0, 1, and 2-rank cells of a simplicial complex.

When $\mathcal{X}$ is a graph, 0-cochains correspond to graph signals [216]. Ordering the cells in $\mathcal{X}^k$, we canonically identify $\mathcal{C}^k(\mathcal{X}, \mathbb{R}^d)$ with the Euclidean vector space $\mathbb{R}^{|\mathcal{X}^k| \times d}$ and explicitly write $\mathbf{H}_k$ as the vector $[\mathbf{h}_{x_1^k}, \dots, \mathbf{h}_{x_{|\mathcal{X}^k|}^k}]$, where $\mathbf{h}_{x_j^k} \in \mathbb{R}^d$ is a feature vector associated with the cell x_j^k. The notation $\mathbf{H}_{k,j}$ refers to the feature vector $\mathbf{h}_{x_j^k}$ to avoid explicit reference to cell x_j^k. We also work with maps between cochain spaces, which we call cochain maps.

Definition 22 (Cochain maps). *For $r < k$, an incidence matrix $B_{r,k}$ induces a map*

$$B_{r,k} \colon \mathcal{C}^k(\mathcal{X}) \to \mathcal{C}^r(\mathcal{X}),$$
$$\mathbf{H}_k \to B_{r,k}(\mathbf{H}_k),$$

where $B_{r,k}(\mathbf{H}_k)$ denotes the usual product $B_{r,k}\mathbf{H}_k$ of matrix $B_{r,k}$ with vector $\mathbf{H}_k$. Similarly, an (r, k)-adjacency matrix $A_{r,k}$ induces a map

$$A_{r,k} \colon \mathcal{C}^r(\mathcal{X}) \to \mathcal{C}^r(\mathcal{X}),$$
$$\mathbf{H}_r \to A_{r,k}(\mathbf{H}_r).$$

These two types of maps between cochain spaces are called **cochain maps**.

Cochain maps serve as operators that 'shuffle' and 'redistribute' the data on the underlying CC. In the context of TDL, cochain maps are the main tools for defining higher-order message passing (Section 6.1) as well as (un)pooling operations (Section 7.1). Each adjacency matrix $A_{r,k}$ or coadjacency matrix $coA_{r,k}$ defines a cochain map between cochain spaces of equal dimension, while each incidence matrix $B_{r,k}$ defines a cochain map between different dimensions. Figure 16(b) shows examples of cochain maps on a CC of dimension 4.

5   Combinatorial complex neural networks (CCNNs)

The modelling flexibility of CCs enables the exploration and analysis of a wide spectrum of CC-based neural network architectures. A CC-based neural network can exploit all neighborhood matrices or a subset of them, thus accounting for multi-way interactions among various cells in the CC to solve a learning task. In this
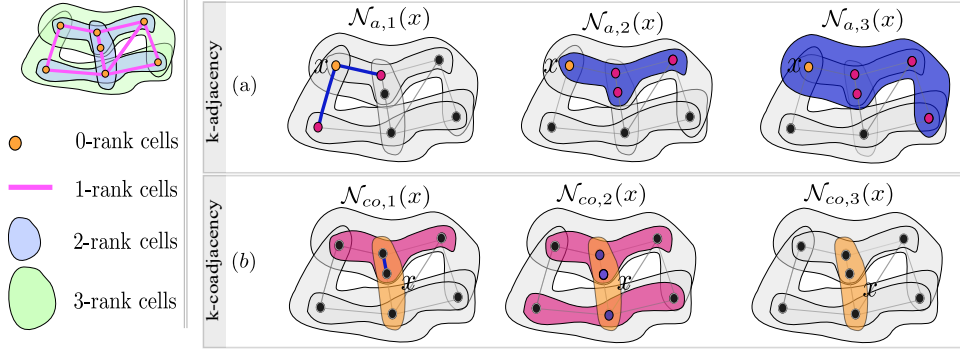
Figure 15: Illustration of k-(co)adjacency neighborhood functions on a CC of dimension three. (a): Illustration of k-adjacency neighborhood functions. The target orange cell x has rank zero. From left to right, the red cells represent $\mathcal{N}_{a,1}(x)$, $\mathcal{N}_{a,2}(x)$ and $\mathcal{N}_{a,3}(x)$. (b): Illustration of k-coadjacency neighborhood functions. The target orange cell x has rank two. From left to right, the red cells represent $\mathcal{N}_{co,1}(x)$, $\mathcal{N}_{co,2}(x)$ and $\mathcal{N}_{co,3}(x)$.
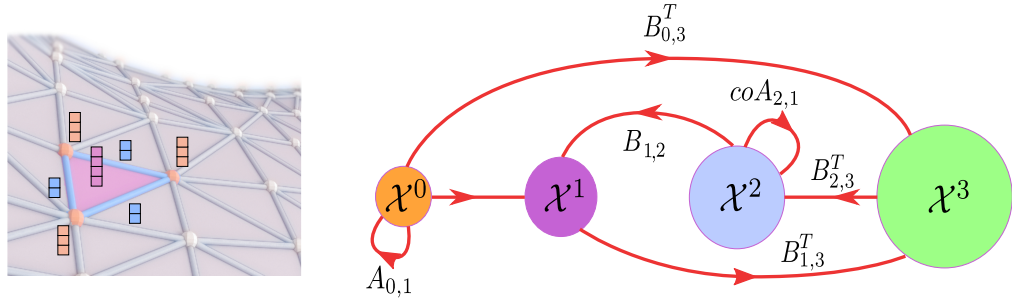
Figure 16: Examples of k-cochains (left) and cochain maps (right) supported on a CC of dimension four. Left: a k-cochain can be interpreted as a signal or a feature vector defined on the k-cells. In the figure, a 3-dimensional cochain is attached to the vertices, 2-dimensional cochains are attached to the 1-cells, and 4-dimensional cochains to the 2-cells. Right: each of $coA_{r,k}$ and $A_{r,k}$ defines a cochain map between cochain spaces of equal dimension, whereas each $B_{r,k}$ defines a cochain map between cochain spaces of different dimensions.

section, we introduce the blueprint for TDL by developing the general principles of CC-based TDL models. We utilize our TDL blueprint framework for examining current approaches and offer directives for designing novel models.

The learning tasks in TDL can be broadly classified into three categories: cell classification, complex classification, and cell prediction. Our numerical experiments in Section 9 provide examples on cell and complex classification. In more detail, the learning tasks of the three categories are the following:

- *Cell classification*: the goal is to predict targets for each cell in a complex. To accomplish this, we can utilize a TDL classifier that takes into account the topological neighbors of the target cell and their associated features. An example of cell classification is triangular mesh segmentation, in which the task is to predict the class of each face or edge in a given mesh.

- *Complex classification*: the aim is to predict targets for an entire complex. To achieve this, we can reduce the topology of the complex into a common representation using higher-order cells, such as pooling, and then learn a TDL classifier over the resulting flat vector. An example of complex classification is class prediction for each input mesh.

- *Cell prediction*: the objective is to predict properties of cell-cell interactions in a complex, and, in some cases, to predict whether a cell exists in the complex. This can be achieved by utilizing the
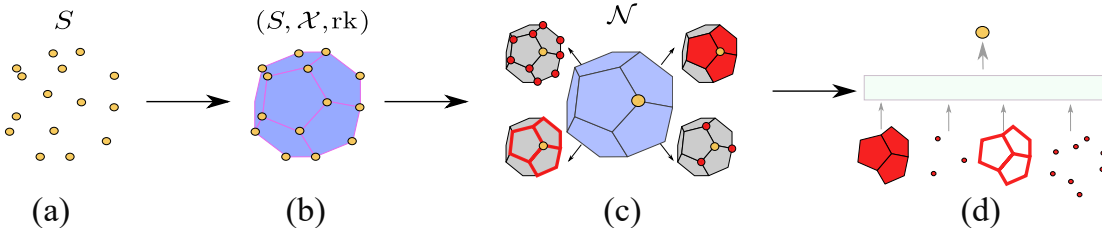
Figure 17: A TDL blueprint. (a): A set of abstract entities. (b): A CC $(S, \mathcal{X}, \mathrm{rk})$ is defined on S. (c): For an element $x \in \mathcal{X}$, we select a collection of neighborhood functions defined on the CC. (d): We build a neural network on the CC using the neighborhood functions selected in (c). The neural network exploits the neighborhood functions selected in (c) to update the data supported on x.

topology and associated features of the cells. A relevant example is the prediction of linkages among entities in hyperedges of a hypergraph.

Figure 17 outlines our general setup for TDL. Initially, a higher-order domain, represented by a CC, is constructed on a set S. A set of neighborhood functions defined on the domain is then selected. The neighborhood functions are usually selected based on the learning problem at hand and they are used to build a topological neural network. To develop our general TDL framework, we introduce *combinatorial complex neural networks (CCNNs)*, an abstract class of neural networks supported on CCs that effectively captures the pipeline of Figure 17. CCNNs can be thought of as a *template* that generalizes many popular architectures, such as convolutional and attention-based neural networks. The abstraction of CCNNs offers many advantages. First, any result that holds for CCNNs is immediately applicable to any particular instance of CCNN architecture. Indeed, the theoretical analysis and results in this paper are applicable to any CC-based neural network as long as it satisfies the CCNN definition. Second, working with a particular parametrization might be cumbersome if the neural network has a complicated architecture. In Section 5.1, we elaborate on the intricate architectures of parameterized TDL models. The more abstract high-level representation of CCNNs simplifies the notation and the general purpose of the learning process, thereby making TDL modelling more intuitive to handle.

Definition 23 (CCNN). *Let $\mathcal{X}$ be a CC. Let $\mathcal{C}^{i_1} \times \mathcal{C}^{i_2} \times \ldots \times \mathcal{C}^{i_m}$ and $\mathcal{C}^{j_1} \times \mathcal{C}^{j_2} \times \ldots \times \mathcal{C}^{j_n}$ be a Cartesian product of m and n cochain spaces defined on $\mathcal{X}$. A **combinatorial complex neural network (CCNN)** is a function of the form*

$$\mathrm{CCNN} : \mathcal{C}^{i_1} \times \mathcal{C}^{i_2} \times \ldots \times \mathcal{C}^{i_m} \longrightarrow \mathcal{C}^{j_1} \times \mathcal{C}^{j_2} \times \ldots \times \mathcal{C}^{j_n}.$$

Intuitively, a CCNN takes a vector of cochains $(\mathbf{H}_{i_1}, \ldots, \mathbf{H}_{i_m})$ as input and returns a vector of cochains $(\mathbf{K}_{j_1}, \ldots, \mathbf{K}_{j_n})$ as output. In Section 5.1, we show how neighborhood functions play a central role in the construction of a general CCNN. Definition 23 does not show how a CCNN can be computed in general. Sections 6 and 7 formalize the computational workflow in CCNNs.

5.1 Building CCNNs: tensor diagrams

Unlike graphs that involve vertex or edge signals, higher-order networks entail a higher number of signals (see Figure 16). Thus, constructing a CCNN requires building a non-trivial amount of interacting sub-networks. Due to the relatively large number of cochains in a CCNN, we introduce *tensor diagrams*, a diagrammatic notation for higher-order networks.

Remark 5.1. *Diagrammatic notation is common in the geometric topology literature [138, 269], and it is typically used to construct functions built from simpler building blocks. See Appendix C for further discussion. See also [235] for related constructions on simplicial neural networks.*
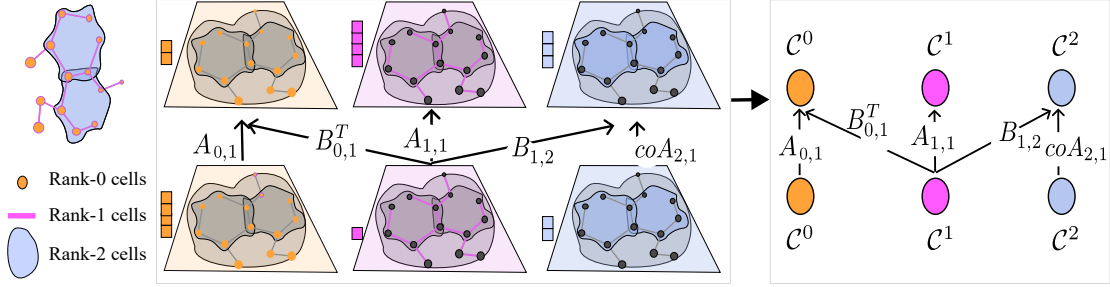
Figure 18: A tensor diagram is a diagrammatic representation of a CCNN that captures the flow of signals on the CCNN.
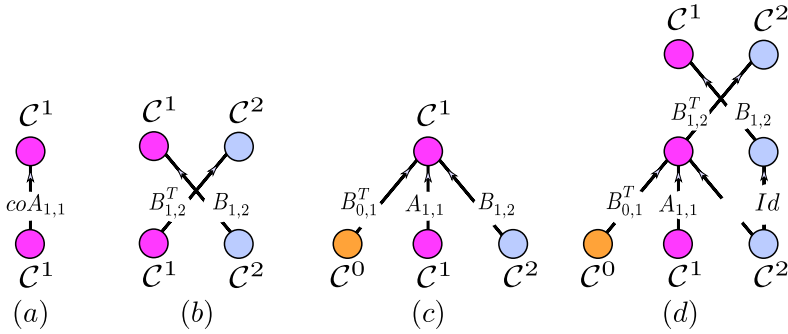

Figure 19: Examples of tensor diagrams. (a): Tensor diagram of a $\mathrm{CCNN}_{coA_{1,1}}\colon \mathcal{C}^1 \to \mathcal{C}^1$. (b): Tensor diagram of a $\mathrm{CCNN}_{\{B_{1,2}, B_{1,2}^T\}}\colon \mathcal{C}^1 \times \mathcal{C}^2 \to \mathcal{C}^1 \times \mathcal{C}^2$. (c): A merge node that merges three cochains. (d): A tensor diagram generated by vertical concatenation of the tensor diagrams in (c) and (b). The edge label *Id* denotes the identity matrix.

> **Definition 24** (Tensor diagram). *A **tensor diagram** represents a CCNN via a directed graph. The signal on a tensor diagram flows from the **source nodes** to the **target nodes**. The source and target nodes correspond to the domain and codomain of the CCNN.*

Figure 18 depicts an example of a tensor diagram. On the left, a CC of dimension three is shown. Consider a 0-cochain $\mathcal{C}^0$, a 1-cochain $\mathcal{C}^1$ and a 2-cochain $\mathcal{C}^2$. The middle figure displays a CCNN that maps a cochain vector in $\mathcal{C}^0 \times \mathcal{C}^1 \times \mathcal{C}^2$ to a cochain vector in $\mathcal{C}^0 \times \mathcal{C}^1 \times \mathcal{C}^2$. On the right, a tensor diagram representation of the CCNN is shown. We label each edge on the tensor diagram by a cochain map or by its matrix representation. The edge labels on the tensor diagram of Figure 18 are $A_{0,1}, B_{0,1}^T, A_{1,1}, B_{1,2}$ and $coA_{2,1}$. Thus, the tensor diagram specifies the flow of cochains on the CC.

The labels on the arrows of a tensor diagram form a sequence $\mathbf{G} = (G_i)_{i=1}^l$ of cochain maps defined on the underlying CC. In Figure 18 for example, $\mathbf{G} = (G_i)_{i=1}^5 = (A_{0,1}, B_{0,1}^T, A_{1,1}, B_{1,2}, coA_{2,1})$. When a tensor diagram is used to represent a CCNN, we use the notation $\mathrm{CCNN}_{\mathbf{G}}$ for the tensor diagram and for its corresponding CCNN. The cochain maps $(G_i)_{i=1}^l$ reflect the structure of the CC and are used to determine the flow of signals on the CC. Any of the neighborhood matrices mentioned in Section 4.4 can be used as cochain maps. The choice of cochain maps depends on the learning task.

Figure 19 visualizes additional examples of tensor diagrams. The *height* of a tensor diagram is the number of edges on a longest path from a source node to a target node. For instance, the heights of the tensor diagrams in Figures 19(a) and 19(d) are one and two, respectively. The vertical concatenation of two tensor diagrams represents the composition of their corresponding CCNNs. For example, the tensor diagram in Figure 19(d) is the vertical concatenation of the tensor diagrams in Figures 19(c) and (b).

If a node in a tensor diagram receives one or more signals, we call it a *merge node*. Mathematically, a merge node is a function $\mathcal{M}_{G_1,\ldots,G_m}\colon \mathcal{C}^{i_1} \times \mathcal{C}^{i_2} \times \ldots \times \mathcal{C}^{i_m} \to \mathcal{C}^j$ given by

$$(\mathbf{H}_{i_1}, \ldots, \mathbf{H}_{i_m}) \xrightarrow{\mathcal{M}} \mathbf{K}_j = \mathcal{M}_{G_1,\ldots,G_m}(\mathbf{H}_{i_1}, \ldots, \mathbf{H}_{i_m}), \tag{1}$$

where $G_k\colon C^{i_k}(\mathcal{X}) \to C^j(\mathcal{X}), k = 1,\ldots,m$, are cochain maps. We think of $\mathcal{M}$ as a message-passing function that takes into account the messages outputted by maps $G_1, \ldots, G_m$, which collectively act on a cochain vector $(\mathbf{H}_{i_1}, \ldots, \mathbf{H}_{i_m})$, to obtain an updated cochain $\mathbf{K}_j$. See Sections 5.2 and 6.2 for more details. Figure 19(c) shows a merge node example.

5.2 Push-forward operator and merge node

We introduce the push-forward operation, a computational scheme that enables sending a cochain supported on i-cells to j-cells. The push-forward operation is a computational building block used to formalize the definition of the merge nodes given in Equation 1, the higher-order message passing introduced in Section 6, and the (un)pooling operations introduced in Section 7.

Definition 25 (Cochain push-forward). *Consider a CC $\mathcal{X}$, a cochain map $G\colon \mathcal{C}^i(\mathcal{X}) \to \mathcal{C}^j(\mathcal{X})$, and a cochain $\mathbf{H}_i$ in $\mathcal{C}^i(\mathcal{X})$. A **(cochain) push-forward** induced by G is an operator $\mathcal{F}_G\colon \mathcal{C}^i(\mathcal{X}) \to \mathcal{C}^j(\mathcal{X})$ defined via*

$$\mathbf{H}_i \to \mathbf{K}_j = [\mathbf{k}_{y_1^j}, \ldots, \mathbf{k}_{y_{|\mathcal{X}^j|}^j}] = \mathcal{F}_G(\mathbf{H}_i), \tag{2}$$

such that for $k = 1,\ldots,|\mathcal{X}^j|$,

$$\mathbf{k}_{y_k^j} = \bigoplus_{x_l^i \in \mathcal{N}_{G^T(y_k^j)}} \alpha_G(\mathbf{h}_{\mathbf{x^i}}), \tag{3}$$

where $\bigoplus$ is a permutation-invariant aggregation function and α_G is a differentiable function.

The operator $\mathcal{F}_G$ pushes forward an i-cochain $\mathbf{H}_i$ supported on $\mathcal{X}^i$ to a j-cochain $\mathcal{F}_G(\mathbf{H}_i)$ supported on $\mathcal{X}^j$. For every cell $y \in \mathcal{X}^j$, Equation 3 constructs the vector $\mathbf{k}_y$ by aggregating all vectors $\mathbf{h}_x$ attached to the neighbors $x \in \mathcal{X}^i$ of y with respect to the neighborhood function $\mathcal{N}_{G^T}$, and by then applying a differentiable function α_G on the set of aggregated vectors $\{\mathbf{h}_x | x \in \mathcal{N}_{G^T}(y)\}$.

Figure 20 visualizes two examples of push-forward operators. Example 5.2 provides a push-forward function induced by an indicence matrix. The push-forward function in Example 5.2 does not contain any parameters, therefore it is not trainable. In Section 5.4, we give examples of parameterized push-forward operations, whose parameters can be learnt.

Example 5.2. *Consider a CC $\mathcal{X}$ of dimension 2. Let $B_{0,2}\colon \mathcal{C}^2(\mathcal{X}) \to \mathcal{C}^0(\mathcal{X})$ be an incidence matrix. The function $\mathcal{F}_{B_{0,2}}^m\colon \mathcal{C}^2(\mathcal{X}) \to \mathcal{C}^0(\mathcal{X})$ defined by $\mathcal{F}_{B_{0,2}}^m(\mathbf{H_2}) = B_{0,2}(\mathbf{H_2})$ is a push-forward induced by $B_{0,2}$. $\mathcal{F}_{B_{0,2}}^m$ pushes forward the cochain $\mathbf{H}_2 \in \mathcal{C}^2$ to cochain $B_{0,2}(\mathbf{H}_2) \in \mathcal{C}^0$.*

In Definition 26, we formulate the notion of merge node using push-forward operators. Figure 21 visualizes Definition 26 of merge node via a tensor diagram.

Definition 26 (Merge node). *Let $\mathcal{X}$ be a CC. Moreover, let $G_1\colon \mathcal{C}^{i_1}(\mathcal{X}) \to \mathcal{C}^j(\mathcal{X})$ and $G_2\colon \mathcal{C}^{i_2}(\mathcal{X}) \to \mathcal{C}^j(\mathcal{X})$ be two cochain maps. Given a cochain vector $(\mathbf{H}_{i_1}, \mathbf{H}_{i_2}) \in \mathcal{C}^{i_1} \times \mathcal{C}^{i_2}$, a **merge node** $\mathcal{M}_{G_1,G_2}\colon \mathcal{C}^{i_1} \times \mathcal{C}^{i_2} \to \mathcal{C}^j$ is defined as*

$$\mathcal{M}_{G_1,G_2}(\mathbf{H}_{i_1}, \mathbf{H}_{i_2}) = \beta\left(\mathcal{F}_{G_1}(\mathbf{H}_{i_1}) \bigotimes \mathcal{F}_{G_2}(\mathbf{H}_{i_2})\right), \tag{4}$$

where $\bigotimes\colon \mathcal{C}^j \times \mathcal{C}^j \to \mathcal{C}^j$ is an aggregation function, $\mathcal{F}_{G_1}$ and $\mathcal{F}_{G_2}$ are push-forward operators induced by G_1 and G_2, and β is an activation function.
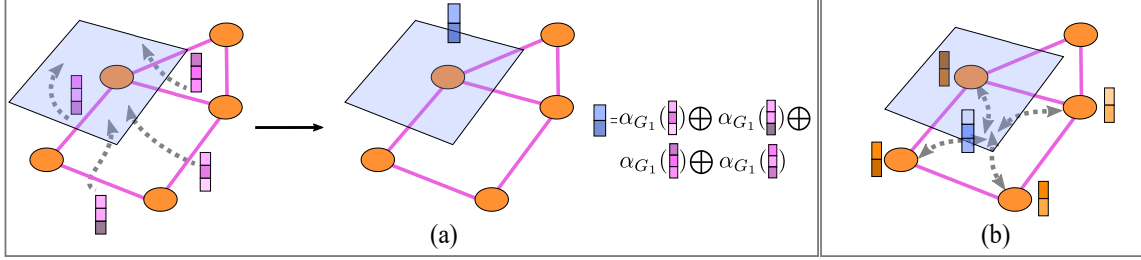

Figure 20: Examples of push-forward operators. (a): Let $G_1 \colon \mathcal{C}^1 \to \mathcal{C}^2$ be a cochain map. A push-forward $\mathcal{F}_{G_1}$ induced by G_1 takes as input a 1-cochain $\mathbf{H}_1$ defined on the edges of the underlying CC $\mathcal{X}$ and 'pushes-forward' this cochain to a 2-cochain $\mathbf{K}_2$ defined on $\mathcal{X}^2$. The cochain $\mathbf{K}_2$ is formed by aggregating the information in $\mathbf{H}_1$ using the neighborhood function $\mathcal{N}_{G_1^T}$. In this case, the neighbors of the 2-rank (blue) cell with respect to G_1 are the four (pink) edges on the boundary of this cell. (b): Similarly, $G_2 \colon \mathcal{C}^0 \to \mathcal{C}^2$ induces a push-forward map $\mathcal{F}_{G_2} \colon \mathcal{C}^0 \to \mathcal{C}^2$ that sends a 0-cochain $\mathbf{H}_0$ to a 2-cochain $\mathbf{K}_2$. The cochain $\mathbf{K}_2$ is defined by aggregating the information in $\mathbf{H}_0$ using the neighborhood function $\mathcal{N}_{G_2^T}$.
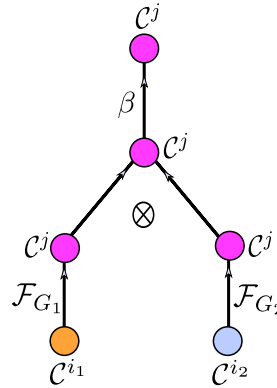
Figure 21: A tensor diagram depicting Definition 26 of merge node.

5.3   Three tensor operations for the construction of CCNNs

Any tensor diagram representation of a CCNN can be built from two elementary operations: the push-forward operator and the merge node. In practice, it is convenient to introduce other operations that facilitate building involved neural network architectures more effectively. For example, one useful operation is the dual operation of the merge node, which we call the split node.

Definition 27 (Split node)**.** *Let $\mathcal{X}$ be a CC. Moreover, let $G_1 \colon \mathcal{C}^j(\mathcal{X}) \to \mathcal{C}^{i_1}(\mathcal{X})$ and $G_2 \colon \mathcal{C}^j(\mathcal{X}) \to \mathcal{C}^{i_2}(\mathcal{X})$ be two cochain maps. Given a cochain $\mathbf{H}_j \in \mathcal{C}^j$, a **split node** $\mathcal{S}_{G_1,G_2} \colon \mathcal{C}^j \to \mathcal{C}^{i_1} \times \mathcal{C}^{i_2}$ is defined as*

$$\mathcal{S}_{G_1,G_2}(\mathbf{H}_j) = \left(\beta_1(\mathcal{F}_{G_1}(\mathbf{H}_j)), \beta_2(\mathcal{F}_{G_2}(\mathbf{H}_j)) \right), \tag{5}$$

where $\mathcal{F}_{G_i}$ is a push-forward operator induced by G_i, and β_i is an activation function for $i = 1, 2$.

While it is clear from Definition 27 that split nodes are simply tuples of push-forward operations, using split nodes allows us to build neural networks more effectively and intuitively. Definition 28 puts forward a set of elementary tensor operations, including split nodes, to facilitate the formulation of CCNNs in terms of tensor diagrams.
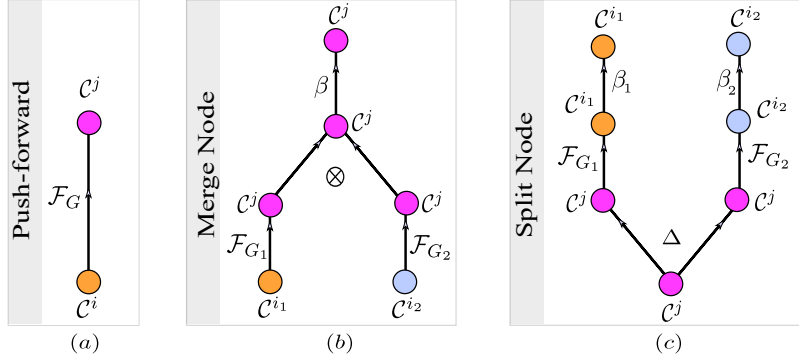
Figure 22: Tensor diagrams of the elementary tensor operations, namely of push-forward operations, merge nodes and split nodes. These three elementary tensor operations are building blocks for constructing tensor diagrams of general CCNNs. A general tensor diagram can be formed using compositions and horizontal concatenations of the three elementary tensor operations. (a): A tensor diagram of a push-forward operation induced by a cochain map $G\colon \mathcal{C}^i \to \mathcal{C}^j$. (b): A merge node induced by two cochain maps $G_1\colon \mathcal{C}^{i_1} \to \mathcal{C}^j$ and $G_2\colon \mathcal{C}^{i_2} \to \mathcal{C}^j$. (c): A split node induced by two cochain maps $G_1\colon \mathcal{C}^j \to \mathcal{C}^{i_1}$ and $G_2\colon \mathcal{C}^j \to \mathcal{C}^{i_2}$. In this illustration, the function $\Delta\colon \mathcal{C}^j \to \mathcal{C}^j \times \mathcal{C}^j$ is defined as $\Delta(\mathbf{H}_j) = (\mathbf{H}_j, \mathbf{H}_j)$.
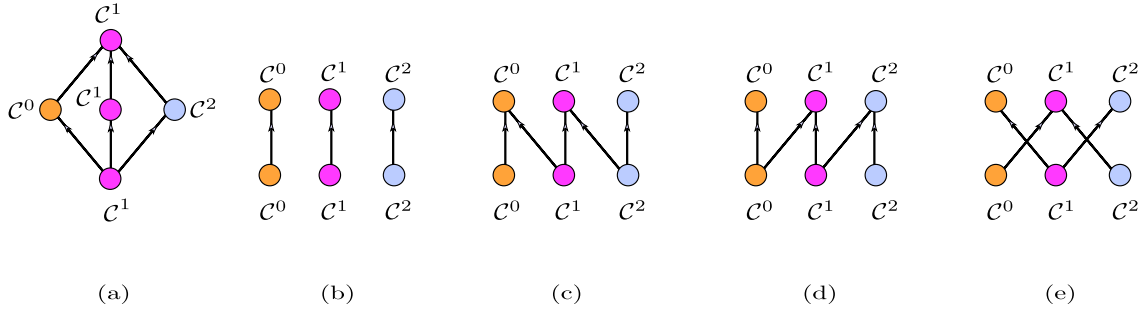
Figure 23: Examples of existing neural networks that can be realized in terms of the elementary operations given in Figure 22. Edge labels are dropped to simplify exposition. (a): The simplicial complex net (SCoNe), proposed by [235], can be realized as a composition of a split node that splits an input 1-cochain to three cochains of dimensions zero, one, and two, followed by a merge node that merges these cochains into a 1-cochain. (b): The simplicial neural network (SCN), proposed by [96], can be realized in terms of push-forward operations. (c)–(e): Examples of cell complex neural networks (CXNs); see [128]. Note that (e) can be realized in terms of a single merge node that merges the 0 and 2-cochains to a 1-cochain as well as a single split node that splits the 1-cochain to 0- and 2-cochains.

Definition 28 (Elementary tensor operations)**.** *We refer collectively to push-forward operations, merge nodes and split nodes as **elementary tensor operations**.*

Figure 22 displays tensor diagrams of elementary tensor operations, and Figure 23 exemplifies how existing topological neural networks are expressed via tensor diagrams based on elementary tensor operations. For example, the simplicial complex net (SCoNe), a Hodge decomposition-based neural network proposed by [235], can be effectively realized in terms of split and merge nodes, as shown in Figure 23(a).

Remark 5.3. *The elementary tensor operations constitute the only framework needed to define any parameterized topological neural network. Indeed, since tensor diagrams can be built via the three elementary tensor operations, then it suffices to define the push-forward and the merge operators in order to fully define a parameterized class of CCNNs (recall that the split node is completely determined by the push-forward*

operator). In Sections 5.4 and 5.5, we build two parameterized classes of CCNNs: the convolutional and attention classes. In both cases, we only define their corresponding parameterized elementary tensor operations. Beyond convolutional and attention versions of CCNNs, the three elementary tensor operations allow us to build arbitrary parameterized tensor diagrams, therefore providing scope to discover novel topological neural network architectures on which our theory remains applicable.

An alternative way of constructing CCNNs draws ideas from topological quantum field theory (TQFT). In Appendix C, we briefly discuss this relationship in more depth.

5.4   Combinatorial complex convolutional networks (CCCNNs)

One of the fundamental computational requirements for deep learning on higher-order domains is the ability to define and compute convolutional operations. Here, we introduce CCNNs equipped with convolutional operators, which we call *combinatorial complex convolutional neural networks (CCCNNs)*. In particular, we put forward two convolutional operators for CCCNNs: CC-convolutional push-forward operators and CC-convolutional merge nodes.

We demonstrate how CCCNNs can be introduced from the two basic blocks: the push-forward and the merge operations which have been defined abstractly in Section 5.2. In its simplest form, a CC-convolutional push-forward, as conceived in Definition 29, is a generalization of the convolutional graph neural network introduced in [160].

Definition 29 (CC-convolutional push-forward). *Consider a CC $\mathcal{X}$, a cochain map $G\colon \mathcal{C}^i(\mathcal{X}) \to \mathcal{C}^j(\mathcal{X})$, and a cochain $\mathbf{H}_i \in C^i(\mathcal{X}, \mathbb{R}^{s_{in}})$. A **CC-convolutional push-forward** is a cochain map $\mathcal{F}_{G;W}^{conv}\colon C^i(\mathcal{X}, \mathbb{R}^{s_{in}}) \to C^j(\mathcal{X}, \mathbb{R}^{t_{out}})$ defined as*

$$\mathbf{H}_i \to \mathbf{K}_j = G\mathbf{H}_i W, \tag{6}$$

where $W \in \mathbb{R}^{d_{s_{in}} \times d_{s_{out}}}$ are trainable parameters.

Having defined the CC-convolutional push-forward, the CC-convolutional merge node (Definition 30) is a straightforward application of Definition 26. Variants of Definition 30 have appeared in recent works on higher-order networks [56, 248, 249, 235, 128, 236, 96, 132, 58, 288].

Definition 30 (CC-convolutional merge node). *Let a $\mathcal{X}$ be a CC. Moreover, let $G_1\colon \mathcal{C}^{i_1}(\mathcal{X}) \to \mathcal{C}^j(\mathcal{X})$ and $G_2\colon \mathcal{C}^{i_2}(\mathcal{X}) \to \mathcal{C}^j(\mathcal{X})$ be two cochain maps. Given a cochain vector $(\mathbf{H}_{i_1}, \mathbf{H}_{i_2}) \in \mathcal{C}^{i_1} \times \mathcal{C}^{i_2}$, a **CC-convolutional merge node** $\mathcal{M}_{\mathbf{G};\mathbf{W}}^{conv}\colon \mathcal{C}^{i_1} \times \mathcal{C}^{i_2} \to \mathcal{C}^j$ is defined as*

$$\begin{aligned} \mathcal{M}_{\mathbf{G};\mathbf{W}}^{conv}(\mathbf{H}_{i_1}, \mathbf{H}_{i_2}) &= \beta\left(\mathcal{F}_{G_1;W_1}^{conv}(\mathbf{H}_{i_1}) + \mathcal{F}_{G_2;W_2}^{conv}(\mathbf{H}_{i_2})\right) \\ &= \beta(G_1\mathbf{H}_{i_1}W_1 + G_2\mathbf{H}_{i_2}W_2), \end{aligned} \tag{7}$$

where $\mathbf{G} = (G_1, G_2)$, $\mathbf{W} = (W_1, W_2)$ is a tuple of trainable parameters, and β is an activation function.

In practice, the matrix representation of the cochain map G in Definition 29 might require problem-specific normalization during training. For various types of normalization in the context of higher-order convolutional operators, we refer the reader to [160, 56, 248].

We have used the notation CCNN$_{\mathbf{G}}$ for a tensor diagram and its corresponding CCNN. Our notation indicates that the CCNN is composed of elementary tensor operations based on a sequence $\mathbf{G} = (G_i)_{i=1}^l$ of cochain maps defined on the underlying CC. When the elementary tensor operations that make up the CCNN are parameterized by a sequence $\mathbf{W} = (W_i)_{i=1}^k$ of trainable parameters, we denote the CCNN and its tensor diagram representation by CCNN$_{\mathbf{G};\mathbf{W}}$.

5.5 Combinatorial complex attention neural networks (CCANNs)

The majority of higher-order deep learning models focus on layers that use *isotropic aggregation*, which means that neighbors in the vicinity of an element contribute equally to an update of the element's representation. As information is aggregated in a diffusive manner, such isotropic aggregation can limit the expressiveness of these learning models, leading to phenomena such as oversmoothing [32]. In contrast, *attention-based learning* [76] allows deep learning models to assign a probability distribution to neighbors in the local vicinity of elements in the underlying domain, thus highlighting components with the most task-relevant information [273]. Attention-based models are successful in practice as they ignore noise in the domain, thereby improving the signal-to-noise ratio [179, 206]. Accordingly, attention-based models have achieved remarkable success on traditional machine learning tasks on graphs, including node classification and link prediction [183], node ranking [262], and attention-based embeddings [76, 178].

After introducing the CC-convolutional push-forward in Section 5.4, our second example of a push-forward operation is the CC-attention push-forward, which is introduced in the present section. Thus, it becomes possible to use CCNNs equipped with CC-attention push-forward operators, which we call *combinatorial complex attention neural networks (CCANNs)*. We first provide the general notion of attention of a sub-CC $\mathcal{Y}_0$ of a CC with respect to other sub-CCs in the CC.

Definition 31 (Higher-order attention)**.** *Let $\mathcal{X}$ be a CC, $\mathcal{N}$ a neighborhood function defined on $\mathcal{X}$, and $\mathcal{Y}_0$ a sub-CC of $\mathcal{X}$. Let $\mathcal{N}(\mathcal{Y}_0) = \{\mathcal{Y}_1, \ldots, \mathcal{Y}_{|\mathcal{N}(\mathcal{Y}_0)|}\}$ be a set of sub-CCs that are in the vicinity of $\mathcal{Y}_0$ with respect to the neighborhood function $\mathcal{N}$. A **higher-order attention** of $\mathcal{Y}_0$ with respect to $\mathcal{N}$ is a function $a\colon \mathcal{Y}_0 \times \mathcal{N}(\mathcal{Y}_0) \to [0,1]$ that assigns a weight $a(\mathcal{Y}_0, \mathcal{Y}_i)$ to each element $\mathcal{Y}_i \in \mathcal{N}(\mathcal{Y}_0)$ such that $\sum_{i=1}^{|\mathcal{N}(\mathcal{Y}_0)|} a(\mathcal{Y}_0, \mathcal{Y}_i) = 1$.*

As seen from Definition 31, a higher-order attention of a sub-CC $\mathcal{Y}_0$ with respect to a neighborhood function $\mathcal{N}$ assigns a discrete distribution to the neighbors of $\mathcal{Y}_0$. Attention-based learning typically aims to learn the function a. Observe that the function a relies on the neighborhood function $\mathcal{N}$. In our context, we aim to learn the function a whose neighborhood function is either an incidence or a (co)adjacency function, as introduced in Section 4.4.

Recall from Definition 31 that a weight $a(\mathcal{Y}_0, \mathcal{Y}_i)$ requires both a source sub-CC $\mathcal{Y}_0$ and a target sub-CC $\mathcal{Y}_i$ as inputs. Thus, a CC-attention push-forward operation requires two cochain spaces. Definition 32 introduces a notion of CC-attention push-forward in which the two underlying cochain spaces contain cochains supported on cells of equal rank.

Definition 32 (CC-attention push-forward for cells of equal rank)**.** *Let $G\colon C^s(\mathcal{X}) \to C^s(\mathcal{X})$ be a neighborhood matrix. A **CC-attention push-forward** induced by G is a cochain map $\mathcal{F}_G^{att}\colon C^s(\mathcal{X}, \mathbb{R}^{d_{s_{in}}}) \to C^s(\mathcal{X}, \mathbb{R}^{d_{s_{out}}})$ defined as*

$$\mathbf{H}_s \to \mathbf{K}_s = (G \odot att)\mathbf{H}_s W_s, \tag{8}$$

*where $\odot$ is the Hadamard product, $W_s \in \mathbb{R}^{d_{s_{in}} \times d_{s_{out}}}$ are trainable parameters, and $att\colon C^s(\mathcal{X}) \to C^s(\mathcal{X})$ is a **higher-order attention matrix** that has the same dimension as matrix G. The (i,j)-th entry of matrix att is defined as*

$$att(i,j) = \frac{e_{ij}}{\sum_{k \in \mathcal{N}_G(i)} e_{ik}}, \tag{9}$$

where $e_{ij} = \phi(a^T[W_s\mathbf{H}_{s,i}||W_s\mathbf{H}_{s,j}])$, $a \in \mathbb{R}^{2 \times s_{out}}$ is a trainable vector, $[a||b]$ denotes the concatenation of a and b, ϕ is an activation function, and $\mathcal{N}_G(i)$ is the neighborhood of cell i with respect to matrix G.

Definition 33 treats a more general case than Definition 32. Specifically, Definition 33 introduces a notion of CC-attention push-forward in which the two underlying cochain spaces contain cochains supported on cells of different ranks.

Definition 33 (CC-attention push-forward for cells of unequal ranks). *For $s \neq t$, let $G \colon C^s(\mathcal{X}) \to C^t(\mathcal{X})$ be a neighborhood matrix. A **CC-attention block** induced by G is a cochain map $\mathcal{F}_G^{att} \mathcal{A} \colon C^s(\mathcal{X}, \mathbb{R}^{d_{s_{in}}}) \times C^t(\mathcal{X}, \mathbb{R}^{d_{t_{in}}}) \to C^t(\mathcal{X}, \mathbb{R}^{d_{t_{out}}}) \times C^s(\mathcal{X}, \mathbb{R}^{d_{s_{out}}})$ defined as*

$$(\mathbf{H}_s, \mathbf{H}_t) \to (\mathbf{K}_t, \mathbf{K}_s), \tag{10}$$

with

$$\mathbf{K}_t = (G \odot att_{s \to t})\mathbf{H}_s W_s, \ \mathbf{K}_s = (G^T \odot att_{t \to s})\mathbf{H}_t W_t, \tag{11}$$

*where $W_s \in \mathbb{R}^{d_{s_{in}} \times d_{t_{out}}}, W_t \in \mathbb{R}^{d_{t_{in}} \times d_{s_{out}}}$ are trainable parameters, and $att_{s \to t}^k \colon C^s(\mathcal{X}) \to C^t(\mathcal{X}), att_{t \to s}^k \colon C^t(\mathcal{X}) \to C^s(\mathcal{X})$ are **higher-order attention matrices** that have the same dimensions as matrices G and G^T, respectively. The (i,j)-th entries of matrices $att_{s \to t}$ and $att_{t \to s}$ are defined as*

$$(att_{s \to t})_{ij} = \frac{e_{ij}}{\sum_{k \in \mathcal{N}_G(i)} e_{ik}}, \ (att_{t \to s})_{ij} = \frac{f_{ij}}{\sum_{k \in \mathcal{N}_{G^T}(i)} f_{ik}}, \tag{12}$$

with

$$e_{ij} = \phi((a)^T[W_s \mathbf{H}_{s,i} || W_t \mathbf{H}_{t,j}]), \ f_{ij} = \phi(rev(a)^T[W_t \mathbf{H}_{t,i} || W_s \mathbf{H}_{s,j}]), \tag{13}$$

where $a \in \mathbb{R}^{t_{out} + s_{out}}$ is a trainable vector, and $rev(a) = [a^l[: t_{out}] || a^l[t_{out} :]]$.

The incidence matrices of Definition 16 can be employed as neighborhood matrices in Definition 33. In Figure 24, we illustrate the notion of CC-attention for incidence neighborhood matrices. Figure 24(c) shows the non-squared incidence matrix $B_{1,2}$ associated with the CC displayed in Figure 24(a). The attention block $\mathrm{HB}_{B_{1,2}}$ learns two incidence matrices $att_{s \to t}$ and $att_{t \to s}$. The matrix $att_{s \to t}$ has the same shape as $B_{1,2}$, and non-zero elements exactly where $B_{1,2}$ has elements equal to one. Each column i in $att_{s \to t}$ represents a probability distribution that defines the attention of the i-th 2-cell to its incident 1-cells. The matrix $att_{t \to s}$ has the same shape as $B_{1,2}^T$, and similarly represents the attention of 1-cells to 2-cells.
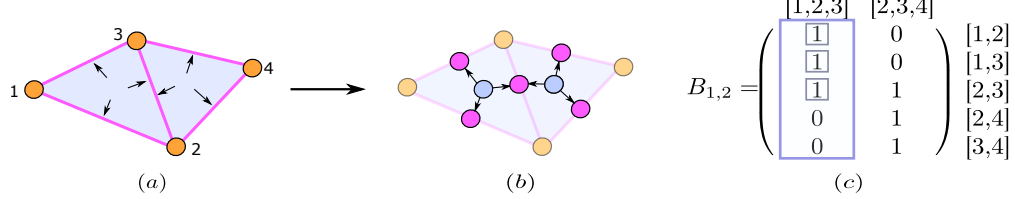
Figure 24: Illustration of notion of CC-attention for cells of unequal ranks. (a): A CC. Each 2-cell (blue face) of the CC attends to its incident 1-cells (pink edges). (b): The attention weights reside on a graph constructed from the cells and their incidence relations; see Section 8.1 for details. (c): Incidence matrix $B_{1,2}$ of the CC given in (a). The non-zero elements in column $[1, 2, 3]$ correspond to the neighborhood $\mathcal{N}_{B_{1,2}}([1, 2, 3])$ of $[1, 2, 3]$ with respect to $B_{1,2}$.

Remark 5.4. *The computation of a push-forward cochain $\mathbf{K}_t$ requires two cochains, namely $\mathbf{H}_s$ and $\mathbf{H}_t$. While $\mathbf{K}_t$ depends on $\mathbf{H}_s$ directly in Equation 11, it depends on $\mathbf{H}_t$ only indirectly via $att_{s \to t}$ as seen from Equations 11–13. Moreover, the cochain $\mathbf{H}_t$ is only needed for $att_{s \to t}$ during training, and not during inference. In other words, the computation of a CC-attention push-forward block requires only a single cochain, $\mathbf{H}_s$, during inference, in agreement with the computation of a general cochain push-forward as specified in Definition 25.*

The operators $G \odot att$ and $G \odot att_{s \to t}$ in Equations 8 and 11 can be viewed as learnt attention versions of G. This perspective allows to employ CCANNs to learn arbitrary types of discrete exterior calculus operators, as elaborated in Appendix D.
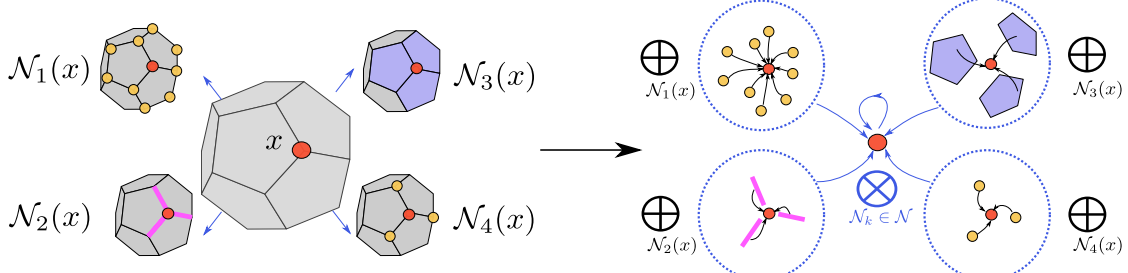
Figure 25: An illustration of higher-order message passing (Definition 34). Left-hand side: a collection of neighborhood functions $\mathcal{N}_1, \ldots, \mathcal{N}_k$ are selected. The selection typically depends on the learning task. Right-hand side: for each $\mathcal{N}_k$, the messages are aggregated using an intra-neighborhood function $\bigoplus$. The inter-neighborhood function $\bigotimes$ aggregates the final messages obtained from all neighborhoods.

6   Higher-order message passing

In this section, we explain the relation between the notion of the merge node introduced in Section 5.2 and higher-order message passing. In particular, we prove that higher-order message passing on CCs can be realized in terms of the elementary tensor operations introduced in Section 5.3. Further, we demonstrate the connection between CCANNs (Section 5.5) and higher-order message passing, and introduce an attention version of higher-order message passing. We first define higher-order message passing on CCs, generalizing notions introduced in [128].

We remark that many of the constructions discussed here are presented in their most basic form, but can be extended further. An important aspect in this direction is the construction of message-passing protocols that are invariant or equivariant with respect to the action of a specific group.

6.1   Definition of higher-order message passing

Higher-order message passing refers to a computational framework that involves exchanging messages among entities and cells in a higher-order domain using a set of neighborhood functions. In Definition 34, we formalize the notion of higher-order message passing for CCs. Figure 25 illustrates Definition 34.

Definition 34 (Higher-order message passing on a CC)**.** *Let $\mathcal{X}$ be a CC. Let $\mathcal{N} = \{\mathcal{N}_1, \ldots, \mathcal{N}_n\}$ be a set of neighborhood functions defined on $\mathcal{X}$. Let x be a cell and $y \in \mathcal{N}_k(x)$ for some $\mathcal{N}_k \in \mathcal{N}$. A **message** $m_{x,y}$ between cells x and y is a computation that depends on these two cells or on the data supported on them. Denote by $\mathcal{N}(x)$ the multi-set $\{\!\{\mathcal{N}_1(x), \ldots, \mathcal{N}_n(x)\}\!\}$, and by $\mathbf{h}_x^{(l)}$ some data supported on the cell x at layer l. **Higher-order message passing** on $\mathcal{X}$, induced by $\mathcal{N}$, is defined via the following four update rules:*

$$m_{x,y} = \alpha_{\mathcal{N}_k}(\mathbf{h}_x^{(l)}, \mathbf{h}_y^{(l)}), \tag{14}$$

$$m_x^k = \bigoplus_{y \in \mathcal{N}_k(x)} m_{x,y}, \ 1 \le k \le n, \tag{15}$$

$$m_x = \bigotimes_{\mathcal{N}_k \in \mathcal{N}} m_x^k, \tag{16}$$

$$\mathbf{h}_x^{(l+1)} = \beta(\mathbf{h}_x^{(l)}, m_x). \tag{17}$$

*Here, $\bigoplus$ is a permutation-invariant aggregation function called the **intra-neighborhood** of x, $\bigotimes$ is an aggregation function called the **inter-neighborhood** of x, and $\alpha_{\mathcal{N}_k}, \beta$ are differentiable functions.*

Some remarks on Definition 34 are as follows. First, the message $m_{x,y}$ in Equation 14 does not depend only on the data $\mathbf{h}_x^{(l)}$, $\mathbf{h}_y^{(l)}$ supported on the cells x, y; it also depends on the cells themselves. For instance, if $\mathcal{X}$ is a cell complex, the *orientation* of both x and y factors into the computation of message $m_{x,y}$. Alternatively, $x \cup y$ or $x \cap y$ might be cells in $\mathcal{X}$ and it might be useful to include their data in the computation of message $m_{x,y}$. This unique characteristic only manifests in higher-order domains, and does not occur in graphs-based message-passing frameworks [52, 114][3]. Second, higher-order message passing relies on the choice of a set $\mathcal{N}$ of neighborhood functions. This is also a unique characteristic that only occurs in a higher-order domain, where a neighborhood function is necessarily described by a set of neighborhood relations rather than graph adjacency as in graph-based message passing. Third, in Equation 14, since y is implicitly defined with respect to a neighborhood relation $\mathcal{N}_k \in \mathcal{N}$, the function $\alpha_{\mathcal{N}_k}$ and the message $m_{x,y}$ depend on $\mathcal{N}_k$. Fourth, the inter-neighborhood $\bigotimes$ does not necessarily have to be a permutation-invariant aggregation function. For instance, it is possible to set an order on the multi-set $\mathcal{N}(x)$ and compute m_x with respect to this order. Finally, higher-order message passing relies on two aggregation functions, the intra-neighborhood and inter-neighborhood, whereas graph-based message passing relies on a single aggregation function. The choice of set $\mathcal{N}$, as illustrated in Section 4, enables the use of a variety of neighborhood functions in higher-order message passing.

Remark 6.1. *The push-forward operator given in Definition 25 is related to the update rule of Equation 14. On one hand, Equation 14 requires two cochains $\mathbf{X}_i = [\mathbf{h}_{x_1^i}^{(l)}, \ldots, \mathbf{h}_{x_{|\mathcal{X}^i|}^i}^{(l)}]$ and $\mathbf{Y}_j^{(l)} = [\mathbf{h}_{y_1^j}^{(l)}, \ldots, \mathbf{h}_{y_{|\mathcal{X}^j|}^j}^{(l)}]$ to compute*

$\mathbf{X}_i^{(l+1)} = [\mathbf{h}_{x_1^i}^{(l+1)}, \ldots, \mathbf{h}_{x_{|\mathcal{X}^i|}^i}^{(l+1)}]$, *so signals on both $\mathcal{C}^j$ and $\mathcal{C}^i$ must be present in order to execute Equation 14. From this perspective, it is natural and customary to think about this operation as an update rule. On the other hand, the push-forward operator of Definition 25 computes a cochain $\mathbf{K}_j \in \mathcal{C}^j$ given a cochain $\mathbf{H}_i \in \mathcal{C}^i$. As a single cochain $\mathbf{H}_i$ is required to perform this computation, it is natural to think about Equation 3 as a function. See Section 6.3 for more details.*

The higher-order message-passing framework given in Definition 34 can be used to construct novel neural network architectures on a CC, as we have also alluded in Figure 17. First, a CC $\mathcal{X}$ and cochains $\mathbf{H}_{i_1} \ldots, \mathbf{H}_{i_m}$ supported on $\mathcal{X}$ are given. Second, a collection of neighborhood functions are chosen, taking into account the desired learning task. Third, the update rules of Definition 34 are executed on the input cochains $\mathbf{H}_{i_1} \ldots, \mathbf{H}_{i_m}$ using the chosen neighborhood functions. The second and the third steps are repeated to obtain the final computations.

> **Definition 35** (Higher-order message-passing neural network)**.** *We refer to to any neural network constructed using Definition 34 as a **higher-order message-passing neural network.***

6.2   Higher-order message-passing neural networks are CCNNs

In this section, we show that higher-order message-passing computations can be realized in terms of merge node computations, and therefore that higher-order message-passing neural networks are CCNNs. As a consequence, higher-order message passing unifies message passing on simplicial complexes, cell complexes and hypergraphs through a coherent set of update rules and, alternatively, through the expressive language of tensor diagrams.

Theorem 6.2. *The higher-order message-passing computations of Definition 34 can be realized in terms of merge node computations.*

Proof. Let $\mathcal{X}$ be a CC. Let $\mathcal{N} = \{\mathcal{N}_1, \ldots, \mathcal{N}_n\}$ be a set of neighborhood functions as specified in Definition 34. Let G_k be the matrix induced by the neighborhood function $\mathcal{N}_k$. We assume that the cell x given in Definition 34 is a j-cell and the neighbors $y \in \mathcal{N}_k(x)$ are i_k-cells. We will show that Equations 14–17 can be realized as applications of merge nodes. In what follows, we define the neighborhood function to be $\mathcal{N}_{Id}(x) = \{x\}$ for $x \in \mathcal{X}$. Moreover, we denote the associated neighborhood matrix of $\mathcal{N}_{Id}$ by $Id \colon \mathcal{C}^j \to \mathcal{C}^j$, as it is the identity matrix.

---

[3]The message 'direction' in $m_{x,y}$ is from y to x. In general, $m_{x,y}$ and $m_{y,x}$ are not equal.

Computing message $m_{x,y}$ of Equation 14 involves two cochains:

$$\mathbf{X}_j^{(l)} = [\mathbf{h}_{x_1^j}^{(l)}, \ldots, \mathbf{h}_{x_{|\mathcal{X}^j|}^j}^{(l)}], \ \mathbf{Y}_{i_k}^{(l)} = [\mathbf{h}_{y_1^{i_k}}^{(l)}, \ldots, \mathbf{h}_{y_{|\mathcal{X}^{i_k}|}^{i_k}}^{(l)}].$$

Every message $m_{x_t^j, y_s^{i_k}}$ corresponds to the entry $[G_k]_{st}$ of matrix G_k. In other words, there is a one-to-one correspondence between non-zero entries of matrix G_k and messages $m_{x_t^j, y_s^{i_k}}$.

It follows from Section 5.2 that computing $\{m_x^k\}_{k=1}^n$ corresponds to a merge node $\mathcal{M}_{Id_j, G_k} \colon \mathcal{C}^j \times \mathcal{C}^{i_k} \to \mathcal{C}^j$ that performs the computations determined via α_k and $\bigoplus$, and yields

$$\mathbf{m}_j^k = [m_{x_1^j}^k, \ldots, m_{x_{|\mathcal{X}^j|}^j}^k] = \mathcal{M}_{Id_j, G_k}(\mathbf{X}_j^{(l)}, \mathbf{Y}_{i_k}^{(l)}) \in \mathcal{C}^j.$$

At this stage, we have n j-cochains $\{\mathbf{m}_j^k\}_{k=1}^n$. Equations 16 and 17 merge these cochains with the input j-cochain $\mathbf{X}_j^{(l)}$. Specifically, computing m_x in Equation 16 corresponds to $n-1$ applications of merge nodes of the form $\mathcal{M}_{Id_k, Id_k} \colon \mathcal{C}^j \times \mathcal{C}^j \to \mathcal{C}^j$ on the cochains $\{\mathbf{m}_j^k\}_{k=1}^n$. Explicitly, we first merge $\mathbf{m}_j^1$ and $\mathbf{m}_j^2$ to obtain $\mathbf{n}_j^1 = \mathcal{M}_{Id_j, Id_j}(\mathbf{m}_j^1, \mathbf{m}_j^2)$. Next, we merge the j-cochain $\mathbf{n}_j^1$ with the j-cochain $\mathbf{m}_j^3$, and so on. The final merge node in this stage performs the merge $\mathbf{n}_j^{n-1} = \mathcal{M}_{Id_j, Id_j}(\mathbf{n}_j^{n-2}, \mathbf{m}_j^n)$, which is $\mathbf{m}_j = [m_{x_1^j}, \ldots, m_{x_{|\mathcal{X}^j|}^j}]$[4]. Finally, computing $\mathbf{X}_j^{(l+1)}$ is realized by a merge node $\mathcal{M}_{(Id_j, Id_j)}(\mathbf{m}_j, \mathbf{X}_j^{(l)})$ whose computations are determined by function β of Equation 17. $\qquad\square$

Theorem 6.2 shows that higher-order message-passing networks defined on CCs can be constructed from the elementary tensor operations, and hence they are special cases of CCNNs. We state this result formally in Theorem 6.3.

Theorem 6.3. *A higher-order message-passing neural network is a CCNN.*

Proof. The conclusion follows immediately from Definition 35 and Theorem 6.2. $\qquad\square$

It follows from Theorem 6.3 that higher-order message-passing neural networks defined on higher-order domains that are less general than CCs (such as simplicial complexes, cell complexes and hypergraphs) are also special cases of CCNNs. Thus, tensor diagrams, as introduced in Definition 24, form a general diagrammatic method for expressing neural networks defined on commonly studied higher-order domains.

Theorem 6.4. *Message-passing neural networks defined on simplicial complexes, cell complexes or hypergraphs can be expressed in terms of tensor diagrams and their computations can be realized in terms of the three elementary tensor operators.*

Proof. The conclusion follows from Theorem 6.3 and from the fact that simplicial complexes, cell complexes and hypergraphs can be realized as special cases of CCs. $\qquad\square$

Theorems 6.3 and 6.4 put forward a unifying TDL framework based on tensor diagrams, thus providing scope for future developments. For instance, [218] have already used our framework to express existing TDL architectures for simplicial complexes, cell complexes and hypergraphs in terms of tensor diagrams.

6.3   Merge nodes and higher-order message passing: a qualitative comparison

Higher-order message passing, as given in Definition 34, provides an update rule to obtain the vector $\mathbf{h}_x^{l+1}$ from vector $\mathbf{h}_x^l$ using a set of neighborhood vectors $\mathbf{h}_y^l$ determined by $\mathcal{N}(x)$. Clearly, this computational framework assumes that vectors $\mathbf{h}_x^{(l)}$ and $\mathbf{h}_y^{(l)}$ are provided as inputs. In other words, performing higher-order message passing according to Definition 34 requires the cochain $\mathbf{X}_j^{(l)} \in \mathcal{C}^j$ in the target domain as well as the

---

[4]Recall that while we use the same notation $\mathcal{M}_{Id_k, Id_k}$ for all merge nodes, these nodes have in general different parameters.
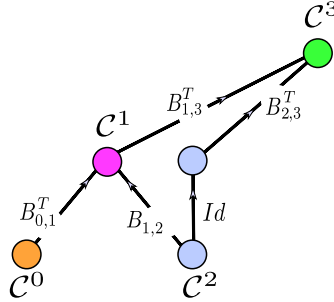
Figure 26: The depicted neural network can be realized as a composition of two merge nodes. More specifically, the input is a cochain vector $(\mathbf{H}_0, \mathbf{H}_2)$. The first merge node computes the 1-chain $\mathbf{H}_1 = \mathcal{M}_{B_{0,1}^T, B_{1,2}}(\mathbf{H}_0, \mathbf{H}_2)$. Similarly, the second merge node $\mathcal{M}_{B_{1,3}^T, B_{2,3}} : \mathcal{C}^1 \times \mathcal{C}^2 \to \mathcal{C}^3$ computes the 3-cochain $\mathbf{H}_3 = \mathcal{M}_{B_{1,3}^T, B_{2,3}}(\mathbf{H}_1, \mathbf{H}_2)$. The merge node perspective allows to compute a cochain supported on the 1-cells and 3-cells without having initial cochains of these cells. On the other hand, the higher-order message-passing framework has two major constraints: it assumes as input initial cochains supported on all cells of all dimensions of the domain, and it updates all cochains supported on all cells of all dimensions of the input domain at every iteration.

cochains $\mathbf{Y}_{i_k}^{(l)} \in \mathcal{C}^{i_k}$ in order to compute the updated j-cochain $\mathbf{X}_j^{(l+1)}$. On the other hand, performing a merge node computation requires a cochain vector $(\mathbf{H}_{i_1}, \mathbf{H}_{i_2})$, as seen from Equation 1 and Definition 26.

The difference between these two computational frameworks might seem notational and the message passing perspective might seem more intuitive, especially when working with graph-based models. However, we argue that the merge node framework is more natural and flexible computationally in the presence of a custom higher-order network architecture. To illustrate this, we consider the example visualized in Figure 26.

In Figure 26, the displayed neural network has a cochain input vector $(\mathbf{H}_0, \mathbf{H}_2) \in \mathcal{C}^0 \times \mathcal{C}^2$. In the first layer, the neural network computes the cochain $\mathbf{H}_1 \in \mathcal{C}^1$, while in the second layer it computes the cochain $\mathbf{H}_3 \in \mathcal{C}^3$. To obtain cochain $\mathbf{H}_1$ in the first layer, we need to consider the neighborhood functions induced by $B_{0,1}^T$ and $B_{1,2}$. However, if we employ Equations 14 and 15 to perform the computations determined by the first layer of the tensor diagram in Figure 26, then we notice that no cochain is provided on $\mathcal{C}^1$ as part of the input. Hence, when applying Equations 14 and 15, a special treatment is required since the vectors $\mathbf{h}_{x_j^1}$ have not been computed yet. Note that such an artifact is not present in GNNs, since they often update node features, which are typically provided as part of the input. To be specific, in GNNs, the first two arguments in the update rule of Equation 14 are cochains that are supported on the 0-cells of the underlying graph.

Similarly, to compute the cochain $\mathbf{H}_3 \in \mathcal{C}^3$ in the second layer of Figure 26, we must consider the neighborhood functions induced by $B_{1,3}^T$ and $B_{2,3}$, and we must use the cochain vector $(\mathbf{H}_1, \mathbf{H}_2)$. This means that the cochains $\mathbf{H}_1$ and $\mathbf{H}_3$ resulting from the computation of the neural network given in Figure 26 are not obtained from an iterative process. Further, the input vectors $\mathbf{H}_0$ and $\mathbf{H}_2$ are never updated at any step of the procedure. Finally, the cochains $\mathbf{H}_1$ and $\mathbf{H}_3$ are never updated. From the perspective of update rules such as the ones appearing in the higher-order message passing framework (Definition 34), this setting is unnatural in the sense that it assumes *initial cochains supported on all cells* of all dimensions as input, and in the sense that it *updates all cochains supported on all cells* in the complex of the input domain at every iteration.

In practice, such difficulties in using the higher-order message passing framework can be overcome with ad hoc engineering solutions based on turning on and off iterations on certain cochains or based on introducing auxiliary cochains. The merge node is designed to overcome these limitations. Specifically, from the merge node perspective, we can think of the first layer of Figure 26 as a function $\mathcal{M}_{B_{0,1}^T, B_{1,2}} : \mathcal{C}^0 \times \mathcal{C}^1 \to \mathcal{C}^1$; see Equation 3. The function $\mathcal{M}_{B_{0,1}^T, B_{1,2}}$ takes as input the cochain vector $(\mathbf{H}_0, \mathbf{H}_2)$, and computes the 1-chain $\mathbf{H}_1 = \mathcal{M}_{B_{0,1}^T, B_{1,2}}(\mathbf{H}_0, \mathbf{H}_2)$. Similarly, we compute the 3-cochain $\mathbf{H}_3 = \mathcal{M}_{B_{1,3}^T, B_{2,3}}(\mathbf{H}_1, \mathbf{H}_2)$ using a merge node $\mathcal{M}_{B_{1,3}^T, B_{2,3}} : \mathcal{C}^1 \times \mathcal{C}^2 \to \mathcal{C}^3$.

6.4 Attention higher-order message passing and CCANNs

Here, we demonstrate the connection between higher-order message passing (Definition 34) and CCANNs (Section 5.5). Initially, we introduce an attention version of Definition 34.

Definition 36 (Attention higher-order message passing on a CC)**.** *Let $\mathcal{X}$ be a CC. Let $\mathcal{N} = \{\mathcal{N}_1, \ldots, \mathcal{N}_n\}$ be a set of neighborhood functions defined on $\mathcal{X}$. Let x be a cell and $y \in \mathcal{N}_k(x)$ for some $\mathcal{N}_k \in \mathcal{N}$. A **message** $m_{x,y}$ between cells x and y is a computation that depends on these two cells or on the data supported on them. Denote by $\mathcal{N}(x)$ the multi-set $\{\!\{\mathcal{N}_1(x), \ldots, \mathcal{N}_n(x)\}\!\}$, and by $\mathbf{h}_x^{(l)}$ some data supported on the cell x at layer l. **Attention higher-order message passing** on $\mathcal{X}$, induced by $\mathcal{N}$, is defined via the following four update rules:*

$$m_{x,y} = \alpha_{\mathcal{N}_k}(\mathbf{h}_x^{(l)}, \mathbf{h}_y^{(l)}), \tag{18}$$

$$m_x^k = \bigoplus_{y \in \mathcal{N}_k(x)} a^k(x,y) m_{x,y},\ 1 \le k \le n, \tag{19}$$

$$m_x = \bigotimes_{\mathcal{N}_k \in \mathcal{N}} b^k m_x^k, \tag{20}$$

$$\mathbf{h}_x^{(l+1)} = \beta(\mathbf{h}_x^{(l)}, m_x). \tag{21}$$

Here, $a^k \colon \{x\} \times \mathcal{N}_k(x) \to [0,1]$ is a higher-order attention function (Definition 31), b^k are trainable attention weights satisfying $\sum_{k=1}^n b^k = 1$, $\bigoplus$ is a permutation-invariant aggregation function, $\bigotimes$ is an aggregation function, $\alpha_{\mathcal{N}_k}$ and β are differentiable functions.

Definition 36 distinguishes two types of attention weights. The first type is determined by the function a^k. The attention weight $a^k(x,y)$ of Equation 19 depends on the neighborhood function $\mathcal{N}_k$ and on cells x and y. Further, $a^k(x,y)$ determines the attention a cell x pays to its surrounding neighbors $y \in \mathcal{N}_k$, as determined by the neighborhood function $\mathcal{N}_k$. The CC-attention push-forward operations defined in Section 5.5 are a particular parameterized realization of these weights. On the other hand, the weights b^k of Equation 20 are only a function of the neighborhood $\mathcal{N}_k$, and therefore determine the attention that cell x pays to the information obtained from each neighborhood function $\mathcal{N}_k$. In our CC-attention push-forward operations given in Section 5.5, we set b^k equal to one. However, the notion of merge node (Definition 26) can be easily extended to introduce a corresponding notion of *attention merge node*, which in turn can be used to realize Equation 20 in practice. Note that the attention determined by weights b^k is unique to higher-order domains, and does not arise in graph-based attention models.

7 Push-forward and higher-order (un)pooling

This section shows how the push-forward operation of Definition 25 can be used to realize (un)pooling operations on CCs, and subsequently introduces (un)pooling operations for CCNNs. Further, this section demonstrates how CC-based pooling provides a unifying framework for image and graph-based pooling, and how shape-preserving pooling on CCs is related to the mapper on graphs.

In particular, we establish yet another unifying mathematical principle: pooling, as message passing, can be fundamentally built from push-forward operations. Thus, push-forward operations form the main fundamental building block from which all higher-order computations can be realized. This realization is important because it establishes a mathematical foundation for a unifying deep learning application programming interface (API) on complexes that combines pooling as well as message passing-based computations as a single operation. Indeed, in TopoModelX[5], one of our contributed Python packages, higher-order message passing and the pooling/unpooling operations are implemented as a single function across various topological domains.

[5]https://github.com/pyt-team/TopoModelX
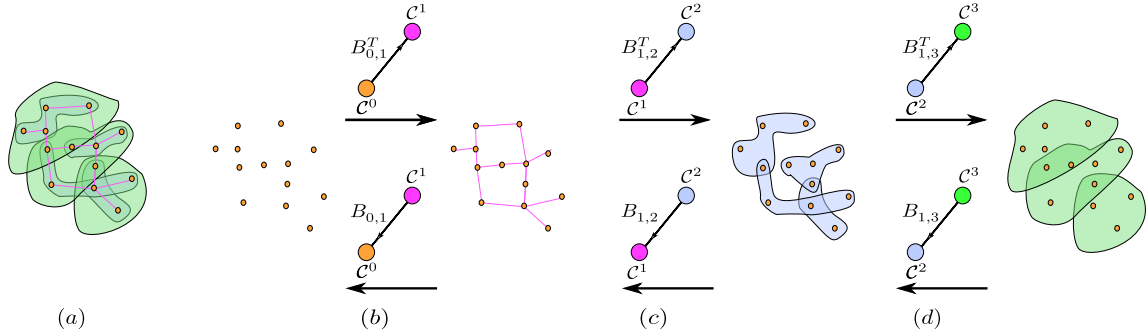
Figure 27: An example of successive CC-(un)pooling operations. A CC-pooling operation exploits the hierarchical structure of the underlying CC to coarsen a lower-rank cochain by pushing it forward to higher-order cells. CC-pooling operations improve invariance to certain distortions. Pink, blue, and green cells have ranks one, two, and three, respectively. A CC $\mathcal{X}$ of dimension three is shown in (a). On $\mathcal{X}$, we consider three cochain operators: $B_{0,1} \colon \mathcal{C}^1 \to \mathcal{C}^0$, $B_{1,2} \colon \mathcal{C}^2 \to \mathcal{C}^1$ and $B_{2,3} \colon \mathcal{C}^3 \to \mathcal{C}^2$. For the top row in Figures (b), (c), and (d), we assume that we are initially given a 0-cochain $\mathbf{H}_0$, while for the bottom row in the same figure, we assume that we are initially given a 3-cochain $\mathbf{H}_3$. For instance, at the top row of Figure (b), the input 0-cochain $\mathbf{H}_0$ gets pushed forward via the functional $\mathcal{F}_{B_{0,1}^T} \colon \mathcal{C}^0 \to \mathcal{C}^1$ to a 1-cochain $\mathbf{H}_1$. This push-forward operator induced by $B_{0,1}^T$ is a CC-pooling operator, since it sends a 0-cochain to a cochain of higher rank. At the bottom row of Figure (b), the push-forward operator $\mathcal{F}_{B_{0,1}} \colon \mathcal{C}^1 \to \mathcal{C}^0$ induced by $B_{0,1}$ is an unpooling operator that sends a 1-cochain to a 0-cochain. Figures (c) and (d) are similar to (b), demonstrating the pooling operators induced by $B_{1,2}^T$ and $B_{2,3}^T$ (top), and the unpooling operators induced by $B_{1,2}$ and $B_{2,3}$ (bottom).

7.1 CC-(un)pooling

We define a CC-based pooling operation that extends the main characteristics of image-based and graph-based pooling operations. Specifically, we build a pooling operation that 'downscales' the size of a signal supported on a CC $\mathcal{X}$. To this end, we exploit the hierarchical nature of CCs and define the pooling operation as a push-forward operation induced by a cochain map $G \colon \mathcal{C}^i(\mathcal{X}) \to \mathcal{C}^j(\mathcal{X})$ that pushes an i-cochain to a j-cochain. To obtain a useful pooling operation that downscales the size of its input i-cochain, we impose the constraint $j > i$. Definition 37 realizes our idea of CC-pooling. Figure 27 visualizes the intuition behind Definition 37. In particular, Figure 27 shows an example of successive applications of pooling operations on cochains supported on a CC of dimension three.

> **Definition 37** (CC-pooling operation). *Let $\mathcal{X}$ be a CC and $G \colon \mathcal{C}^i(\mathcal{X}) \to \mathcal{C}^j(\mathcal{X})$ a cochain map. The push-forward operation induced by G is called a **CC-pooling operation** if $j > i$.*

In Definition 38, we introduce an unpooling operation on CCs that pushes forward a cochain to a lower-rank cochain. Figure 27 shows as example of unpooling on CCs.

> **Definition 38** (CC-unpooling operation). *Let $\mathcal{X}$ be a CC and $G \colon \mathcal{C}^i(\mathcal{X}) \to \mathcal{C}^j(\mathcal{X})$ a cochain map. The push-forward operation induced by G is called a **CC-unpooling operation** if $j < i$.*

7.2 Formulating common pooling operations as CC-pooling

In this section, we formulate common pooling operations in terms of CC-pooling. In particular, we demonstrate that graph and image pooling can be cast as CC-pooling.

(a) (b) (c) (d)
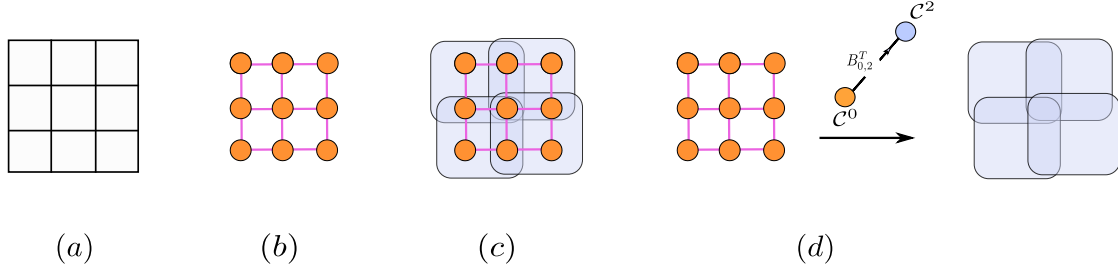
Figure 28: Realizing image pooling in terms of CC-pooling. (a): An image of size 3×3. (b): The lattice graph that corresponds to the image given in (a). (c): Augmenting the lattice graph with 2-cells. Choosing these particular cells shown in (c) is equivalent to choosing the image-pooling window size to be 2×2 and the pooling stride to be one. (d): Performing the image-pooling computation is equivalent to performing a CC-pooling operation induced by the cochain map $B_{0,2}^T \colon \mathcal{C}^0 \to \mathcal{C}^2$, which pushes forward the image signal (the 0-cochain supported on $\mathcal{X}^2$) to a signal supported on $\mathcal{X}^2$.

7.2.1 Graph pooling as CC-pooling

Here, we briefly demonstrate that the CC-pooling operation (Definition 37) is consistent with a graph-based pooling algorithm. Let $\mathbf{H}_0$ be a cochain defined on the vertices and edges of a graph $\mathcal{G}$. Moreover, let $\mathbf{H}_0'$ be a cochain defined on the vertices of a coarsened version $\mathcal{G}'$ of $\mathcal{G}$. Under such a setup, $\mathbf{H}_0'$ represents a coarsened version of $\mathbf{H}_0$. A graph pooling function supported on the pair $(\mathcal{G}, \mathbf{H}_0)$ is a function of the form $\mathcal{POOL} \colon (\mathcal{G}, \mathbf{H}_0) \to (\mathcal{G}', \mathbf{H}_0')$ that sends every vertex in $\mathcal{G}$ to a vertex in $\mathcal{G}'$, which corresponds to a cluster of vertices in $\mathcal{G}$. We now elucidate how the function $\mathcal{POOL}$ can be realized in terms of CC-pooling.

Proposition 7.1. *The function $\mathcal{POOL}$ can be realized in terms of CC-pooling operations.*

Proof. Each vertex in the graph $\mathcal{G}'$ represents a cluster of vertices in the original graph $\mathcal{G}$. Using the membership of these clusters, we construct a CC by augmenting $\mathcal{G}$ by a collection of 2-cells, so that each of these cells corresponds to a supernode of $\mathcal{G}'$. We denote the resulting CC structure by $\mathcal{X}_\mathcal{G}$, consisting of $\mathcal{G}$ augmented by the 2-cells. Hence, any 0-cochain $\mathbf{H}_0'$ defined on $\mathcal{G}'$ can be written as a 2-cochain $\mathbf{H}_2 \in \mathcal{C}^2(\mathcal{X}_\mathcal{G})$. The relation between the vertices of the original graph $\mathcal{G}$ and the vertices of the pooled graph $\mathcal{G}'$, or equivalently the CC $\mathcal{X}_\mathcal{G}$, is described via the incidence matrix $B_{0,2}^T$. Hence, learning the signal $\mathbf{H}_2$ can be realized in terms of a map $B_{0,2}^T \colon \mathcal{C}^2(\mathcal{X}_\mathcal{G}) \to \mathcal{C}^0(\mathcal{X}_\mathcal{G})$ that pushes forward the cochain $\mathbf{H}_0$ to $\mathbf{H}_2$. $\square$

The 2-cells defined on $\mathcal{X}_\mathcal{G}$ can be practically constructed using the *mapper on graphs* [130], a classification tool in TDA. See Section 7.4 for more details of such a construction.

7.2.2 Image pooling as CC-pooling

Since images can be realized as lattice graphs, a signal stored on an image grid can be realized as a 0-cochain of the lattice graph that corresponds to the image. See Figures 28(a–b) for an example. Here, we demonstrate that the CC-pooling operation (Definition 37) is consistent with the known image-pooling definition. Indeed, one may augment the lattice graph of Figure 28(b) by 2-cells, as shown in Figure 28(c), to perform the image pooling operation. Usually, these cells have a regular window size. In Figure 28(c), we have chosen the pooling window size, or equivalently the size of the 2-cell, to be 2×2, and the pooling stride to be 1. The image pooling operation in this case can be realized as a CC-pooling operation induced by the cochain map $B_{0,2}^T \colon \mathcal{C}^0 \to \mathcal{C}^2$, as visualized in Figure 28(d). We formally record this in the following proposition.

Proposition 7.2. *An image pooling operator can be realized in terms of a push-forward operator from the underlying image domain to a 2-dimensional CC obtained by augmenting the image by appropriate 2-cells where image pooling computations occur.*

Proof. The proof is a straightforward conclusion from the definition of image pooling. $\square$
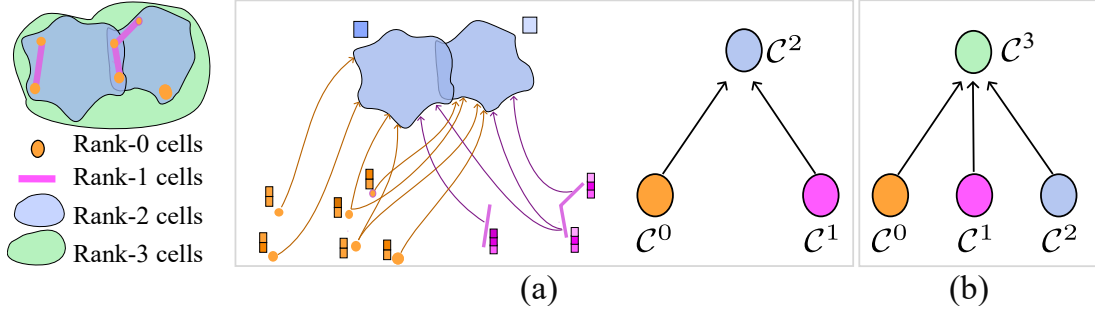
Figure 29: Examples of pooling operations. In this example, a CC of dimension three is displayed. A rank cell of rank 3 (shown in green) has the highest rank among all cells in the CC. (a): A pooling CCNN of height one pools a cochain vector $(\mathbf{H}_0, \mathbf{H}_1)$ to a 2-cochain $\mathbf{H}_2$. (b): A readout operation can be realized as a pooling CCNN of height one by encapsulating the entire CC by a single (green) cell of rank higher than all other cells in the CC, and by pooling (reading out) all signals of lower-order cells to the encapsulating (green) cell.

7.3   (Un)pooling CCNNs

The pooling operator of Definition 37 considers only the special case in which the tensor diagram of a CCNN has a single edge. In what follows, we generalize the notion of pooling by identifying the defining properties that characterize a CCNN as a pooling CCNN. To this end, we start with a CCNN whose tensor diagram has a height of one.

Definition 39 (Pooling CCNN of height one). *Consider a CCNN represented by a tensor diagram* $\mathrm{CCNN}_{\mathbf{G};\mathbf{W}}$ *of height one. Let* $\mathcal{C}^{i_1} \times \mathcal{C}^{i_2} \times \cdots \times \mathcal{C}^{i_m}$ *be the domain and let* $\mathcal{C}^{j_1} \times \mathcal{C}^{j_2} \times \cdots \times \mathcal{C}^{j_n}$ *be the codomain of the CCNN. Let* $i_{min} = min(i_1, \ldots, i_m)$ *and* $j_{min} = min(j_1, \ldots, j_n)$*. We say that the CCNN is a **pooling CCNN of height one** if*

  1. $i_{min} < j_{min}$, and

  2. the tensor diagram $\mathrm{CCNN}_{\mathbf{G};\mathbf{W}}$ *has an edge labeled by a cochain operator* $G \colon \mathcal{C}^{i_{min}} \to \mathcal{C}^k$ *for some* $k \geq j_{min}$*.*

Intuitively, a CCNN represented by a tensor diagram of height one is a pooling CCNN of height one if it pushes forward its lowest-rank signals to higher-rank cells. Observe that a readout operation can be realized as a pooling CCNN of height one; see Figure 29 for an illustration.

A CCNN may not perform a pooling operation at every layer, and it may preserve the dimensionality of the lowest-rank signal. Before we give the general definition of pooling CCNNs, we first define lowest rank-preserving CCNNs of height one.

Definition 40 (Lowest rank-preserving CCNN of height one). *Consider a CCNN represented by a tensor diagram of height one. Let* $\mathcal{C}^{i_1} \times \mathcal{C}^{i_2} \times \cdots \times \mathcal{C}^{i_m}$ *be the domain and let* $\mathcal{C}^{j_1} \times \mathcal{C}^{j_2} \times \cdots \times \mathcal{C}^{j_n}$ *be the codomain of the CCNN. Let* $i_{min} = min(i_1, \ldots, i_m)$ *and* $j_{min} = min(j_1, \ldots, i_n)$*. We say that the CCNN is a **lowest rank-preserving CCNN of height one** if* $i_{min} = j_{min}$*.*

Every CCNN is a composition of CCNNs that are represented by tensor diagrams of height one. Hence, pooling CCNNs can be characterized in terms of tensor diagrams of height one, as elaborated in Definition 41.

Definition 41 (Pooling CCNN)**.** *Let* $\mathrm{CCNN}_{\mathbf{G};\mathbf{W}}$ *be a tensor diagram representation of a CCNN. We decompose the CCNN as*

$$\mathrm{CCNN}_{\mathbf{G};\mathbf{W}} = \mathrm{CCNN}_{\mathbf{G}_N;\mathbf{W}_N} \circ \cdots \circ \mathrm{CCNN}_{\mathbf{G}_1;\mathbf{W}_1},$$

where $\mathrm{CCNN}_{\mathbf{G}_i;\mathbf{W}_i}, i = 1, \ldots, N$, *is a tensor diagram of height one representing the i-th layer of the CCNN, and* $\mathbf{G}_i \subseteq \mathbf{G}$. *We call the CCNN represented by* $\mathrm{CCNN}_{\mathbf{G};\mathbf{W}}$ *a* **pooling CCNN** *if*

1. *every* $\mathrm{CCNN}_{\mathbf{G}_i;\mathbf{W}_i}$ *is either a pooling CCNN of height one or a lowest rank-preserving CCNN of height one, and*

2. *at least one of the layers* $\mathrm{CCNN}_{\mathbf{G}_i;\mathbf{W}_i}$ *is a pooling CCNN of height one.*

Intuitively, a pooling CCNN is a CCNN whose tensor diagram forms a 'ladder' that pushes signals to higher-rank cells at every layer. Figure 19(d) gives an example of a pooling CCNN of height two.

An unpooling CCNN of height one is defined similarly to a pooling CCNN of height one (Definition 39), with the only difference being that the inequality $i_{min} < j_{min}$ becomes $i_{min} > j_{min}$. Moreover, an unpooling CCNN (Definition 42) is defined analogously to a pooling CCNN (Definition 41).

Definition 42 (Unpooling CCNN)**.** *Let* $\mathrm{CCNN}_{\mathbf{G};\mathbf{W}}$ *be a tensor diagram representation of a CCNN. We decompose the CCNN as*

$$\mathrm{CCNN}_{\mathbf{G};\mathbf{W}} = \mathrm{CCNN}_{\mathbf{G}_N;\mathbf{W}_N} \circ \cdots \circ \mathrm{CCNN}_{\mathbf{G}_1;\mathbf{W}_1},$$

where $\mathrm{CCNN}_{\mathbf{G}_i;\mathbf{W}_i}, i = 1, \ldots, N$, *is a tensor diagram of height one representing the i-th layer of the CCNN, and* $\mathbf{G}_i \subseteq \mathbf{G}$. *We call the CCNN represented by* $\mathrm{CCNN}_{\mathbf{G};\mathbf{W}}$ *an* **unpooling CCNN** *if*

1. *every* $\mathrm{CCNN}_{\mathbf{G}_i;\mathbf{W}_i}$ *is either an unpooling CCNN of height one or a lowest rank-preserving CCNN of height one, and*

2. *at least one of the layers* $\mathrm{CCNN}_{\mathbf{G}_i;\mathbf{W}_i}$ *is an unpooling CCNN of height one.*

7.4 Mapper and the CC-pooling operation

In practice, constructing a useful CC-pooling operation on a higher-order domain is determined by the higher-rank cells in the input CC. Similar to image-based models, CC-pooling operations can be applied sequentially at the end of a higher-order network to provide a summary representation of the input domain; see Figure 27 for an example. Such a hierarchical summary might not be readily available in the input CC. For instance, if $\mathcal{X}$ is a graph, then a CC-pooling operation, as given in Definition 37, can only push forward an input node-signal to an edge-signal, which may not always provide a compact summary of the input signal.

In such situations, one may choose to *augment the input CC* $\mathcal{X}$ with a collection of new cells of dimension $\dim(\mathcal{X}) + 1$ so that the new cells approximate the shape of the input CC $\mathcal{X}$. Figure 30 displays an example of augmenting a graph $\mathcal{X}$, which is a CC of dimension one, with new cells of dimension two using the *mapper on graphs (MOG)* construction suggested in [130, 90, 258][6]. The augmented higher-rank cells obtained from the MOG construction summarize the shape features of the underlying graph, which is a desirable pooling characteristic (e.g., in shape analysis). We refer to Appendix E for details about the MOG construction of topology-preserving CC-pooling operations.

8 Hasse graph interpretation and equivariances of CCNNs

In this section, we scrutinize the properties of our topological learning machines by establishing connections to the pre-existing findings regarding GNNs. We begin our inquiry by elucidating the interpretation of

---

[6]While graph skeletonization using the mapper algorithm [258] has been studied in [90], our implementation and discussion here relies on the notions suggested in [130].

(a) $\qquad$ (b) $\qquad$ (c) $\qquad$ (d)
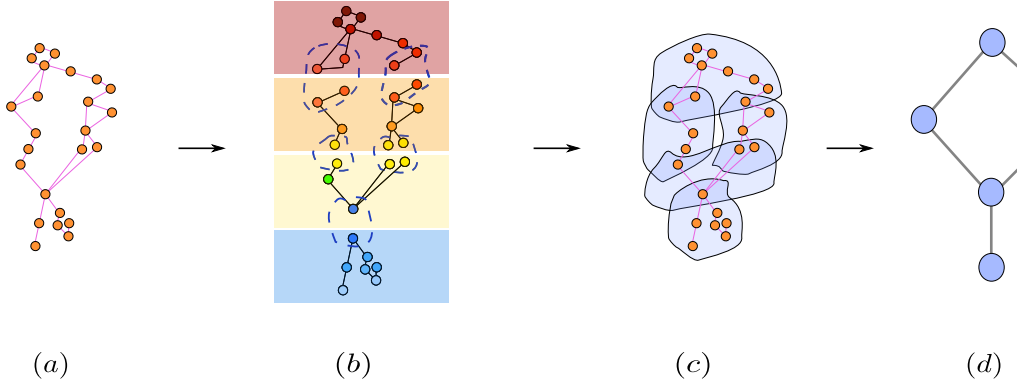
Figure 30: An example of constructing a shape-preserving pooling operation on a CC $\mathcal{X}$. Here, we demonstrate the case in which $\mathcal{X}$ is a graph. We utilize the *mapper on graphs (MOG)* construction [130, 258], a graph skeletonization algorithm that can be used to augment $\mathcal{X}$ with topology-preserving cells of rank 2. (a): An input graph $\mathcal{X}$, which is a CC of dimension one. (b): The MOG algorithm receives three elements as input, namely the graph $\mathcal{X}$, a feature-preserving scalar function $g\colon \mathcal{X}^0 \to [a,b]$, and a cover $\mathcal{U}$ of range $[a,b]$, that is a collection of open sets that covers the closed interval $[a,b]$. The scalar function g is used to pull back a covering $\mathcal{U}$ on the range $[a,b]$ to a covering on $\mathcal{X}$. The colors of nodes in Figure (b) indicate the scalar values of g. In Figure (b), $\mathcal{X}$ is split into four segments so that each segment corresponds to a cover element of $\mathcal{U}$. (c): The figure shows the connected components in pull-back cover elements. Each connected component is enclosed by a blue cell. Each of these blue cells is considered as a cell of rank 2. We augment $\mathcal{X}$ with the blue cells to form a CC of dimension two, consisting of the original 0-cells and 1-cells in $\mathcal{X}$ as well as the augmented 2-cells. This augmented CC is denoted by $\mathcal{X}_{g,\mathcal{U}}$. (d): The MOG algorithm constructs a graph, whose nodes are the connected components contained in each cover element in the pull-back of the cover $\mathcal{U}$, and whose edges are formed by the intersection between these connected components. In other words, the MOG-generated graph summarizes the connectivity between the augmented cells of rank 2 added via the MOG algorithm. Observe that the adjacency matrix of the MOG-generated graph given in Figure (d) is equivalent to the adjacency matrix $A_{2,2}$ of $\mathcal{X}_{g,\mathcal{U}}$, since 2-cells in $\mathcal{X}$ are 2-adjacent if and only if they intersect on a node (and the latter occurs if and only if there is an edge between the nodes of the MOG-generated graph). Given this CC structure, the cochain map $B_{0,2}^T\colon \mathcal{C}^0(X_{g,\mathcal{U}}) \to \mathcal{C}^2(X_{g,\mathcal{U}})$ can be used to induce a shape-preserving CC-pooling operation. Moreover, a signal $\mathbf{H}_0$ supported on the nodes of $\mathcal{X}$ can be push-forwarded and pooled to a signal $\mathbf{H}_2$ supported on the augmented 2-cells. This figure is inspired from [130].

CCs as specialized graphs, known as *Hasse graphs*, followed by characterizing their equivariance properties against the actions of permutations and orientations. We further link our definitions of equivariances to the conventional ones under the Hasse graph representation.

8.1   Hasse graph interpretation of CCNNs

We first demonstrate that every CC can be reduced to a unique and special graph known as the *Hasse graph*. This reduction enables us to analyze and understand various computational and conceptual aspects of CCNNs in terms of graph-based models.

8.1.1   CCs as Hasse graphs

Definition 10 implies that a CC is a poset, that is a partially ordered set whose partial order relation is the set inclusion relation. It also implies that two CCs are equivalent if and only if their posets are equivalent[7]. Definition 43 introduces the *Hasse graph* [1, 274] of a CC, which is a directed graph associated with a finite poset.

---

[7]For related structures (e.g., simplicial/cell complexes), this poset is typically called the *face poset* [274].
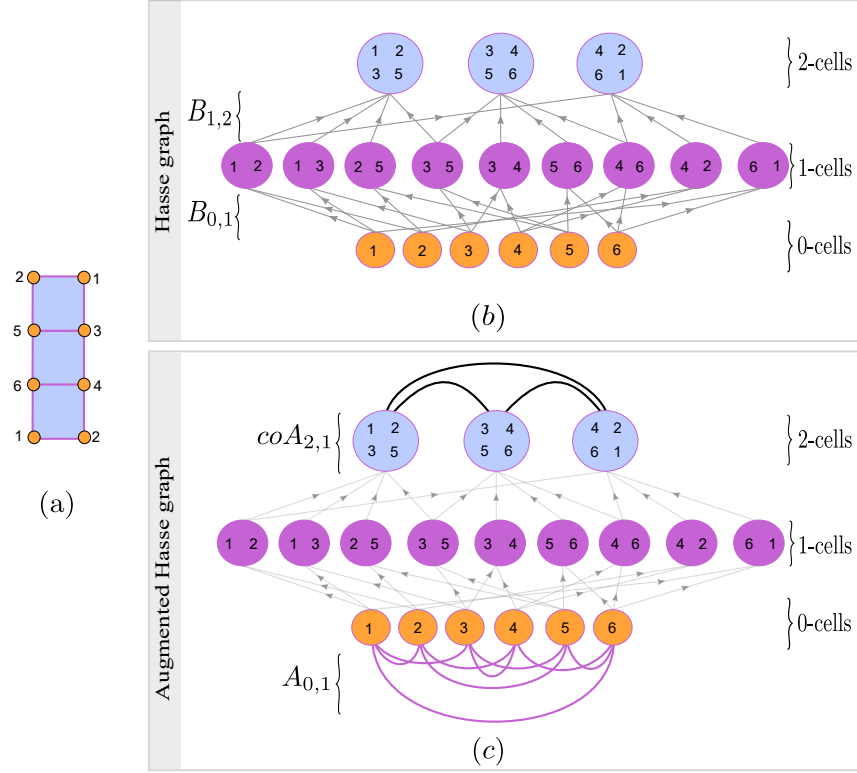
Figure 31: Example of the Hasse graph of a CC. (a): CC of a Möbius strip. (b): Hasse graph of the CC, describing the poset structure between cells. (c): Hasse graph augmented with the edges defined via $A_{0,1}$ and $coA_{2,1}$.

> **Definition 43** (Hasse graph)**.** *The **Hasse graph** of a CC $(S, \mathcal{X}, \mathrm{rk})$ is a directed graph $\mathcal{H}_{\mathcal{X}} = (V(\mathcal{H}_{\mathcal{X}}), E(\mathcal{H}_{\mathcal{X}}))$ with vertices $V(\mathcal{H}_{\mathcal{X}}) = \mathcal{X}$ and edges $E(\mathcal{H}_{\mathcal{X}}) = \{(x, y) : x \subsetneq y, \mathrm{rk}(x) = \mathrm{rk}(y) - 1\}$.*

The vertices of the Hasse graph $\mathcal{H}_{\mathcal{X}}$ of a CC $(S, \mathcal{X}, \mathrm{rk})$ are the cells of $\mathcal{X}$, while the edges of $\mathcal{H}_{\mathcal{X}}$ are determined by the immediate incidence among these cells. Figure 31 shows an example of the Hasse graph of a CC.

The *CC structure class* is the set of CCs determined up to isomorphism, according to Definition 10. Proposition 8.1 provides sufficient criteria for determining CC structure classes. The proof of Proposition 8.1 relies on the observations that CC structure classes are determined by the underlying Hasse graph representation and that the Hasse graph provides the same information as the incidence matrices $\{B_{k,k+1}\}_{k=0}^{\dim(\mathcal{X})-1}$. Figure 32 supports visually the proofs of parts 2 and 3 in Proposition 8.1.

Proposition 8.1. *Let $(S, \mathcal{X}, \mathrm{rk})$ be a CC. For the CC structure class indicated by $(S, \mathcal{X}, \mathrm{rk})$, the following sufficient conditions hold:*

1. *The CC structure class is determined by the incidence matrices $\{B_{k,k+1}\}_{k=0}^{\dim(\mathcal{X})-1}$.*

2. *The CC structure class is determined by the adjacency matrices $\{A_{k,1}\}_{k=0}^{\dim(\mathcal{X})-1}$.*

3. *The CC structure class is determined by the coadjacency matrices $\{coA_{k,1}\}_{k=1}^{\dim(\mathcal{X})}$.*

Proof. The proof of the three parts of the proposition follows by noting that the structure of a CC is determined completely by its Hasse graph representation. The first part of the proposition follows from the fact that the edges in the Hasse graph are precisely the non-zero entries of matrices $\{B_{k,k+1}\}_{k=0}^{\dim(\mathcal{X}-1)}$. The
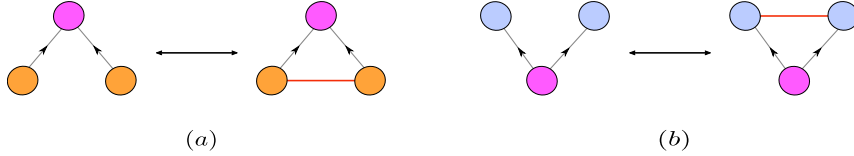
Figure 32: Relation between immediate incidence and (co)adjacency on the Hasse graph of a CC. This figure supports visually the proofs of parts 2 and 3 in Proposition 8.1. (a): Two $(k-1)$ cells x^{k-1} and y^{k-1} (orange vertices) are 1-adjacent if and only if there exists a k-cell z^k (pink vertex) that is incident to x^{k-1} and $y^{k-1}$. (b): Two $(k+1)$ cells x^{k+1} and y^{k+1} (blue vertices) are 1-coadjacent if and only if there exists a k-cell z^k (pink vertex) that is incident to x^{k+1} and y^{k+1}.

second part follows by observing that two $(k-1)$ cells x^{k-1} and y^{k-1} are 1-adjacent if and only if there exists a k-cell z^k that is incident to x^{k-1} and y^{k-1}. The third part is confirmed by noting that two $(k+1)$-cells x^{k+1} and y^{k+1} are 1-coadjacent if and only if there exists a k-cell z^k that is incident to x^{k+1} and y^{k+1}. $\square$

8.1.2   Augmented Hasse graphs

The Hasse graph of a CC is useful because it shows that computations for a higher-order deep learning model can be reduced to computations for a graph-based model. Particularly, a k-cochain (signal) being processed on a CC $\mathcal{X}$ can be thought as a signal on the corresponding vertices of the associated Hasse graph $\mathcal{H}_{\mathcal{X}}$. The edges specified by the matrices $B_{k,k+1}$ determine the message-passing structure of a given higher-order model defined on $\mathcal{X}$. However, the message-passing structure determined via the matrices $A_{r,k}$ is not directly supported on the corresponding edges of $\mathcal{H}_{\mathcal{X}}$. Thus, it is sometimes desirable to *augment the Hasse graph* with additional edges other than the ones specified by the poset partial order relation of the CC. Along these lines, Definition 44 introduces the notion of augmented Hasse graph.

> **Definition 44** (Augmented Hasse graph). *Let $\mathcal{X}$ be a CC, and let $\mathcal{H}_{\mathcal{X}}$ be its Hasse graph with vertex set $V(\mathcal{H}_{\mathcal{X}})$ and edge set $E(\mathcal{H}_{\mathcal{X}})$. Let $\mathcal{N} = \{\mathcal{N}_1, \ldots, \mathcal{N}_n\}$ be a set of neighborhood functions defined on $\mathcal{X}$. We say that $\mathcal{H}_{\mathcal{X}}$ has an augmented edge $e_{x,y}$ induced by $\mathcal{N}$ if there exist $\mathcal{N}_i \in \mathcal{N}$ such that $x \in \mathcal{N}_i(y)$ or $y \in \mathcal{N}_i(x)$. Denote by $E_{\mathcal{N}}$ the set of all augmented edges induced by $\mathcal{N}$. The **augmented Hasse graph** of $\mathcal{X}$ induced by $\mathcal{N}$ is defined to be the graph $\mathcal{H}_{\mathcal{X}}(\mathcal{N}) = (V(\mathcal{H}_{\mathcal{X}}), E(\mathcal{H}_{\mathcal{X}}) \cup E_{\mathcal{N}})$.*

It is easier to think of the augmented Hasse graph in Definition 44 in terms of the matrices $\mathbf{G} = \{G_1, \ldots, G_n\}$ associated with the neighborhood functions $\mathcal{N} = \{\mathcal{N}_1, \ldots, \mathcal{N}_n\}$. Each augmented edge in $\mathcal{H}_{\mathcal{X}}(\mathcal{N})$ corresponds to a non-zero entry in some $G_i \in \mathbf{G}$. Since $\mathcal{N}$ and $\mathbf{G}$ store equivalent information, we use $\mathcal{H}_{\mathcal{X}}(\mathbf{G})$ to denote the augmented Hasse graph induced by the edges determined by $\mathbf{G}$. For instance, the graph given in Figure 31(c) is denoted by $\mathcal{H}_{\mathcal{X}}(A_{0,1}, coA_{2,1})$.

8.1.3   Reducibility of CCNNs to graph-based models

In this section, we show that any CCNN-based computational model can be realized as a message-passing scheme over a subgraph of the augmented Hasse graph of the underlying CC. Every CCNN is determined via a computational tensor diagram, which can be built using the elementary tensor operations, namely push-forward operations, merge nodes and split nodes. Thus, the reducibility of CCNN-based computations to message-passing schemes over graphs can be achieved by proving that these three tensor operations can be executed on an augmented Hasse graph. Proposition 8.2 states that push-forward operations are executable on augmented Hasse graphs.

Proposition 8.2. *Let $\mathcal{X}$ be a CC and let $\mathcal{F}_G \colon \mathcal{C}^i(\mathcal{X}) \to \mathcal{C}^j(\mathcal{X})$ be a push-forward operator induced by a cochain map $G \colon \mathcal{C}^i(\mathcal{X}) \to \mathcal{C}^j(\mathcal{X})$. Any computation executed via $\mathcal{F}_G$ can be reduced to a corresponding computation over the augmented Hassed graph $\mathcal{H}_{\mathcal{X}}(G)$ of $\mathcal{X}$.*

Proof. Let $\mathcal{X}$ be a CC. Let $\mathcal{H}_{\mathcal{X}}(G)$ be the augmented Hasse graph of $\mathcal{X}$ determined by G. The definition of the augmented Hasse graph implies that there is a one-to-one correspondence between the vertices $\mathcal{H}_{\mathcal{X}}(G)$ and the cells in $\mathcal{X}$. Given a cell $x \in \mathcal{X}$, let x' be the corresponding vertex in $\mathcal{H}_{\mathcal{X}}(G)$. Let y be a cell in $\mathcal{X}$ with a feature vector $\mathbf{h}_y$ computed via the push-forward operation specified by Equation 3. Recall that the vector $\mathbf{h}_y$ is computed by aggregating all vectors $\mathbf{h}_x$ attached to the neighbors $x \in \mathcal{X}^i$ of y with respect to the neighborhood function $\mathcal{N}_{G^T}$. Let $m_{x,y}$ be a computation (message) that is executed between two cells x and y of $\mathcal{X}$ as a part of the computation of push-forward $\mathcal{F}_G$. It follows from the augmented Hasse graph definition that the cells x and y must have a corresponding non-zero entry in matrix G. Moreover, this non-zero entry corresponds to an edge in $\mathcal{H}_{\mathcal{X}}(G)$ between x' and y'. Thus, the computation $m_{x,y}$ between the cells x and y of $\mathcal{X}$ can be carried out as the computation (message) $m_{x',y'}$ between the corresponding vertices x' and y' of $\mathcal{H}_{\mathcal{X}}(G)$. $\qquad\square$

Similarly, computations on an arbitrary merge node can be characterized in terms of computations on a subgraph of the augmented Hasse graph of the underlying CC. Proposition 8.3 formalizes this statement.

Proposition 8.3. *Any computation executed via a merge node $\mathcal{M}_{\mathbf{G},\mathbf{W}}$ as given in Equation 1 can be reduced to a corresponding computation over the augmented Hasse graph $\mathcal{H}_{\mathcal{X}}(\mathbf{G})$ of the underlying CC.*

Proof. Let $\mathcal{X}$ be a CC. Let $\mathbf{G} = \{G_1, \ldots, G_n\}$ be a sequence of cochain operators defined on $\mathcal{X}$. Let $\mathcal{H}_{\mathcal{X}}(\mathbf{G})$ be the augmented Hasse graph determined by $\mathbf{G}$. By the augmented Hasse graph definition, there is a one-to-one correspondence between the vertices of $\mathcal{H}_{\mathcal{X}}(\mathbf{G})$ and the cells of $\mathcal{X}$. For each cell $x \in \mathcal{X}$, let x' be the corresponding vertex in $\mathcal{H}_{\mathcal{X}}(\mathbf{G})$. Let $m_{x,y}$ be a computation (message) that is executed between two cells x and y of $\mathcal{X}$ as part of the evaluation of function $\mathcal{M}_{\mathbf{G},W}$. Hence, the two cells x and y must have a corresponding non-zero entry in a matrix $G_i \in \mathbf{G}$. By the augmented Hasse graph definition, this non-zero entry corresponds to an edge in $\mathcal{H}_{\mathcal{X}}(\mathbf{G})$ between x' and y'. Thus, the computation $m_{x,y}$ between the cells x and y of $\mathcal{X}$ can be carried out as the computation (message) $m_{x',y'}$ between the corresponding vertices x' and y' of $\mathcal{H}_{\mathcal{X}}(\mathbf{G})$. $\qquad\square$

Propositions 8.2 and 8.3 ensure that push-forward and merge node computations can be realized on augmented Hasse graphs. Theorem 8.4 generalizes Propositions 8.2 and 8.3, stating that any computation on tensor diagrams is realizable on augmented Hasse graphs.

Theorem 8.4. *Any computation executed via a tensor diagram $\mathrm{CCNN}_{\mathbf{G};\mathbf{W}}$ can be reduced to a corresponding computation on the augmented Hasse graph $\mathcal{H}_{\mathcal{X}}(\mathbf{G})$.*

Proof. The conclusion follows directly from Propositions 8.1.1 and 8.2, along with the fact that any tensor diagram can be realized in terms of the three elementary tensor operations. $\qquad\square$

According to Theorem 8.4, a tensor diagram and its corresponding augmented Hasse graph encode the same computations in alternative forms. Figure 33 illustrates that the augmented Hasse graph provides a computational summary of the associated tensor diagram representation of a CCNN.

8.1.4   Augmented Hasse graphs and CC-pooling

The Hasse graph and its augmented version are graph representations of the poset structure of the underlying CC. It is instructive to interpret the (un)pooling operations (Definitions 37 and 38) with respect to these graphs. The CC-pooling operation of Definition 37 maps a signal in the poset structure from lower-rank cells to higher-rank ones. On the other hand, the CC-unpooling operation of Definition 38 maps a signal in the opposite direction. Figure 34 presents an example of CC (un)-pooling operations visualized over the augmented Hasse graph of the underlying CC.

8.1.5   Augmented Hasse diagrams, message passing, and merge nodes

The difference between constructing a CCNN using the higher-order message passing paradigm given in Section 6.1 versus using the three elementary tensor operations given in Section 5.3 has been demonstrated in Section 6.3. In particular, Section 6.3 mentions that merge nodes naturally allow for a more flexible
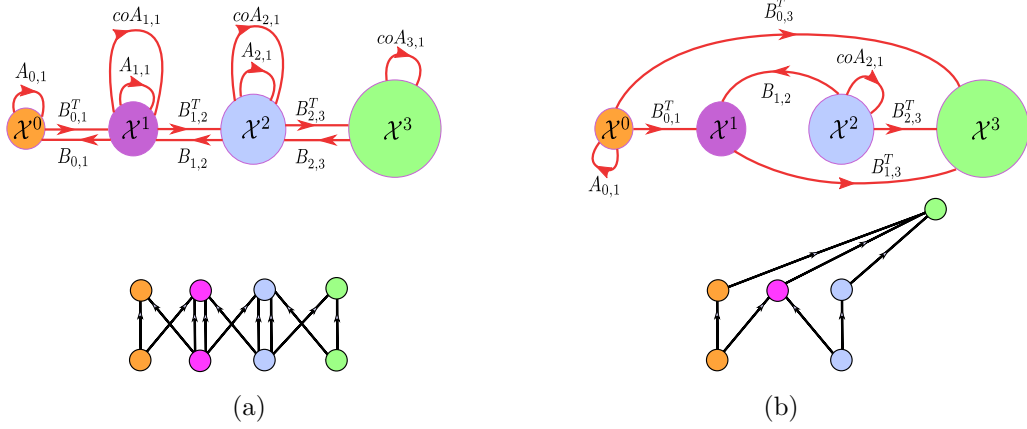
Figure 33: Tensor diagrams of two CCNNs and their corresponding augmented Hasse graphs. Edge labels are dropped from the tensor diagrams to avoid clutter, as they can be inferred from the corresponding augmented Hasse graphs. (a): A tensor diagram obtained from a higher-order message-passing scheme. (b): A tensor diagram obtained by using the three elementary tensor operations introduced in Section 5.3.
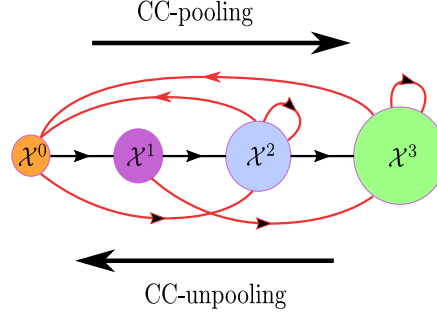
Figure 34: CC (un)-pooling operations viewed on the augmented Hasse graph of a CC. The vertices in the figure represent skeletons in the underlying CC. Black edges represent edges in the Hasse graph between these vertices, whereas red edges represent edges obtained from the augmented Hasse graph structure. CC-pooling corresponds to pushing a signal in the poset structure from lower-rank to higher-rank vertices, whereas CC-unpooling corresponds to pushing a signal in the poset structure from higher-rank to lower-rank vertices.

computational framework in comparison to the higher-order message-passing paradigm. This flexibility manifests in terms of the underlying tensor diagram as well as the input for the network under consideration. The difference between tensor operations and higher-order message passing can also be highlighted with augmented Hasse graphs, as demonstrated in Figure 33. Figure 33(a) shows a tensor diagram obtained from a higher-order message-passing scheme on a CCNN. We observe two key properties of this CCNN: the initial input cochains are supported on all cells of all dimensions of the domain, and the CCNN updates all cochains supported on all cells of all dimensions of the domain at every iteration given a predetermined set of neighborhood functions. As a consequence, the corresponding augmented Hasse graph exhibits a uniform topological structure. In contrast, Figure 33(b) shows a tensor diagram constructed using the three elementary tensor operations. As the higher-order message-passing rules do not impose constraints, the resulting augmented Hasse graph exhibits a more flexible structure.

8.1.6   Higher-order representation learning

The relation between augmented Hasse graphs and CCs given by Theorem 8.4 suggests that many graph-based deep learning constructions have analogous constructions for CCs. In this section, we demonstrate how *higher-order representation learning* can be reduced to graph representation learning [135], as an application of certain CC computations as augmented Hasse graph computations.

The goal of graph representation is to learn a mapping that embeds the vertices, edges or subgraphs of a graph into a Euclidean space, so that the resulting embedding captures useful information about the graph. Similarly, higher-order representation learning [128] involves learning an embedding of various cells in a given topological domain into a Euclidean space, preserving the main structural properties of the topological domain. More precisely, given a complex $\mathcal{X}$, higher-order representation learning refers to learning a pair (enc, dec) of functions, consisting of the *encoder map enc*: $\mathcal{X}^k \to \mathbb{R}^d$ and the *decoder map dec*: $\mathbb{R}^d \times \mathbb{R}^d \to \mathbb{R}$. The encoder function associates to every k-cell x^k in $\mathcal{X}$ a feature vector $enc(x^k)$, which encodes the structure of x^k with respect to the structures of other cells in $\mathcal{X}$. On the other hand, the decoder function associates to every pair of cell embeddings a measure of similarity, which quantifies some notion of relation between the corresponding cells. We optimize the trainable functions (enc, dec) using a context-specific *similarity measure sim*: $\mathcal{X}^k \times \mathcal{X}^k \to \mathbb{R}$ and an objective function

$$\mathcal{L}_k = \sum_{x^k \in \mathcal{X}^k} l(dec(enc(x^k), enc(y^k)), sim(x^k, y^k)), \tag{22}$$

where $l: \mathbb{R} \times \mathbb{R} \to \mathbb{R}$ is a loss function. The precise relation between higher-order and graph representation learning is given by Proposition 8.5.

Proposition 8.5. *Higher-order representation learning can be reduced to graph representation learning.*

Proof. Let $sim: \mathcal{X}^k \times \mathcal{X}^k \to \mathbb{R}$ be a similarity measure. The graph $\mathcal{G}_{\mathcal{X}^k}$ is defined as the graph whose vertex set corresponds to cells in $\mathcal{X}^k$ and whose edges correspond to cell pairs in $\mathcal{X}^k \times \mathcal{X}^k$ mapped to non-zero values by the function sim. Thus, the pair (enc, dec) corresponds to a pair $(enc_\mathcal{G}, dec_\mathcal{G})$ of the form $enc_\mathcal{G}: \mathcal{G}_{\mathcal{X}^k} \to \mathbb{R}$ and $dec_\mathcal{G}: \mathbb{R}^d \times \mathbb{R}^d \to \mathbb{R}$. Thereby, learning the pair (enc, dec) is reduced to learning the pair $(enc_\mathcal{G}, dec_\mathcal{G})$. $\square$

TopoEmbedX[8], one of our three contributed software packages, supports higher-order representation learning on cell complexes, simplicial complexes, and CCs. The main computational principle underlying TopoEmbedX is Proposition 8.5. Specifically, TopoEmbedX converts a given higher-order domain into a subgraph of the corresponding augmented Hasse graph, and then utilizes existing graph representation learning algorithms to compute the embedding of elements of this subgraph. Given the correspondence between the elements of the augmented Hasse graph and the original higher-order domain, this results in obtaining embeddings for the higher-order domain.

Remark 8.6. *Following our discussion on Hasse graphs, and particularly the ability to transform computations on a CCNN to computations on a (Hasse) graph, one may argue that GNNs are sufficient and that there is no need for CCNNs. However, this is a misleading clue, in the sense that any computation can be represented by a computational graph. Applying a standard GNN over the augmented Hasse graph of a CC is not equivalent to applying a CCNN. This point will become clearer in Section 8.2, where we introduce CCNN equivariances.*

8.2 On the equivariance of CCNNs

Analogous to their graph counterparts, higher-order deep learning models, and CCNNs in particular, should always be considered in conjunction with their underlying *equivariance* [52]. We now provide novel definitions for *permutation* and *orientation equivariance for CCNNs* and draw attention to their relations with conventional notions of equivariance defined for GNNs.

8.2.1 Permutation equivariance of CCNNs

Motivated by Proposition 8.1, which characterizes the structure of a CC, this section introduces permutation-equivariant CCNNs. We first define the action of the permutation group on the space of cochain maps.

Definition 45 (Permutation action on space of cochain maps). *Let $\mathcal{X}$ be a CC. Define* $\mathrm{Sym}(\mathcal{X}) = \prod_{i=0}^{\dim(\mathcal{X})} \mathrm{Sym}(\mathcal{X}^k)$ *the group of rank-preserving permutations of the cells of $\mathcal{X}$. Let $\mathbf{G} = \{G_k\}$ be a sequence of cochain maps defined on $\mathcal{X}$ with $G_k: \mathcal{C}^{i_k} \to \mathcal{C}^{j_k}$, $0 \leq i_k, j_k \leq \dim(\mathcal{X})$. Let $\mathcal{P} = (\mathbf{P}_i)_{i=0}^{\dim(\mathcal{X})} \in \mathrm{Sym}(\mathcal{X})$. Define the **permutation (group) action** of $\mathcal{P}$ on $\mathbf{G}$ by $\mathcal{P}(\mathbf{G}) = (\mathbf{P}_{j_k} G_k \mathbf{P}_{i_k}^T)_{i=0}^{\dim(\mathcal{X})}$.*

---

[8]https://github.com/pyt-team/TopoEmbedX

We introduce permutation-equivariant CCNNs in Definition 46, using the group action given in Definition 45. Definition 46 generalizes the relevant definitions in [235, 249]. We refer the reader to [272, 154] for a related discussion. Hereafter, we use $\mathrm{Proj}_k\colon \mathcal{C}^1 \times \cdots \times \mathcal{C}^m \to \mathcal{C}^k$ to denote the standard k-th projection for $1 \le k \le m$, defined via $\mathrm{Proj}_k(\mathbf{H}_1, \ldots, \mathbf{H}_k, \ldots, \mathbf{H}_m) = \mathbf{H}_k$.

Definition 46 (Permutation-equivariant CCNN). *Let $\mathcal{X}$ be a CC and let $\mathbf{G} = \{G_k\}$ be a finite sequence of cochain maps defined on $\mathcal{X}$. Let $\mathcal{P} = (\mathbf{P}_i)_{i=0}^{\dim(\mathcal{X})} \in \mathrm{Sym}(\mathcal{X})$. A CCNN of the form*

$$\mathrm{CCNN}_{\mathbf{G};\mathbf{W}}\colon \mathcal{C}^{i_1} \times \mathcal{C}^{i_2} \times \cdots \times \mathcal{C}^{i_m} \to \mathcal{C}^{j_1} \times \mathcal{C}^{j_2} \times \cdots \times \mathcal{C}^{j_n}$$

*is called a **permutation-equivariant CCNN** if*

$$\mathrm{Proj}_k \circ \mathrm{CCNN}_{\mathbf{G};\mathbf{W}}(\mathbf{H}_{i_1}, \ldots, \mathbf{H}_{i_m}) = \mathbf{P}_k \, \mathrm{Proj}_k \circ \mathrm{CCNN}_{\mathcal{P}(\mathbf{G});\mathbf{W}}(\mathbf{P}_{i_1}\mathbf{H}_{i_1}, \ldots, \mathbf{P}_{i_m}\mathbf{H}_{i_m}) \quad (23)$$

for all $1 \le k \le m$ and for any $(\mathbf{H}_{i_1}, \ldots, \mathbf{H}_{i_m}) \in \mathcal{C}^{i_1} \times \mathcal{C}^{i_2} \times \cdots \times \mathcal{C}^{i_m}$.

Equation 23 generalizes the corresponding notion of permutation equivariance of GNNs. Consider a graph with n vertices and adjacency matrix A. Denote a GNN on this graph by $\mathrm{GNN}_{A;W}$. Let $H \in \mathbb{R}^{n \times k}$ be vertex features. Then $\mathrm{GNN}_{A;W}$ is permutation equivariant in the sense that for $P \in \mathrm{Sym}(n)$ we have $P\,\mathrm{GNN}_{A;W}(H) = \mathrm{GNN}_{PAP^T;W}(PH)$.

In general, working with Definition 46 may be cumbersome. It is easier to characterize the equivariance in terms of merge nodes. To this end, recall that the height of a tensor diagram is the longest path from any source node to any target node. Proposition 8.7 allows us to express tensor diagrams of height one in terms of merge nodes.

Proposition 8.7. *Let $\mathrm{CCNN}_{\mathbf{G};\mathbf{W}}\colon \mathcal{C}^{i_1} \times \mathcal{C}^{i_2} \times \cdots \times \mathcal{C}^{i_m} \to \mathcal{C}^{j_1} \times \mathcal{C}^{j_2} \times \cdots \times \mathcal{C}^{j_n}$ be a CCNN with a tensor diagram of height one. Then*

$$\mathrm{CCNN}_{\mathbf{G};\mathbf{W}} = (\mathcal{M}_{\mathbf{G}_{j_1};\mathbf{W}_1}, \ldots, \mathcal{M}_{\mathbf{G}_{j_n};\mathbf{W}_n}), \quad (24)$$

where $\mathbf{G}_k \subseteq \mathbf{G}$.

Proof. Let $\mathrm{CCNN}_{\mathbf{G};\mathbf{W}}\colon \mathcal{C}^{i_1} \times \mathcal{C}^{i_2} \times \cdots \times \mathcal{C}^{i_m} \to \mathcal{C}^{j_1} \times \mathcal{C}^{j_2} \times \cdots \times \mathcal{C}^{j_n}$ be a CCNN with a tensor diagram of height one. Since the codomain of the function $\mathrm{CCNN}_{\mathbf{G};\mathbf{W}}$ is $\mathcal{C}^{j_1} \times \mathcal{C}^{j_2} \times \ldots \times \mathcal{C}^{j_n}$, then $\mathrm{CCNN}_{\mathbf{G};\mathbf{W}}$ is determined by n functions $F_k\colon \mathcal{C}^{i_1} \times \mathcal{C}^{i_2} \times \cdots \times \mathcal{C}^{i_m} \to \mathcal{C}^{j_k}$ for $1 \le k \le n$. Since the height of the tensor diagram of $\mathrm{CCNN}_{\mathbf{G};\mathbf{W}}$ is one, then each function F_k is also of height one and it is thus a merge node by definition. The result follows. $\square$

Proposition 8.7 states that every target node j_k in a tensor diagram of height one is a merge node specified by the operators $\mathbf{G}_{j_k}$ formed by the labels of the edges with target j_k. Definition 46 introduces the general notion of permutation equivariance of CCNNs. Definition 47 introduces the notion of permutation-equivariant merge node. Since a merge node is a CCNN, Definition 47 is a special case of Definition 46.

Definition 47 (Permutation-equivariant merge node). *Let $\mathcal{X}$ be a CC and let $\mathbf{G} = \{G_k\}$ be a finite sequence of cochain operators defined on $\mathcal{X}$ with $G_k\colon C^{i_k}(\mathcal{X}) \to C^j(\mathcal{X})$. Let $\mathcal{P} = (\mathbf{P}_i)_{i=0}^{\dim(\mathcal{X})} \in \mathrm{Sym}(\mathcal{X})$. We say that the merge node given in Equation 1 is a **permutation-equivariant merge node** if*

$$\mathcal{M}_{\mathbf{G};\mathbf{W}}(\mathbf{H}_{i_1}, \ldots, \mathbf{H}_{i_m}) = \mathbf{P}_j \mathcal{M}_{\mathcal{P}(\mathbf{G});\mathbf{W}}(\mathbf{P}_{i_1}\mathbf{H}_{i_1}, \ldots, \mathbf{P}_{i_1}\mathbf{H}_{i_m}) \quad (25)$$

for any $(\mathbf{H}_{i_1}, \ldots, \mathbf{H}_{i_m}) \in \mathcal{C}^{i_1} \times \mathcal{C}^{i_2} \times \cdots \times \mathcal{C}^{i_m}$.

Proposition 8.8. *Let $\mathrm{CCNN}_{\mathbf{G};\mathbf{W}}\colon \mathcal{C}^{i_1} \times \mathcal{C}^{i_2} \times \cdots \times \mathcal{C}^{i_m} \to \mathcal{C}^{j_1} \times \mathcal{C}^{j_2} \times \cdots \times \mathcal{C}^{j_n}$ be a CCNN with a tensor diagram of height one. Then $\mathrm{CCNN}_{\mathbf{G};\mathbf{W}}$ is permutation equivariant if and only the merge nodes $\mathcal{M}_{\mathbf{G}_{j_k};\mathbf{W}_k}$ given in Equation 24 are permutation equivariant for $1 \le k \le n$.*

Proof. If a CCNN is of height one, then by Proposition 8.7, $\mathrm{Proj}_k \circ \mathrm{CCNN}_{\mathbf{G};\mathbf{W}}(\mathbf{H}_{i_1}, \ldots, \mathbf{H}_{i_m}) = \mathcal{M}_{\mathbf{G}_{j_k};\mathbf{W}_k}$. Hence, the result follows from the definition of merge node permutation equivariance (Definition 47) and the definition of CCNN permutation equivariance (Definition 46). □

Finally, Theorem 8.9 characterizes the permutation equivariance of CCNNs in terms of merge nodes. From this point of view, Theorem 8.9 provides a practical version of permutation equivariance for CCNNs.

Theorem 8.9. *A* $\mathrm{CCNN}_{\mathbf{G};\mathbf{W}}$ *is permutation equivariant if and only if every merge node in* $\mathrm{CCNN}_{\mathbf{G};\mathbf{W}}$ *is permutation equivariant.*

Proof. Proposition 8.8 proves this fact for CCNNs of height one. For CCNNs of height n, it is enough to observe that a CCNN of height n is a composition of n CCNNs of height one and that the composition of two permutation-equivariant networks is a permutation-equivariant network. □

Remark 8.10. *Our permutation equivariance assumes that all cells in each dimension are independently labeled with indices. However, if we label the cells in a CC with subsets of the powerset* $\mathcal{P}(S)$ *rather than with indices, then we only need to consider permutations of the powerset that are induced by permutations of the 0-cells in order to ensure permutation equivariance.*

Remark 8.11. *A GNN is equivariant in that a permutation of the vertex set of the graph and the input signal over the vertex set yields the same permutation of the GNN output. Applying a standard GNN over the augmented Hasse graph of the underlying CC is thus not equivalent to applying a CCNN. Although the message-passing structures are the same, the weight-sharing and permutation equivariance of the standard GNN and CCNN are different. In particular, Definition 10 gives additional structure, which is not preserved by an arbitrary permutation of the vertices in the augmented Hasse graph. Thus, care is required in order to reduce message passing over a CCNN to message passing over the associated augmented Hasse graph. Specifically, one need only consider the subgroup of permutations of vertex labels in the augmented Hasse graph which are induced by permutations of 0-cells in the corresponding CC. Thus, there is merit in adopting the rich notions of topology to think about distributed, structured learning architectures, as topological constructions facilitate reasoning about computation in ways that are not within the scope of graph-based approaches.*

Remark 8.12. *Note that Proposition 8.5 does not contradict Remark 8.11. In fact, the computations described in Proposition 8.5 are conducted on a particular subgraph of the Hasse graph whose vertices are the k-cells of the underlying complex. Differences between graph-based networks and TDL networks start to emerge particularly once different dimensions are considered simultaneously during computations.*

8.2.2   Orientation equivariance of CCNNs

When CC are reduced to regular cell complexes, then orientation equivariance can also be introduced to CCNNs. Analogous to Definition 45, we introduce the following definition of orientation actions on CCs.

Definition 48 (Orientation action on space of diagonal-cochain maps)**.** *Let* $\mathcal{X}$ *be a CC. Let* $\mathbf{G} = \{G_k\}$ *be a sequence of cochain operators defined on* $\mathcal{X}$ *with* $G_k \colon \mathcal{C}^{i_k} \to \mathcal{C}^{j_k}$, $0 \leq i_k, j_k \leq \dim(\mathcal{X})$. *Let* $O(\mathcal{X})$ *be the group of tuples* $\mathcal{D} = (\mathbf{D}_i)_{i=0}^{\dim(\mathcal{X})}$ *of diagonal matrices with diagonals* ± 1 *of size* $|\mathcal{X}^k| \times |\mathcal{X}^k|$ *such that* $\mathbf{D}_0 = I$. *Define the* ***orientation (group) action*** *of* $\mathcal{D}$ *on* $\mathbf{G}$ *by* $\mathcal{D}(\mathbf{G}) = (\mathbf{D}_{j_k} G_k \mathbf{D}_{i_k})_{i=0}^{\dim(\mathcal{X})}$.

We introduce orientation-equivariant CCNNs in Definition 49, using the group action given in Definition 48. Orientation equivariance for CCNNs (Definition 49) is put forward in analogous way to permutation equivariance for CCNNs (Definition 46).

> **Definition 49** (Orientation-equivariant CCNN)**.** *Let $\mathcal{X}$ be a CC and let $\mathbf{G} = \{G_k\}$ be a finite sequence of cochain operators defined on $\mathcal{X}$. Let $\mathcal{D} \in O(\mathcal{X})$. A CCNN of the form*
>
> $$\mathrm{CCNN}_{\mathbf{G};\mathbf{W}} \colon \mathcal{C}^{i_1} \times \mathcal{C}^{i_2} \times \cdots \times \mathcal{C}^{i_m} \to \mathcal{C}^{j_1} \times \mathcal{C}^{j_2} \times \cdots \times \mathcal{C}^{j_n}$$
>
> *is called an **orientation-equivariant CCNN** if*
>
> $$\mathrm{Proj}_k \circ \mathrm{CCNN}_{\mathbf{G};\mathbf{W}}(\mathbf{H}_{i_1}, \ldots, \mathbf{H}_{i_m}) = \mathbf{D}_k \,\mathrm{Proj}_k \circ \mathrm{CCNN}_{\mathcal{D}(\mathbf{G});\mathbf{W}}((\mathbf{D}_{i_1}\mathbf{H}_{i_1}, \ldots, \mathbf{D}_{i_1}\mathbf{H}_{i_m})) \qquad (26)$$
>
> *for all $1 \leq k \leq m$ and for any $(\mathbf{H}_{i_1}, \ldots, \mathbf{H}_{i_m}) \in \mathcal{C}^{i_1} \times \mathcal{C}^{i_2} \times \cdots \times \mathcal{C}^{i_m}$.*

Propositions 8.7 and 8.8 can be stated analogously for the orientation equivariance case. We skip stating these facts here, and only state the main theorem that characterizes the orientation equivariance of CCNNs in terms of merge nodes.

Theorem 8.13. *A* $\mathrm{CCNN}_{\mathbf{G};\mathbf{W}}$ *is orientation equivariant if and only if every merge node in* $\mathrm{CCNN}_{\mathbf{G};\mathbf{W}}$ *is orientation equivariant.*

Proof. The proof of Theorem 8.13 is similar to the proof of Theorem 8.9. $\qquad\square$

9   Implementation and numerical experiments

The proposed CCNNs can be used to construct different neural network architectures for diverse learning tasks. In this section, we demonstrate the generality and the efficacy of CCNNs by evaluating their predictive performance on shape analysis and graph learning tasks. In our geometric processing experiments, we compare CCNNs against state-of-the-art methods, which are highly engineered and trained towards specific tasks. Furthermore, we conduct our experiments on various data modalities commonly studied in geometric data processing, namely on point clouds and 3D meshes. We also perform experiments on graph data. In our experiments, we tune three main components: the choice of CCNN architecture, the learning rate, and the number of replications in data augmentation. We justify the choice of CCNN architecture for each learning task. We have implemented our pipeline in PyTorch, and ran the experiments on a single GPU NVIDIA GeForce RTX 3060 Ti using a Microsoft Windows back-end.

9.1   Software: TopoNetX, TopoEmbedX, and TopoModelX

All our software development and experimental analysis have been carried out using Python. We have developed three Python packages, which we have also used to run our experiments: TopoNetX[9],TopoEmbedX[10] and TopoModelX[11]. TopoNetX supports the construction of several topological structures, including cell complex, simplicial complex, and combinatorial complex classes. These classes provide methods for computing boundary operators, Hodge Laplacians and higher-order adjacency operators on cell, simplicial, and combinatorial complexes, respectively. TopoEmbedX supports representation learning of higher-order relations on cell complexes, simplicial complexes, and combinatorial complexes. TopoModelX supports computing deep learning models defined on these topological domains.

In addition to our software package implementations, we have utilized PyTorch [219] for training the neural networks reported in this section. Also, we have utilized Scikit-learn [220] to compute the eigenvectors of the 1-Hodge Laplacians. The normal vectors of point clouds have been computed using the Point Cloud Utils package [281]. Finally, we have used NetworkX [127] and HyperNetX [155], both in the development of our software packages as well as in our computations.

---

[9]https://github.com/pyt-team/TopoNetX
[10]https://github.com/pyt-team/TopoEmbedX
[11]https://github.com/pyt-team/TopoModelX

9.2 Datasets

In our evaluation of CCNNs, we use four datasets: the Human Body, the COSEG, the SHREC11, and a benchmark dataset for graph classification taken from [39]. A summary of these datasets follows.

Human Body segmentation dataset. The original Human Body segmentation dataset presented in [12] contains relatively large meshes with a size up to 12,000 vertices. The segmentation labels provided in this dataset are set per-face, and the segmentation accuracy is defined to be the ratio of the correctly classified faces over the total number of faces in the entire dataset. In this work, we use a simplified version of the original Human Body dataset, as provided by [136], in which meshes have less than 1,000 nodes and segmentation labels are remapped to edges. We use this simplified version of the Human Body dataset for the shape analysis (i.e., mesh segmentation) task in Section 9.3.1.

COSEG segmentation dataset. The original COSEG dataset [278] contains eleven sets of shapes with ground-truth segmentation. In this work, we use a subset of the original COSEG dataset that contains relatively large sets of aliens, vases, and chairs. These three sets consist of 200, 300, and 400 shapes, respectively. We use this custom subset of the COSEG dataset for the shape analysis (i.e., mesh segmentation) task in Section 9.3.1.

SHREC11 classification dataset. SHREC 2011 [184], abbreviated as SHREC11, is a large-scale dataset that contains 600 nonrigid deformed shapes (watertight triangle meshes) from 30 categories, where each category contains an equal number of objects. Examples of these categories include hand, lamp, woman, man, flamingo, and rabbit. The dataset is available as a training and test set consisting of 480 and 120 shapes, respectively. We use the SHREC11 dataset for the shape analysis tasks in Sections 9.3.2 and 9.4.

Benchmark dataset for graph classification. This dataset has graphs belonging to three different classes [39]. For each graph, the feature vector on each vertex (the 0-cochain) is a one-hot vector of size five, and it stores the relative position of the vertices on the graph. This dataset has easy and hard versions. The easy version has highly connected graphs, while the hard version has sparse graphs. We use this dataset for the graph classification task in Section 9.3.3.

9.3 Shape analysis: mesh segmentation and classification

The CC structure used for the shape analysis experiments (mesh segmentation and classification) is simply induced by the triangulation of the meshes. Specifically, the 0-, 1-, and 2-cells are the vertices, edges, and faces of the mesh, respectively. The matrices used for the CCNNs are $B_{0,1}$, $B_{0,2}$, their transpose matrices, and the (co)adjacency matrices $A_{1,1}$, $coA_{1,1}$, and $coA_{2,1}$.

A CCNN takes a vector of cochains as input features. For shape analysis tasks, we consider cochains, whose features are built directly from the vertex coordinates of the underlying mesh. We note that other choices (e.g., spectral-based cochains as in [199]) can also be included. Our shape analysis tasks have three input cochains: the vertex, edge and face cochains. Each vertex cochain has two input features: the position and the normal vectors associated with the vertex. Similar to [136], each edge cochain consists of five features: the length of the edge, the dihedral angle, two inner angles, and two edge-length ratios for each face. Finally, each input face cochain consists of three input features: the face area, face normal, and the three face angles.

9.3.1 Mesh segmentation

For the Human Body dataset [196], we built a CCNN that produces an edge class. The tensor diagram of the architecture is shown in Figure 35(a). For the COSEG dataset [278], we built a CCNN that combines our proposed feature vectors defined on vertices, edges, and faces to learn the final face class. The architecture uses incidence matrices as well as (co)adjacency matrices to construct a signal flow as demonstrated in Figure 35(b). Specifically, the tensor diagram displays three non-squared attention-blocks and three squared attention blocks. The depth of the model is chosen to be two, as indicated in Figure 35(b).
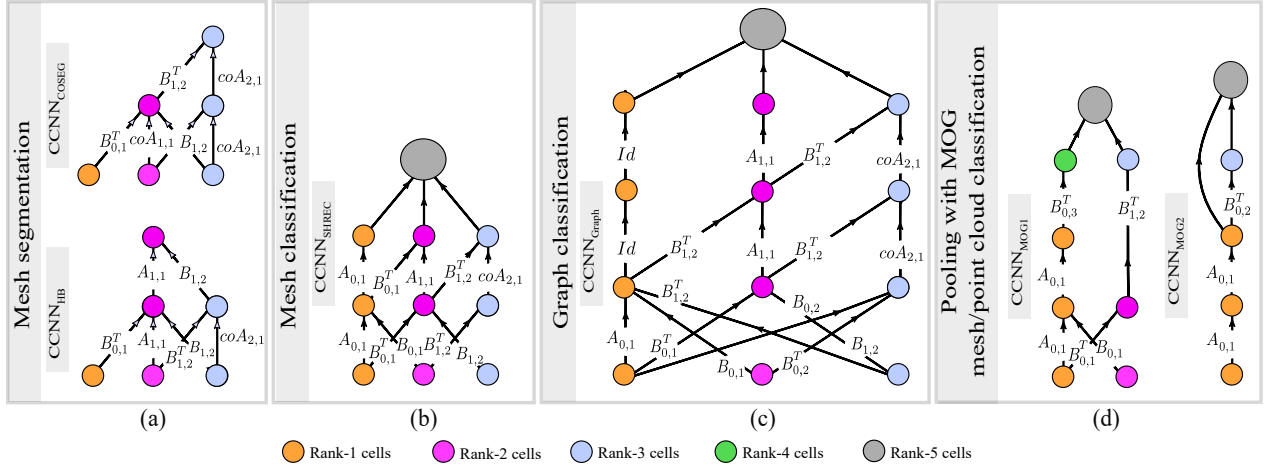
Figure 35: The tensor diagrams of the CCNNs used in our experiments. (a): The CCNNs used in the mesh segmentation tasks. In particular, CCNN$_{HB}$ and CCNN$_{COSEG}$ are the architectures used on the Human Body dataset [12] and on the COSEG dataset [278], respectively. (b): The mesh classification CCNN used on the SHREC11 dataset [184]. (c): The graph classification CCNN used on the dataset provided in [39]. (d): The mesh/point cloud classification CCNNs used in conjunction with the MOG algorithm on the SHREC11 dataset.

Table 2: Predictive accuracy on test sets related to shape analysis, namely on Human Body and COSEG (vase, chair, alien) datasets. Red and blue colors indicate best and second best results, respectively. The results reported here are based on the CCNN$_{COSEG}$ and CCNN$_{HB}$ architectures, which are visualized in Figure 35(a). In particular, the result for CCNN$_{HB}$ is reported in the first column, whereas the results for CCNN$_{COSEG}$ are reported in the second, third and forth columns.

Method	Segmentation tasks			
	Human Body	COSEG vase	COSEG chair	COSEG alien
HodgeNet	85.03	90.30	95.68	96.03
PD-MeshNet	85.61	95.36	97.23	98.18
MeshCNN	85.39	92.36	92.99	96.26
CCNN	87.30	93.40	98.30	93.70

Note that the architectures chosen for the COSEG and for the Human Body datasets have the same number and types of building blocks; compare Figures 35(a) and (b). We use a random $85\% - 15\%$ train-test split. For both of these architectures, a softmax activation is applied to the output tensor. All our segmentation models are trained for 600 epochs using a learning rate of 0.0001 and the standard cross-entropy loss. These results are consistent across Human Body and Shape COSEG datasets

We test the proposed CCNNs on mesh segmentation using the Human Body [196] and the Shape COSEG (vase, chair, and alien) [278] datasets. For each mesh in these datasets, the utilized CC structure is the one induced by the triangulation of the meshes, although other variations in the CC structure yield comparable results. Further, three k-cochains are constructed for $0 \leq k \leq 2$ and are utilized in CCNN training. As shown in Table 2, CCNNs outperform three neural networks tailored to mesh analysis (HodgeNet [260], PD-MeshNet [203] and MeshCCN [136]) on two out of four datasets, and are among the best two neural networks on all four datasets.

Architecture of CCNN$_{COSEG}$ **and** CCNN$_{HB}$**.**   In CCNN$_{COSEG}$, as shown in Figure 35(a), we choose a CCNN pooling architecture as given in Definition 41, which pushes signals from vertices, edges and faces, and aggregates their information towards the final face prediction class. We choose CCNN$_{HB}$ similarly, except that the predicted signal is an edge class. The reason for this choice is that the Human Body dataset [12] encodes the segmentation information on edges.

Table 3: Predictive accuracy on the SHREC11 test dataset. The left and right column report the mesh and point cloud classification results, respectively. The CCNN for mesh classification is $CCNN_{SHREC}$, shown in Figure 35(b), while the CCNN for point cloud classification is $CCNN_{MOG2}$, shown in Figure 35(d).

Method	Classification tasks	
	Mesh	Point cloud
HodgeNet	99.10	94.70
PD-MeshNet	99.70	99.10
MeshCNN	98.60	91.00
CCNN	99.17	95.20

Table 4: Predictive accuracy on the test set of [39] related to graph classification; red and blue colors indicate best and second best results, respectively. All results are reported using the $CCNN_{Graph}$ architecture shown in Figure 35(c).

Dataset	Method						
	Graclus	NDP	DiffPool	Top-K	SAGPool	MinCutPool	$CCNN_{Graph}$
Easy	97.81	97.93	98.64	82.47	84.23	99.02	98.90
Hard	69.08	72.67	69.98	42.80	37.71	73.80	75.79

9.3.2 Mesh and point cloud classification

We evaluate our method on mesh classification using the SHREC11 dataset [184] based on the same cochains and CC structure used in the segmentation experiment of Section 9.3.1. The CCNN architecture for our mesh classification task, denoted by $CCNN_{SHREC}$, is demonstrated in Figure 35(b). The final layer of $CCNN_{SHREC}$, depicted as a grey node in Figure 35(b), is a simple pooling operation that sums all embeddings of the CC after mapping them to the same Euclidean space. The $CCNN_{SHREC}$ is trained for 40 epochs with both tanh and identity activation functions using a learning rate of 0.005 and the standard cross-entropy loss. We use anisotropic scaling and random rotations for data augmentation. Each mesh is augmented 30 times, is centered around the vertex center of the mass, and is rescaled to fit inside the unit cube.

The $CCNN_{SHREC}$ with identity activations and tanh activations achieve predictive accuracies of 96.67% and 99.17%, respectively. Table 3 shows that CCNNs outperform two neural networks tailored to mesh analysis (HodgeNet and MeshCCN), being the second best model behind PD-MeshNet in mesh and point cloud classification. It is worth mentioning that the mesh classification CCNN requires a significantly lower number of epochs to train (40 epochs) as compared to the mesh segmentation CCNNs (600 epochs).

Architecture of $CCNN_{SHREC}$**.** The $CCNN_{SHREC}$ has two layers and is chosen as a pooling CCNN in the sense of Definition 41, similar to $CCNN_{COSEG}$ and $CCNN_{HB}$. The main difference is that the final layer of $CCNN_{SHREC}$, represented by the grey point in Figure 35(b), is a global pooling function that sums all embeddings of all dimensions (zero, one and two) of the underlying CC after mapping them to the same Euclidean space.

9.3.3 Graph classification

For the graph classification task, we use the graph classification benchmark provided in [39]; the dataset consists of graphs with three different labels. For each graph, the feature vector on each vertex (the 0-cochain) is a one-hot vector of size five, and it stores the relative position of the vertex on the graph. To construct the CC structure, we use the 2-clique complex of the input graph. We then proceed to build the CCNN for graph classification, denoted by $CCNN_{Graph}$, which is visualized in Figure 35(c). The matrices used for the construction of $CCNN_{Graph}$ are $B_{0,1}$, $B_{1,2}$, $B_{0,2}$, their transpose matrices, and the (co)adjacency matrices $A_{0,1}, A_{1,1}, coA_{2,1}$. The cochains of $CCNN_{Graph}$ are constructed as follows. For each graph in the dataset, we set the 0-cochain to be the one-hot vector of size 5 provided by the dataset. This one-hot vector stores the relative position of the vertex on the graph. We also construct the 1-cochain and 2-cochain on the 2-clique complex of the graph by considering the coordinate-wise max value of the one-hot vectors attached to the vertices of each cell. The input to $CCNN_{graoh}$ consists of the 0-cochain provided as a part of the dataset as
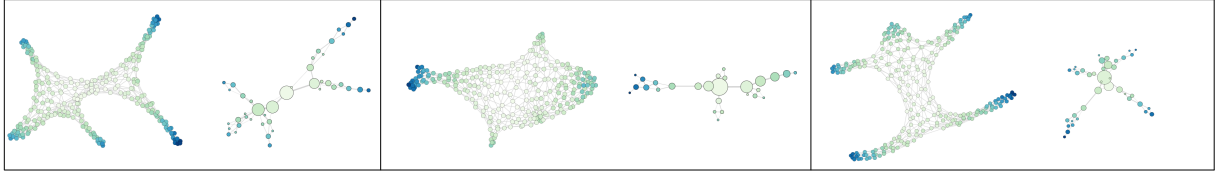
Figure 36: Examples of applying the MOG algorithm on the SHREC11 dataset [184]. In each figure, we show the original mesh graph on the left and the mapper graph on the right. The scalar function chosen for the MOG algorithm is the average geodesic distance (AGD). We observe that the pooled mapper graph has similar overall shape to the original graphs.

well as the constructed 1 and 2-cochains. The grey node in Figure 35(c) indicates a simple mean pooling operation. We train this network with a learning rate of 0.005 and no data augmentation.

Table 4 reports the results on the *easy* and the *hard* versions of the datasets[12], and compares them to six state-of-the-art GNNs. As shown in Table 4, CCNNs outperform all six GNNs on the hard dataset, and five of the GNNs on the easy dataset. The proposed CCNN outperforms MinCutPool on the hard dataset, while it attains comparable performance to MinCutPool on the easy dataset.

Architecture of $CCNN_{Graph}$**.**   In the $CCNN_{Graph}$ displayed in Figure 35(c) we choose a CCNN pooling architecture as given in Definition 41 that pushes signals from vertices, edges and faces, and aggregate their information towards the higher-order cells before making making the final prediction. For the dataset of [39], we experiment with two architectures; the first one is identical to the $CCNN_{SHREC}$ shown in Figure 35(b), and the second one is the $CCNN_{Graph}$ shown in Figure 35(c). We report the results for $CCNN_{Graph}$, as it provides superior performance. Note that when this neural network is conducted on an underlying simplicial complex, the neighborhood matrices $B_{0,1}$ and $B_{1,3}$ are typically not considered, hence the CC-structure equipped with these additional incidence matrices improves the generalization performance of the $CCNN_{Graph}$.

9.4   Pooling with mapper on graphs and data classification

We perform experiments to measure the effectiveness of the MOG pooling strategy discussed in Section 7.4. Recall that the MOG algorithm requires two pieces of input: the 1-skeleton of a CC $\mathcal{X}$, and a scalar function on the vertices of $\mathcal{X}$. Our choice for the input scalar function is the average geodesic distance (AGD) [159], which is suitable for shape detection as it is invariant to reflection and rotation. For two entities u and v on a graph, the geodesic distance between u and v, denoted by $d(v,u)$, is computed using Dijkstra's shortest path algorithm. The AGD is given by the following equation:

$$AGD(v) = \frac{1}{|V|} \sum_{u \in V} d(v,u). \tag{27}$$

From Equation 27, it is immediate that the vertices near the center of the graph are likely to have low function values, while points on the periphery are likely to have high values. This observation has been utilized to study graph symmetry [159], and it provides a justification for selecting the AGD for the MOG pooling strategy. Figure 36 presents a few examples of applying the MOG pooling strategy using AGD on the SHREC11 dataset.

In order to demonstrate the effectiveness of our MOG pooling approach, we conduct three experiments on the SHREC11 dataset: mesh classification based on CC-pooling with input vertex and edge features (Section 9.4.1), mesh classification based on CC-pooling with input vertex features only (Section 9.4.2), and point cloud classification based on CC-pooling with input vertex features only (Section 9.4.3). The experiments in Sections 9.4.1 and 9.4.2 utilize the mesh structure in the SHREC11 dataset, whereas the

---

[12]The difficulty in these datasets is controlled by the compactness degree of the graph clusters; clusters in the 'easy' data have more in-between cluster connections, while clusters in the 'hard' data are more isolated [39].

experiment in Section 9.4.3 utilizes its own point cloud version. In particular, we choose two simple CCNN architectures shown in Figure 35(d), denoted by CCNN_{MOG1} and CCNN_{MOG2}, as opposed to the more complicated architecture of CCNN_{SHREC} in Figure 35(b). The main difference between CCNN_{MOG1} and CCNN_{MOG2} is the choice of the input feature vectors as described next.

9.4.1   Mesh classification: CC-pooling with input vertex and edge features

In this experiment, we consider the vertex feature vector to be the position concatenated with the normal vectors for each vertex in the underlying mesh. For the edge features, we compute the first ten eigenvectors of the 1-Hodge Laplacian [97, 94] and attach a 10-dimensional feature vector to the edges of the underlying mesh. The CC that we consider here is 3-dimensional, as it consists of the triangular mesh (vertices, edges and faces) and of 3-cells. The 3-cells are obtained using the MOG algorithm, and are used for augmenting each mesh. We calculate the 3-cells via the MOG algorithm using the AGD scalar function as input. We conduct this experiment using the CCNN defined via the tensor diagram CCNN_{MOG1} given in Figure 35(d). During training, we augment each mesh with ten additional meshes, with each of these additional meshes being obtained by a random rotation as well as 0.1% noise perturbation to the vertex positions. We train CCNN_{MOG1} for 100 epochs using a learning rate of 0.0002 and the standard cross-entropy loss, and obtain an accuracy of 98.1%. While the accuracy of CCNN_{MOG1} is lower than the one we report for CCNN_{SHREC} (99.17%) in Table 3, we note that CCNN_{MOG1} requires a significantly smaller number of replications for mesh augmentation to achieve a similar accuracy (CCNN_{MOG1} requires 10, whereas CCNN_{SHREC} required 30 replications).

Architecture of CCNN_{MOG1}**.**   The tensor diagram CCNN_{MOG1} of Figure 35(d) corresponds to a pooling CCNN. In particular, CCNN_{MOG1} pushes forward the signal towards two different higher-order cells: the faces of the mesh as well as the 3-cells obtained from the MOG algorithm.

9.4.2   Mesh classification: CC-pooling with input vertex features only

In this experiment, we consider the position and the normal vectors of the input vertices. The CC structure that we consider is the underlying graph structure obtained from each mesh; i.e., we only use the vertices and the edges, and ignore the faces. We augment this structure by 2-cells obtained via the MOG algorithm using the AGD scalar function as input. We choose the network architecture to be relatively simpler than CCNN_{MOG1}, and report it in Figure 35(d) as CCNN_{MOG2}. During training we augment each mesh with 10 additional meshes, with each of these additional meshes being obtained by a random rotation as well as 0.05% noise perturbation to the vertex positions. We train CCNN_{MOG2} for 100 epochs using a learning rate of 0.0003 and the standard cross-entropy loss, and obtain an accuracy of 97.1%.

Architecture of CCNN_{MOG2} **for mesh classification.**   The tensor diagram CCNN_{MOG2} of Figure 35(d) corresponds to a pooling CCNN. In particular, CCNN_{MOG2} pushes forward the signal towards a single 2-cell obtained from the MOG algorithm. Observe that the overall architecture of CCNN_{MOG2} is similar in principle to AlexNet [165], where convolutional layers are followed by pooling layers.

9.4.3   Point cloud classification: CC-pooling with input vertex features only

In this experiment, we consider point cloud classification on the SHREC11 dataset. The setup is similar in principle to the one studied in Section 9.4.2 where we consider only the features supported on the vertices of the point cloud as input. Specifically, for each mesh in the SHREC11 dataset, we sample $1,000$ points from the surface of the mesh. Additionally, we estimate the normal vectors of the resulting point clouds using the Point Cloud Utils package [281]. To build the CC structure, we first consider the k-nearest neighborhood graph obtained from each point cloud using $k = 7$. We then augment this graph by 2-cells obtained via the MOG algorithm using the AGD scalar function as input. We train the CCNN_{MOG2} shown in Figure 35(d). During training, we augment each point cloud with 12 additional instances, each one of these instances being obtained by random rotation. We train CCNN_{MOG2} for 100 epochs using a learning rate of 0.0003 and the standard cross-entropy loss, and obtain an accuracy of 95.2% (see Table 3).

9.5   Ablation studies

In this section, we perform two ablation studies. The first ablation study reveals that pooling strategies in CCNNs have a crucial effect on predictive performance. The second ablation study demonstrates that CCNNs have better predictive capacity than GNNs; the advantage of CCNNs arises from their topological pooling operations and from their ability to learn from topological features.

Pooling strategies in CCNNs.   To evaluate the impact of the choice of pooling strategy on predictive performance, we experiment with two pooling strategies using the SHREC11 classification dataset. The first pooling strategy is the MOG algorithm described in Section 9.4; the results of this pooling strategy based on CCNN_{MOG2} are discussed in Section 9.4.2 (97.1%). The second pooling strategy is briefly described as follows. For each mesh, we consider the 2-dimensional CC obtained by considering each 1-hop neighborhood to be the 1-cells in the CC and each 2-hop neighborhood to be the 2-cells in the CC. We train CCNN_{MOG2}, and obtain an accuracy of 89.2%, which is lower than 97.1%. These experiments suggest that the choice of pooling strategy has a crucial effect on predictive performance.

Comparing CCNNs to GNNs in terms of predictive performance.   Observe that CCNN_{SHREC} has topological features of dimension one and two as inputs. On the other hand, CCNN_{MOG2} has only vertex features as input, but it learns the higher-order cell latent features by using the push-forward operation that pushes the signal from 0-cells to the 2-cells obtained from the MOG algorithm. In both cases, using a higher-order structure is essential for improving predictive performance, even though two different strategies towards exploiting the higher-order structures are utilized. To support our claim, we run an experiment in which we replace the pooling layer in CCNN_{MOG2} by the cochain operator induced by $A_{0,1}$, effectively rendering the neural network as a GNN. In this setting, using the same setup as in experiment 9.4.2, we obtain an accuracy of 84.56%. This experiment reveals the performance advantages of employing higher-order structures, either by utilizing the input topological features supported on higher-order cells or via pooling strategies that augment higher-order cells.

10   Related work

Topological deep learning (TDL) has recently emerged as a new research frontier that lies at the intersection of several areas, including geometric and topological machine learning, and network science. To demonstrate where TDL fits in the existing literature, we review a broad spectrum of prior works, and categorize them into graph-based models, higher-order deep learning models, graph-based pooling, attention-based models, and applied algebraic topology.

10.1   Graph-based models

Graph-based models have been widely used for modeling pairwise interactions (edges) between elements (vertices) of different systems, including social systems (e.g., social network analysis) and biological systems (e.g., protein-protein interactions), see [163, 151]. Based on their edge or vertex properties, graphs can be classified as unweighted graphs (unweighted edges), weighted graphs (weighted edges), signed graphs (signed edges), undirected or directed graphs (undirected or directed edges), and spatio-temporal graphs (spatio-temporal vertices), as discussed in [284, 123]. Each of these graph types can be combined with neural networks to form graph neural networks and model different interactions in various systems [284, 123]. For example, unweighted and undirected graph-based models have been used for omic data mapping [4] and mutual friendship detection in social networks [264]; weighted graph-based models have been widely used with systems related to traffic forecasting [294, 134] and epidemiological modeling/forecasting [186, 195]; signed graph-based models are suitable for tasks such as segmentation [17] and clustering [167, 107]; spatio-temporal graph-based models can describe systems that are spatio-temporal in nature, such as human activity and different types of motion [287, 225, 38].

As graph-based approaches that utilize single-layer or monolayer graphs cannot model multiple types of relations between vertices in a network [284, 123], multilayer or multiplex networks have been proposed [71,

296, 161]. Similar to monolayer graphs, multiplex networks contain vertices and edges, but the edges exist in separate layers, where each layer represents a specific type of interaction or relation. Multiplex networks have been used in various applications, including multilayer modeling of the human brain [84, 5] and online gaming [71]. All these types of networks can only model pairwise relations between vertices, motivating the need for higher-order networks, as discussed in Section 2.2.

10.2   Higher-order deep learning models

In recent years, there has been an increasing interest in higher-order networks [200, 30, 43] due to the ability of these networks to adequately capture higher-order interactions. Hodge-theoretic approaches, message passing schemes, and skip connections have been developed for higher-order networks in the signal processing and deep learning literature.

A Hodge-theoretic approach [185] over simplicial complexes has been introduced by [249, 22]. This effort has been extended to hypergraphs by [25, 249] and to cell complexes by [244, 236]. The work of [234] has defined an edge-based convolutional neural network by exploiting the 1-Hodge Laplacian operator for linear filtering [24, 247, 22, 23, 249].

Convolutional operators and message-passing algorithms have been developed for higher-order neural networks. For example, a convolutional operator on hypergraphs has been proposed by [152, 102, 8] and has been investigated further by [282, 15, 152, 16, 111, 121, 117]. A unifying framework for learning on graphs and hypergraphs has been proposed recently in [148]. The authors in [110] have introduced the so-called general hypergraph neural networks, which constitute a multi-modal/multi-type data correlation modeling framework. As for message passing on complexes, the work of [128] has introduced a higher-order message-passing framework that encompasses those proposed by [96, 56, 114, 139] and has utilized various local neighborhood aggregation schemes. In [204], recurrent simplicial neural networks have been proposed and applied to trajectory prediction. The authors in [58] have addressed the challenge of processing signals supported on multiple cell dimensions concurrently, by introducing a coupling multi-signal approach on higher-order networks that utilizes the Dirac operator. Several simplicial and cellular neural networks have been introduced recently, including [57, 244, 46, 236, 243, 29, 288]. For more details, the reader is referred to the recent survey of [218] on TDL.

A generalization of skip connections [140, 238] to simplicial complexes has been introduced by [131], which allows the training of higher-order deep neural networks. The authors in [209] have proposed a higher-order graph neural network that takes into account higher-order graph structures at multiple scales. While these methods allow for multi-way hierarchical coupling, the coupling is isotropic and weight differences within a particular multi-way connection can not be learned. These limitations can be alleviated by attention-based models.

Higher-order models have achieved promising performance in several real-world applications, including link prediction [75, 131, 224], action recognition [276], visual classification [254], optimal homology generator detection [156], time series [242], dynamical systems [193], spectral clustering [228], node classification [131], and trajectory prediction [235, 35].

10.3   Attention-based models

Real-world relational data is large, unstructured, sparse and noisy. As a result, graph neural networks (GNNs) may learn suboptimal data representations, and therefore may exhibit compromised performance [284, 83, 10]. To address these issues, various attention mechanisms [72] have been incorporated in GNNs, which allow to learn neural architectures that detect the most relevant parts of a given graph while ignoring irrelevant parts. Based on the used attention mechanism, existing graph attention approaches can be divided into weight-based attention, similarity-based attention, and attention-guided walk [179].

The majority of attention-based mechanisms, with the exception of [117, 120, 118, 16, 157, 112], are designed for graphs. For example, the attention model proposed by [120] is a generalization of the graph attention model of [273]. In [118], the authors have utilized a model based on Hodge decomposition, similar to the one suggested in [235], to introduce an attention model for simplicial complexes. The hypergraph attention

models introduced in [16, 157] provide alternative generalizations of the graph attention model of [273]. The aforementioned attention models neither allow nor combine higher-order attention blocks of entities of different dimensions. This limits the space of neural architectures and the scope of applications of existing attention models.

10.4   Graph-based pooling

Several attempts have been made to emulate the success of image-based pooling layers in the context of graphs. Some of the early work employs popular graph clustering algorithms [169, 93] to achieve graph-based pooling architectures [54]. Coarsening operations have been applied to graphs to attain the invariance properties needed in learning tasks [291, 202, 109, 202]. The current state-of-the-art graph-based pooling approaches mostly rely on dynamically learning the pooling needed for the learning task [125]. This includes spectral methods [192], clustering methods such as DiffPool [291] and MinCut [40], top-K methods [108, 180, 298], and hierarchical graph pooling [297, 149, 180, 298, 182, 217]. Pooling on higher-order networks remains unstudied, with the exception of a general simplicial complex pooling strategy developed by [77] along the lines of the proposal made by [125].

10.5   Applied algebraic topology

Although algebraic topology [138] is a relatively old field, applications of this field have only recently started to crystallize [98, 61]. Indeed, topological constructions have been found to be natural tools for the formulation of longstanding problems in many fields. For instance, persistent homology [98] has been successful at finding solutions to various complex data problems [11, 18, 50, 67, 81, 82, 116, 170, 174, 175, 176, 177, 191, 214, 239]. Recent years have witnessed increased interest in the role of topology in machine learning and data science [91, 141]. Topology-based machine learning models have been applied in many areas, including topological signatures of data [42, 66, 231], neuroscience [81, 82, 116, 174, 175, 176, 177], bioscience [70, 89, 187, 214, 265, 266], the study of graphs [19, 69, 279, 144, 222, 223, 129, 230], time series forcasting [293], Trojan detection [146], image segmentation [145], 3D reconstruction [275], and time-varying setups [99, 194, 221, 232].

Topological data analysis (TDA) [98, 61, 91, 189, 113] has emerged as a scientific area that harnesses topological tools to analyze data and develop machine learning algorithms. TDA has found many applications in machine learning, including enhancing existing machine learning models [142, 105, 277, 181, 36, 78], improving the explainability of deep learning models [101, 62, 190], dimensionality reduction [208], filtration learning [143], and topological layers constructions [158]. A notable research trend has been the vectorization of persistence diagrams. Vector representations of persistence diagrams are constructed in order to be utilized in downstream machine learning tasks. These methods include Betti curves [270], persistence landscapes [55], persistence images [2], and other vectorization constructions [73, 37, 168]. A unification of these methods has been proposed recently in [68].

Our work introduces combinatorial complexes (CCs) as a generalized higher-order network on which deep learning models can be defined and studied in a unifying manner. Hence, our work expands TDA by formalizing deep learning notions in topological terms and by realizing constructions in TDA, e.g., mapper [258], in terms of our TDL framework. The construction of CCs and of combinatorial complex neural networks (CCNNs), which are neural networks defined on CCs, is inspired by classical notions in algebraic topology [138] and in topological quantum field theory [269], and by recent advances in TDA [60, 61, 65, 63, 64, 66, 79] as applied to machine learning [226, 91].

11   Conclusions

We have established a topological deep learning (TDL) framework that enables the learning of representations for data supported on topological domains. To this end, we have introduced combinatorial complexes (CCs) as a new topological domain to model and characterize the main components of TDL. Our framework provides a unification for many concepts that may be perceived as separate in the current literature. Specifically, we can reduce most deep learning architectures presented thus far in the literature to particular instances of combinatorial complex neural networks (CCNNs), based on computational operations defined on CCs. Our

framework thus provides a platform for a more systematic exploration and comparison of the large space of deep learning protocols on topological spaces.

Limitations. This work has laid out the foundations of a novel TDL framework. While TDL has great potential, similar to other novel learning frameworks, there are limitations, many of which are still not well-understood. Specifically, some known limitations involve:

- *Computational complexity*: The primary challenge for moving from graphs to richer topological domains is the combinatorial increase in the complexity to store and process data defined on such domains. Training a TDL network can be a computationally intensive task, requiring careful consideration of neighborhood functions and generalization performance. TDL networks also require a large amount of memory, especially when working with a large number of matrices during network construction. The topology of the network can also increase the computational complexity of training.
- *The choice of the neural network architecture*: Choosing the appropriate neural network architecture for a given dataset and a given learning task can be challenging. The performance of a TDL network can be highly dependent on the choice of architecture and its hyperparameters.
- *Interpretability and explainability*: The architecture of a TDL network can make it difficult to interpret the learnt representations and understand how the network is making predictions.
- *Limited availability of datasets*: TDL networks require topological data, which we have found to be of limited availability. Ad hoc conversions of existing data to include higher-order relations may not always be ideal.

Future work. Aforementioned limitations leave ample room for future studies, making the realization of the full potential of TDL an interesting endeavour. While the flexible definition of CCs, as compared to, e.g., simplicial complexes, already provides some mitigation to the associated computational challenges, improving the scaling of CCNNs even further will require the exploration of sparsification techniques, randomization and other algorithmic improvements. Besides addressing the aforementioned limitations, promising directions not treated within this paper include explorations of directed [13], weighted [29], multilayer [201], and time-varying dynamic topological domains [267, 6, 290]. There are also several issues related to the selection of the most appropriate topological domain for a given dataset in the first place, which need further exploration in the future. Additionally, there is a need, but also a research opportunity, to better understand CCNN architectures from a theoretical perspective. This could in turn lead to better architectures. To illustrate this point, consider graph neural networks (GNNs) based on message passing [114], which have recently been shown to be as powerful as the Weisfeiler–Lehman isomorphism test[13] [286, 197, 209]. This connection between GNNs and classical graph-based combinatorial invariants has driven theoretical developments of the graph isomorphism problem and has inspired new architectures [286, 197, 7, 49]. We expect that connecting similar developments will also be important for TDL.

The topological viewpoint we adopt brings about many interesting properties. For example, we are able to model other types of *topological inductive biases* in our computational architectures, such as the properties that do not change under different discretizations of the underlying domain, e.g., the Euler characteristic that is commonly used to distinguish topological spaces. While isomorphisms are the primary *equivalence relation* in graph theory, *homeomorphisms* and *topological equivalence* are more relevant for data defined on topological spaces, and invariants under homeomorphisms have different machine learning applications[14]. Homeomorphism equivalence is more relevant in various applications in which domain discretization is an artifact of data processing, and not an intrinsic part of the data [253]. Further, homeomorphism equivalence translates to a similarity question between two structures. Indeed, topological data analysis has been extensively utilized towards addressing the problem of similarity between meshes [92, 133, 230]. In geometric data processing, neural network architectures that are agnostic to mesh discretization are often desirable and perform better in practice [253]. We anticipate that the development of TDL models will open up new avenues to explore topological invariants across topological domains.

---

[13]The Weisfeiler–Lehman isomorphism test [280] is a widely-used graph isomorphism algorithm that provides a coloring of a graph's vertices, and this coloring gives a necessary condition for two graphs to be isomorphic.

[14]Intuitively, two topological spaces are equivalent if one of them can be deformed to the other via a continuous transformation.

Acknowledgments

References

[1]   Peter Abramenko and Kenneth S. Brown. *Buildings: theory and applications.* Vol. 248. Springer Science & Business Media, 2008.

[2]   Henry Adams et al. "Persistence images: a stable vector representation of persistent homology". In: *J. of Mach. Learn Res.* 18.1 (2017), pp. 218–252.

[3]   Gerardo Adesso. "GPT4: the ultimate brain". In: *Authorea Preprints* (2022).

[4]   David Amar and Ron Shamir. "Constructing module maps for integrated analysis of heterogeneous biological networks". In: *Nucleic Acids Research* 42.7 (2014), pp. 4208–4219.

[5]   D. V. Anand and Moo K. Chung. "Hodge Laplacian of brain networks". In: *IEEE Transactions on Medical Imaging* (2023).

[6]   Md Sayeed Anwar and Dibakar Ghosh. "Stability of synchronization in simplicial complexes with multiple interaction layers". In: *Phys. Rev. E* 106 (3 Sept. 2022), p. 034314.

[7]   Vikraman Arvind et al. "On Weisfeiler-Leman invariance: subgraph counts and related graph properties". In: *Journal of Computer and System Sciences* 113 (2020), pp. 42–59.

[8]   Devanshu Arya and Marcel Worring. "Exploiting relational information in social networks using geometric deep learning on hypergraphs". In: *Proceedings of the 2018 ACM on International Conference on Multimedia Retrieval.* 2018, pp. 117–125.

[9]   Michael Aschbacher. "Combinatorial cell complexes". In: *Progress in Algebraic Combinatorics.* Mathematical Society of Japan, 1996, pp. 1–80.

[10] Nurul A. Asif et al. "Graph neural network: a comprehensive review on non-Euclidean space". In: *IEEE Access* 9 (2021), pp. 60588–60606.

[11] Marco Attene, Silvia Biasotti, and Michela Spagnuolo. "Shape understanding by contour-driven retiling". In: *The Visual Computer* 19.2 (2003), pp. 127–138.

[12] Matan Atzmon, Haggai Maron, and Yaron Lipman. "Point convolutional neural networks by extension operators". In: *ACM Trans. Graph.* 37.4 (July 2018).

[13] Giorgio Ausiello and Luigi Laura. "Directed hypergraphs: introduction and fundamental algorithms—a survey". In: *Theoretical Computer Science* 658 (2017), pp. 293–306.

[14] Dzmitry Bahdanau, Kyunghyun Cho, and Yoshua Bengio. "Neural machine translation by jointly learning to align and translate". In: *arXiv preprint arXiv:1409.0473* (2014).

[15] Junjie Bai et al. "Multi-scale representation learning on hypergraph for 3D shape retrieval and recognition". In: *IEEE Transactions on Image Processing* 30 (2021), pp. 5327–5338.

[16] Song Bai, Feihu Zhang, and Philip H. S. Torr. "Hypergraph convolution and hypergraph attention". In: *Pattern Recognition* 110 (2021), p. 107637.

[17] Alberto Bailoni et al. "GASP, a generalized framework for agglomerative clustering of signed graphs and its application to instance segmentation". In: *IEEE Conf. Comput. Vis. Pattern Recog.* 2022, pp. 11645–11655.

[18] Chandrajit L. Bajaj, Valerio Pascucci, and Daniel R. Schikore. "The contour spectrum". In: *Proceedings of the 8th Conference on Visualization '97*. IEEE Computer Society Press. 1997, 167–ff.

[19] Maria Bampasidou and Thanos Gentimis. "Modeling collaborations with persistent homology". In: *arXiv preprint arXiv:1403.5346* abs/1403.5346 (2014).

[20] Xiaoge Bao et al. "Impact of basic network motifs on the collective response to perturbations". In: *Nature Communications* 13.1 (2022), p. 5301.

[21] Albert-László Barabási. "Network science". In: *Philosophical Transactions of the Royal Society A: Mathematical, Physical and Engineering Sciences* 371.1987 (2013), p. 20120375.

[22] Sergio Barbarossa and Stefania Sardellitti. "Topological signal processing over simplicial complexes". In: *IEEE Transactions on Signal Processing* 68 (2020), pp. 2992–3007.

[23] Sergio Barbarossa and Stefania Sardellitti. "Topological signal processing: making sense of data building on multiway relations". In: *IEEE Signal Processing Magazine* 37.6 (2020), pp. 174–183.

[24] Sergio Barbarossa, Stefania Sardellitti, and Elena Ceci. "Learning from signals defined over simplicial complexes". In: *2018 IEEE Data Science Workshop (DSW)*. IEEE. 2018, pp. 51–55.

[25] Sergio Barbarossa and Mikhail Tsitsvero. "An introduction to hypergraph signal processing". In: *2016 IEEE International Conference on Acoustics, Speech and Signal Processing (ICASSP)*. IEEE. 2016, pp. 6425–6429.

[26] Tathagata Basak. "Combinatorial cell complexes and poincaré duality". In: *Geometriae Dedicata* 147.1 (2010), pp. 357–387.

[27] Peter Battaglia et al. "Interaction networks for learning about objects, relations and physics". In: *Proceedings of the 30th International Conference on Neural Information Processing Systems*. NIPS'16. Barcelona, Spain: Curran Associates Inc., 2016, pp. 4509–4517.

[28] Peter W. Battaglia et al. "Relational inductive biases, deep learning, and graph networks". In: *arXiv preprint arXiv:1806.01261* (2018).

[29] Claudio Battiloro et al. "Topological signal processing over weighted simplicial complexes". In: *arXiv preprint arXiv:2302.08561* (2023).

[30] Federico Battiston et al. "Networks beyond pairwise interactions: structure and dynamics". In: *Physics Reports* 874 (2020), pp. 1–92.

[31] Federico Battiston et al. "The physics of higher-order interactions in complex systems". In: *Nature Physics* 17.10 (2021), pp. 1093–1098.

[32] Dominique Beaini et al. "Directional graph networks". In: *Int. Conf. Mach. Learn.* PMLR. 2021, pp. 748–758.

[33] Austin R. Benson, David F. Gleich, and Desmond J. Higham. "Higher-order network analysis takes off, fueled by classical ideas and new data". In: *arXiv preprint arXiv:2103.05031* (2021).

[34] Austin R. Benson, David F. Gleich, and Jure Leskovec. "Higher-order organization of complex networks". In: *Science* 353.6295 (2016), pp. 163–166.

[35] Austin R. Benson et al. "Simplicial closure and higher-order link prediction". In: *Proceedings of the National Academy of Sciences* 115.48 (2018), E11221–E11230.

[36] Aicha BenTaieb and Ghassan Hamarneh. "Topology aware fully convolutional networks for histology gland segmentation". In: *Medical Image Computing and Computer-Assisted Intervention–MICCAI 2016: 19th International Conference, Athens, Greece, October 17-21, 2016, Proceedings, Part II 19*. Springer. 2016, pp. 460–468.

[37] Eric Berry et al. "Functional summaries of persistence diagrams." In: *J. Appl. Comput. Topol.* 4.2 (2020), pp. 211–262.

[38] Uttaran Bhattacharya et al. "STEP: spatial temporal graph convolutional networks for emotion perception from Gaits". In: *Proceedings of the AAAI Conference on Artificial Intelligence* 34.02 (Apr. 2020), pp. 1342–1350.

[39] Filippo Maria Bianchi, Claudio Gallicchio, and Alessio Micheli. "Pyramidal reservoir graph neural network". In: *Neurocomputing* 470 (2022), pp. 389–404.

[40] Filippo Maria Bianchi, Daniele Grattarola, and Cesare Alippi. "Spectral clustering with graph neural networks for graph pooling". In: *Int. Conf. Mach. Learn.* PMLR. 2020, pp. 874–883.

[41] Ginestra Bianconi. *Higher-order networks*. Cambridge University Press, 2021.

[42] Silvia Biasotti et al. "Describing shapes by geometrical-topological properties of real functions". In: *ACM Computing Surveys (CSUR)* 40.4 (2008), p. 12.

[43] Christian Bick et al. "What are higher-order networks?" In: *arXiv preprint arXiv:2104.11329* (2021).

[44] Jacob Charles Wright Billings et al. "Simplex2Vec embeddings for community detection in simplicial complexes". In: *arXiv preprint arXiv:1906.09068* (2019).

[45] Tolga Birdal et al. "Intrinsic dimension, persistent homology and generalization in neural networks". In: *Advances in Neural Information Processing Systems* 34 (2021), pp. 6776–6789.

[46] Cristian Bodnar et al. "Weisfeiler and Lehman go cellular: CW networks". In: *Advances in Neural Information Processing Systems* 34 (2021), pp. 2625–2640.

[47] Davide Boscaini et al. "Learning class-specific descriptors for deformable shapes using localized spectral convolutional networks". In: *Computer Graphics Forum* 34.5 (2015), pp. 13–23.

[48] Davide Boscaini et al. "Learning shape correspondence with anisotropic convolutional neural networks". In: *Advances in Neural Information Processing Systems*. 2016, pp. 3189–3197.

[49] Giorgos Bouritsas et al. "Improving graph neural network expressivity via subgraph isomorphism counting". In: *IEEE Transactions on Pattern Analysis and Machine Intelligence* 45.1 (2023), pp. 657–668.

[50] Roger L. Boyell and Henry Ruston. "Hybrid techniques for real-time radar simulation". In: *Proceedings of the November 12-14, 1963, Fall Joint Computer Conference*. ACM. 1963, pp. 445–458.

[51] Michael M. Bronstein et al. "Geometric deep learning: going beyond Euclidean data". In: *IEEE Signal Processing Magazine* 34.4 (2017), pp. 18–42.

[52] Michael M. Bronstein et al. "Geometric deep learning: grids, groups, graphs, geodesics, and gauges". In: *arXiv preprint arXiv:2104.13478* (2021).

[53] Ronald Brown. *Topology and groupoids*. www.groupoids.org, 2006.

[54] Joan Bruna et al. "Spectral networks and locally connected networks on graphs". In: *Proceedings of the 2nd International Conference on Learning Representations*. Ed. by Yoshua Bengio and Yann LeCun. ICLR 2014. Banff, AB, Canada, 2014.

[55] Peter Bubenik. "Statistical topological data analysis using persistence landscapes". In: *J. of Mach. Learn Res.* 16.1 (2015), pp. 77–102.

[56] Eric Bunch et al. "Simplicial 2-complex convolutional neural nets". In: *NeurIPS Workshop on Topological Data Analysis and Beyond* (2020).

[57] Thomas F. Burns and Tomoki Fukai. "Simplicial Hopfield networks". In: *The Eleventh International Conference on Learning Representations*. 2023.

[58] Lucille Calmon, Michael T. Schaub, and Ginestra Bianconi. "Higher-order signal processing with the Dirac operator". In: *56th Asilomar Conference on Signals, Systems, and Computers*. Pacific Grove, CA, USA: IEEE, 2022, pp. 925–929.

[59] Wenming Cao et al. "A comprehensive survey on geometric deep learning". In: *IEEE Access* 8 (2020), pp. 35929–35949.

[60] Erik Carlsson, Gunnar Carlsson, and Vin De Silva. "An algebraic topological method for feature identification". In: *International Journal of Computational Geometry & Applications* 16.04 (2006), pp. 291–314.

[61] Gunnar Carlsson. "Topology and data". In: *Bulletin of the American Mathematical Society* 46.2 (2009), pp. 255–308.

[62]   Gunnar Carlsson and Rickard Brüel Gabrielsson. "Topological approaches to deep learning". In: *Topological Data Analysis: The Abel Symposium 2018*. Springer. Springer, 2020, pp. 119–146.

[63]   Gunnar Carlsson and Facundo Mémoli. "Persistent clustering and a theorem of J. Kleinberg". In: *arXiv preprint arXiv:0808.2241* (2008).

[64]   Gunnar Carlsson and Afra Zomorodian. "The theory of multidimensional persistence". In: *Discrete & Computational Geometry* 42.1 (2009), pp. 71–93.

[65]   Gunnar Carlsson et al. "On the local behavior of spaces of natural images". In: *Int. J. Comput. Vis.* 76.1 (2008), pp. 1–12.

[66]   Gunnar Carlsson et al. "Persistence barcodes for shapes". In: *International Journal of Shape Modeling* 11.02 (2005), pp. 149–187.

[67]   Hamish Carr, Jack Snoeyink, and Michiel van de Panne. "Simplifying flexible isosurfaces using local geometric measures". In: *IEEE Visualization*. IEEE. 2004, pp. 497–504.

[68]   Mathieu Carriere et al. "PersLay: a neural network layer for persistence diagrams and new graph topological signatures". en. In: *Proceedings of the Twenty Third International Conference on Artificial Intelligence and Statistics*. PMLR, June 2020, pp. 2786–2796. (Visited on 04/24/2023).

[69]   C. J. Carstens and K. J. Horadam. "Persistent homology of collaboration networks". In: *Mathematical Problems in Engineering* 2013 (2013).

[70]   Joseph Minhow Chan, Gunnar Carlsson, and Raul Rabadan. "Topology of viral evolution". In: *Proceedings of the National Academy of Sciences* 110.46 (2013), pp. 18566–18571.

[71]   Yaomin Chang et al. "GraphRR: a multiplex graph based reciprocal friend recommender system with applications on online gaming service". In: *Knowledge-Based Systems* 251 (2022), p. 109187.

[72]   Sneha Chaudhari et al. "An attentive survey of attention models". In: *ACM Transactions on Intelligent Systems and Technology (TIST)* 12.5 (2021), pp. 1–32.

[73]   Yen-Chi Chen et al. "Statistical analysis of persistence intensity functions". In: *arXiv preprint arXiv:1510.02502* (2015).

[74]   Yunpeng Chen et al. "Graph-based global reasoning networks". In: *IEEE Conf. Comput. Vis. Pattern Recog.* 2019, pp. 433–442.

[75]   Yuzhou Chen, Yulia R. Gel, and H. Vincent Poor. "BScNets: block simplicial complex neural networks". In: *Proceedings of the AAAI Conference on Artificial Intelligence* 36.6 (June 2022), pp. 6333–6341.

[76]   Edward Choi et al. "GRAM: graph-based attention model for healthcare representation learning". In: *Proceedings of the 23rd ACM SIGKDD International Conference on Knowledge Discovery and Data Mining*. 2017, pp. 787–795.

[77]   Domenico Mattia Cinque, Claudio Battiloro, and Paolo Di Lorenzo. "Pooling strategies for simplicial convolutional networks". In: *arXiv preprint arXiv:2210.05490* (2022).

[78]   James R. Clough et al. "Explicit topological priors for deep-learning based image segmentation using persistent homology". In: *Information Processing in Medical Imaging: 26th International Conference, IPMI 2019, Hong Kong, China, June 2–7, 2019, Proceedings 26*. Springer. 2019, pp. 16–28.

[79]   Anne Collins et al. "A barcode shape descriptor for curve point cloud data". In: *Computers & Graphics* 28.6 (2004), pp. 881–894.

[80]   Keenan Crane et al. "Digital geometry processing with discrete exterior calculus". In: *ACM SIGGRAPH 2013 Courses*. Association for Computing Machinery, 2013, pp. 1–126.

[81]   Carina Curto. "What can topology tell us about the neural code?" In: *Bulletin of the American Mathematical Society* 54.1 (2017), pp. 63–78.

[82]   Y. Dabaghian et al. "A topological paradigm for hippocampal spatial map formation using persistent homology". In: *PLoS Computational Biology* 8.8 (2012), e1002581.

[83]   Enyan Dai, Charu Aggarwal, and Suhang Wang. "NRGNN: learning a label noise resistant graph neural network on sparsely and noisily labeled graphs". In: *Proceedings of the 27th ACM SIGKDD Conference on Knowledge Discovery & Data Mining*. 2021, pp. 227–236.

[84]   Manlio De Domenico. "Multilayer modeling and analysis of human brain networks". In: *GigaScience* 6.5 (Feb. 2017).

[85]   Manlio De Domenico et al. "The physics of spreading processes in multilayer networks". In: *Nature Physics* 12.10 (2016), pp. 901–906.

[86]   Haowen Deng, Tolga Birdal, and Slobodan Ilic. "PPFNet: global context aware local features for robust 3D point matching". In: *IEEE Conf. Comput. Vis. Pattern Recog.* 2018, pp. 195–205.

[87]   Songgaojun Deng et al. "Cola-GNN: cross-location attention based graph neural networks for long-term ILI prediction". In: *Proceedings of the 29th ACM International Conference on Information & Knowledge Management.* 2020, pp. 245–254.

[88]   Mathieu Desbrun, Eva Kanso, and Yiying Tong. "Discrete differential forms for computational modeling". In: *Discrete Differential Geometry.* Springer, 2008, pp. 287–324.

[89]   D. DeWoskin et al. "Applications of computational homology to the analysis of treatment response in breast cancer patients". In: *Topology and its Applications* 157.1 (2010), pp. 157–164.

[90]   Tamal K. Dey, Facundo Mémoli, and Yusu Wang. "Multiscale mapper: Topological summarization via codomain covers". In: *Proceedings of the Twenty-Seventh Annual ACM-SIAM Symposium on Discrete Algorithms.* SIAM. 2016, pp. 997–1013.

[91]   Tamal K. Dey and Yusu Wang. *Computational topology for data analysis.* Cambridge University Press, 2022.

[92]   Tamal K. Dey et al. "Persistent heat signature for pose-oblivious matching of incomplete models". In: *Computer Graphics Forum* 29.5 (2010), pp. 1545–1554.

[93]   Inderjit S. Dhillon, Yuqiang Guan, and Brian Kulis. "Weighted graph cuts without eigenvectors a multilevel approach". In: *IEEE Trans. Pattern Anal. Mach. Intell.* 29.11 (2007), pp. 1944–1957.

[94]   Jozef Dodziuk. "Finite-difference approach to the Hodge theory of harmonic forms". In: *American Journal of Mathematics* 98.1 (1976), pp. 79–104.

[95]   Benjamin Dupuis, George Deligiannidis, and Umut Şimşekli. "Generalization bounds with data-dependent fractal dimensions". In: *arXiv preprint arXiv:2302.02766* (2023).

[96]   Stefania Ebli, Michaël Defferrard, and Gard Spreemann. "Simplicial neural networks". In: *NeurIPS Workshop on Topological Data Analysis and Beyond* (2020).

[97]   Beno Eckmann. "Harmonische funktionen und randwertaufgaben in einem komplex". In: *Commentarii Mathematici Helvetici* 17.1 (1944), pp. 240–255.

[98]   Herbert Edelsbrunner and John Harer. *Computational topology: an introduction.* American Mathematical Soc., 2010.

[99]   Herbert Edelsbrunner et al. "Time-varying Reeb graphs for continuous space-time data". In: *Proceedings of the Twentieth Annual Symposium on Computational Geometry.* ACM. 2004, pp. 366–372.

[100]   Athanasios Efthymiou et al. "Graph neural networks for knowledge enhanced visual representation of paintings". In: *arXiv preprint arXiv:2105.08190* (2021).

[101]   Hamza Elhamdadi, Shaun Canavan, and Paul Rosen. "AffectiveTDA: using topological data analysis to improve analysis and explainability in affective computing". In: *IEEE Transactions on Visualization and Computer Graphics* 28.1 (2021), pp. 769–779.

[102]   Yifan Feng et al. "Hypergraph neural networks". In: *Proceedings of the AAAI Conference on Artificial Intelligence* 33.01 (2019), pp. 3558–3565.

[103]   Massimo Ferri, Dott Mattia G. Bergomi, and Lorenzo Zu. "Simplicial complexes from graphs towards graph persistence". In: *arXiv preprint arXiv:1805.10716* (2018).

[104]   Matthias Fey and Jan Eric Lenssen. "Fast graph representation learning with PyTorch Geometric". In: *arXiv preprint arXiv:1903.02428* (2019).

[105]   Rickard Brüel Gabrielsson et al. "A Topology Layer for Machine Learning". In: *Proceedings of the Twenty Third International Conference on Artificial Intelligence and Statistics.* Ed. by Silvia Chiappa and Roberto Calandra. Vol. 108. Proc. of Mach. Learn Res. PMLR, 2020, pp. 1553–1563.

[106]   Claudio Gallicchio and Alessio Micheli. "Graph echo state networks". In: *The 2010 International Joint Conference on Neural Networks (IJCNN).* IEEE. 2010, pp. 1–8.

[107]   Jean Gallier. "Spectral theory of unsigned and signed graphs. Applications to graph clustering: a survey". In: *arXiv preprint arXiv:1601.04692* (2016).

[108] Hongyang Gao and Shuiwang Ji. "Graph U-Nets". In: *Int. Conf. Mach. Learn.* PMLR. 2019, pp. 2083–2092.

[109] Hongyang Gao, Yi Liu, and Shuiwang Ji. "Topology-aware graph pooling networks". In: *IEEE Trans. Pattern Anal. Mach. Intell.* 43.12 (2021), pp. 4512–4518.

[110] Yue Gao et al. "HGNN+: general hypergraph neural networks". In: *IEEE Transactions on Pattern Analysis and Machine Intelligence* (2022).

[111] Yue Gao et al. "Hypergraph learning: methods and practices". In: *IEEE Transactions on Pattern Analysis and Machine Intelligence* (2020).

[112] Dobrik Georgiev, Marc Brockschmidt, and Miltiadis Allamanis. "HEAT: hyperedge attention networks". In: *Transactions on Machine Learning Research* (2022).

[113] Robert W. Ghrist. *Elementary applied topology.* Vol. 1. Createspace Seattle, 2014.

[114] Justin Gilmer et al. "Neural message passing for quantum chemistry". In: *Int. Conf. Mach. Learn.* PMLR. 2017, pp. 1263–1272.

[115] Benjamin Girault, Shrikanth S. Narayanan, and Antonio Ortega. "Towards a definition of local stationarity for graph signals". In: *2017 IEEE International Conference on Acoustics, Speech and Signal Processing (ICASSP).* IEEE. 2017, pp. 4139–4143.

[116] Chad Giusti, Robert Ghrist, and Danielle S. Bassett. "Two's company, three (or more) is a simplex: algebraic-topological tools for understanding higher-order structure in neural data". In: *Journal of Computational Neuroscience* 41 (2016), p. 1.

[117] Lorenzo Giusti et al. "Cell attention networks". In: *arXiv preprint arXiv:2209.08179* (2022).

[118] Lorenzo Giusti et al. "Simplicial attention networks". In: *arXiv preprint arXiv:2203.07485* (2022).

[119] Fernando de Goes, Mathieu Desbrun, and Yiying Tong. "Vector field processing on triangle meshes". In: *ACM SIGGRAPH 2016 Courses.* Association for Computing Machinery, 2016, pp. 1–49.

[120] Christopher Wei Jin Goh, Cristian Bodnar, and Pietro Lio. "Simplicial attention networks". In: *ICLR 2022 Workshop on Geometrical and Topological Representation Learning.* 2022.

[121] Xue Gong, Desmond J. Higham, and Konstantinos Zygalakis. "Generative hypergraph models and spectral embedding". In: *Scientific Reports* 13.1 (2023), p. 540.

[122] Ian Goodfellow et al. *Deep learning.* Vol. 1. MIT press Cambridge, 2016.

[123] Palash Goyal and Emilio Ferrara. "Graph embedding techniques, applications, and performance: a survey". In: *Knowledge-Based Systems* 151 (2018), pp. 78–94.

[124] Leo J. Grady and Jonathan R. Polimeni. *Discrete calculus: applied analysis on graphs for computational science.* Vol. 3. Springer, 2010.

[125] Daniele Grattarola et al. "Understanding pooling in graph neural networks". In: *IEEE Transactions on Neural Networks and Learning Systems* (2022).

[126] Celia Hacker. "K-simplex2vec: a simplicial extension of node2vec". In: *NeurIPS workshop on Topological Data Analysis and Beyond* (2020).

[127] Aric Hagberg, Pieter Swart, and Daniel S Chult. *Exploring network structure, dynamics, and function using NetworkX.* Tech. rep. Los Alamos National Lab.(LANL), Los Alamos, NM (United States), 2008.

[128] Mustafa Hajij, Kyle Istvan, and Ghada Zamzmi. "Cell complex neural networks". In: *NeurIPS 2020 Workshop TDA and Beyond* (2020).

[129] Mustafa Hajij and Paul Rosen. "An efficient data retrieval parallel Reeb graph algorithm". In: *Algorithms* 13.10 (2020), p. 258.

[130] Mustafa Hajij, Bei Wang, and Paul Rosen. "MOG: mapper on graphs for relationship preserving clustering". In: *arXiv preprint arXiv:1804.11242* (2018).

[131] Mustafa Hajij et al. "High skip networks: a higher order generalization of skip connections". In: *ICLR 2022 Workshop on Geometrical and Topological Representation Learning.* 2022.

[132] Mustafa Hajij et al. "Simplicial complex representation learning". In: *Machine Learning on Graphs (MLoG) Workshop at 15th ACM International WSD Conference* (2022).

[133] Mustafa Hajij et al. "Visual detection of structural changes in time-varying graphs using persistent homology". In: *2018 IEEE Pacific Visualization Symposium (PacificVis).* IEEE. 2018, pp. 125–134.

[134]   Hatem F. Halaoui. "Smart traffic online system (STOS): presenting road networks with time-weighted graphs". In: *2010 International Conference on Information Society*. IEEE. 2010, pp. 349–356.

[135]   William L. Hamilton, Rex Ying, and Jure Leskovec. "Representation Learning on Graphs: Methods and Applications". In: *IEEE Data Eng. Bull.* 40.3 (2017), pp. 52–74.

[136]   Rana Hanocka et al. "MeshCNN: a network with an edge". In: *ACM Trans. Graph.* 38.4 (2019), pp. 1–12.

[137]   Jakob Hansen and Robert Ghrist. "Toward a spectral theory of cellular sheaves". In: *Journal of Applied and Computational Topology* 3.4 (2019), pp. 315–358.

[138]   Allen Hatcher. *Algebraic topology.* Cambridge University Press, 2005.

[139]   Mikhail Hayhoe et al. "Stable and transferable hyper-graph neural networks". In: *arXiv preprint arXiv:2211.06513* (2022).

[140]   Kaiming He et al. "Deep Residual Learning for Image Recognition". In: *2016 IEEE Conference on Computer Vision and Pattern Recognition (CVPR)*. 2016, pp. 770–778.

[141]   Felix Hensel, Michael Moor, and Bastian Rieck. "A survey of topological machine learning methods". In: *Frontiers in Artificial Intelligence* 4 (2021), p. 681108.

[142]   Christoph Hofer et al. "Deep learning with topological signatures". In: *Adv. Neural Inform. Process. Syst.* 2017, pp. 1634–1644.

[143]   Christoph Hofer et al. "Graph filtration learning". In: *International Conference on Machine Learning.* PMLR. 2020, pp. 4314–4323.

[144]   Danijela Horak, Slobodan Maletić, and Milan Rajković. "Persistent homology of complex networks". In: *Journal of Statistical Mechanics: Theory and Experiment* (2009), P03034.

[145]   Xiaoling Hu et al. "Topology-preserving deep image segmentation". In: *Advances in Neural Information Processing Systems.* Vol. 32. Curran Associates, Inc., 2019. (Visited on 04/24/2023).

[146]   Xiaoling Hu et al. "Trigger hunting with a topological prior for Trojan detection". In: *International Conference on Learning Representations.* 2022.

[147]   Jiahui Huang et al. "Multiway non-rigid point cloud registration via learned functional map synchronization". In: *IEEE Trans. Pattern Anal. Mach. Intell.* (2022).

[148]   Jing Huang and Jie Yang. "UniGNN: a unified framework for graph and hypergraph neural networks". In: *Proceedings of the Thirtieth International Joint Conference on Artificial Intelligence, IJCAI.* 2021.

[149]   Jingjia Huang et al. "AttPool: towards hierarchical feature representation in graph convolutional networks via attention mechanism". In: *Int. Conf. Comput. Vis.* 2019, pp. 6480–6489.

[150]   Takeshi D. Itoh, Takatomi Kubo, and Kazushi Ikeda. "Multi-level attention pooling for graph neural networks: unifying graph representations with multiple localities". In: *Neural Networks* 145 (2022), pp. 356–373.

[151]   Kanchan Jha, Sriparna Saha, and Hiteshi Singh. "Prediction of protein–protein interaction using graph neural networks". In: *Scientific Reports* 12.1 (2022), pp. 1–12.

[152]   Jianwen Jiang et al. "Dynamic hypergraph neural networks." In: *IJCAI.* 2019, pp. 2635–2641.

[153]   Weiwei Jiang and Jiayun Luo. "Graph neural network for traffic forecasting: a survey". In: *Expert Systems with Applications* (2022), p. 117921.

[154]   Fabian Jogl. "Do we need to improve message passing? Improving graph neural networks with graph transformations". PhD thesis. Vienna University of Technology, 2022.

[155]   Cliff A Joslyn et al. "Hypernetwork science: from multidimensional networks to computational topology". In: *Unifying Themes in Complex Systems X: Proceedings of the Tenth International Conference on Complex Systems.* Springer. 2021, pp. 377–392.

[156]   Alexandros D. Keros, Vidit Nanda, and Kartic Subr. "Dist2Cycle: a simplicial neural network for homology localization". In: *Proceedings of the AAAI Conference on Artificial Intelligence* 36.7 (June 2022), pp. 7133–7142.

[157]   Eun-Sol Kim et al. "Hypergraph attention networks for multimodal learning". In: *IEEE Conf. Comput. Vis. Pattern Recog.* 2020, pp. 14581–14590.

[158]   Kwangho Kim et al. "Pllay: Efficient topological layer based on persistent landscapes". In: *Advances in Neural Information Processing Systems* 33 (2020), pp. 15965–15977.

[159] Vladimir G Kim et al. "Möbius transformations for global intrinsic symmetry analysis". In: *Computer Graphics Forum* 29.5 (2010), pp. 1689–1700.

[160] Thomas N. Kipf and Max Welling. "Semi-supervised classification with graph convolutional networks". In: *arXiv preprint arXiv:1609.02907* (2016).

[161] Mikko Kivelä et al. "Multilayer networks". In: *Journal of complex networks* 2.3 (2014), pp. 203–271.

[162] Reinhard Klette. "Cell complexes through time". In: *Vision Geometry IX*. Vol. 4117. SPIE. 2000, pp. 134–145.

[163] David Knoke and Song Yang. *Social network analysis*. SAGE publications, 2019.

[164] Iasonas Kokkinos et al. "Intrinsic shape context descriptors for deformable shapes". In: *IEEE Conf. Comput. Vis. Pattern Recog.* IEEE. 2012, pp. 159–166.

[165] Alex Krizhevsky, Ilya Sutskever, and Geoffrey E Hinton. "Imagenet classification with deep convolutional neural networks". In: *Communications of the ACM* 60.6 (2017), pp. 84–90.

[166] Alex Krizhevsky, Ilya Sutskever, and Geoffrey E. Hinton. "ImageNet classification with deep convolutional neural networks". In: *Advances in Neural Information Processing Systems*. 2012, pp. 1097–1105.

[167] Jérôme Kunegis et al. "Spectral analysis of signed graphs for clustering, prediction and visualization". In: *Proceedings of the 2010 SIAM international conference on data mining*. SIAM. 2010, pp. 559–570.

[168] Genki Kusano, Yasuaki Hiraoka, and Kenji Fukumizu. "Persistence weighted Gaussian kernel for topological data analysis". In: *Int. Conf. Mach. Learn.* 2016, pp. 2004–2013.

[169] Dan Kushnir, Meirav Galun, and Achi Brandt. "Fast multiscale clustering and manifold identification". In: *Pattern Recognition* 39.10 (2006), pp. 1876–1891.

[170] In So Kweon and Takeo Kanade. "Extracting topographic terrain features from elevation maps". In: *CVGIP: image understanding* 59.2 (1994), pp. 171–182.

[171] Valerio La Gatta et al. "Music recommendation via hypergraph embedding". In: *IEEE Transactions on Neural Networks and Learning Systems* (2022).

[172] Renaud Lambiotte, Martin Rosvall, and Ingo Scholtes. "From networks to optimal higher-order models of complex systems". In: *Nature physics* 15.4 (2019), pp. 313–320.

[173] Yann LeCun et al. "Gradient-based learning applied to document recognition". In: *Proceedings of the IEEE* 86.11 (1998), pp. 2278–2324.

[174] Hyekyoung Lee et al. "Computing the shape of brain networks using graph filtration and gromov-hausdorff metric". In: *International Conference on Medical Image Computing and Computer Assisted Intervention* (2011), pp. 302–309.

[175] Hyekyoung Lee et al. "Discriminative persistent homology of brain networks". In: *IEEE International Symposium on Biomedical Imaging: From Nano to Macro* (2011), pp. 841–844.

[176] Hyekyoung Lee et al. "Persistent brain network homology from the perspective of dendrogram". In: *IEEE Transactions on Medical Imaging* 31.12 (2012), pp. 2267–2277.

[177] Hyekyoung Lee et al. "Weighted functional brain network modeling via network filtration". In: *NIPS Workshop on Algebraic Topology and Machine Learning* (2012).

[178] John Boaz Lee, Ryan Rossi, and Xiangnan Kong. "Graph classification using structural attention". In: *Proceedings of the 24th ACM SIGKDD International Conference on Knowledge Discovery & Data Mining*. 2018, pp. 1666–1674.

[179] John Boaz Lee et al. "Attention models in graphs: a survey". In: *ACM Transactions on Knowledge Discovery from Data (TKDD)* 13.6 (2019), pp. 1–25.

[180] Junhyun Lee, Inyeop Lee, and Jaewoo Kang. "Self-attention graph pooling". In: *Int. Conf. Mach. Learn.* PMLR. 2019, pp. 3734–3743.

[181] Samuel Leventhal et al. "Exploring classification of topological priors with machine learning for feature extraction". In: *IEEE Transactions on Visualization and Computer Graphics* (2023).

[182] Juanhui Li et al. "Graph pooling with representativeness". In: *2020 IEEE International Conference on Data Mining (ICDM)*. IEEE. 2020, pp. 302–311.

[183] Zhifei Li et al. "Learning knowledge graph embedding with heterogeneous relation attention networks". In: *IEEE Transactions on Neural Networks and Learning Systems* (2021).

[184]   Z. Lian et al. "Shape retrieval on non-rigid 3D watertight meshes". In: *Eurographics workshop on 3d object retrieval (3DOR)*. Citeseer. 2011.

[185]   Lek-Heng Lim. "Hodge Laplacians on graphs". In: *SIAM Review* 62.3 (2020), pp. 685–715.

[186]   Kevin Linka et al. "Outbreak dynamics of COVID-19 in Europe and the effect of travel restrictions". In: *Computer methods in biomechanics and biomedical engineering* 23.11 (2020), pp. 710–717.

[187]   Derek Lo and Briton Park. "Modeling the spread of the Zika virus using topological data analysis". In: *arXiv preprint arXiv:1612.03554* (2016).

[188]   Andreas Loukas. "What graph neural networks cannot learn: depth vs width". In: *arXiv preprint arXiv:1907.03199* (2019).

[189]   Ephy R. Love et al. "Topological convolutional layers for deep learning". In: *J. of Mach. Learn Res.* 24.59 (2023), pp. 1–35.

[190]   Ephy R. Love et al. "Topological deep learning". In: *arXiv preprint arXiv:2101.05778* (2021).

[191]   P. Y. Lum et al. "Extracting insights from the shape of complex data using topology". In: *Scientific reports* 3 (2013), p. 1236.

[192]   Yao Ma et al. "Graph convolutional networks with eigenpooling". In: *Proceedings of the 25th ACM SIGKDD international conference on knowledge discovery & data mining*. 2019, pp. 723–731.

[193]   Soumen Majhi, Matjaž Perc, and Dibakar Ghosh. "Dynamics on higher-order networks: a review". In: *Journal of the Royal Society Interface* 19.188 (2022), p. 20220043.

[194]   Slobodan Maletić, Yi Zhao, and Milan Rajković. "Persistent topological features of dynamical systems". In: *Chaos: An Interdisciplinary Journal of Nonlinear Science* 26.5 (2016), p. 053105.

[195]   Ronald Manríéquez, Camilo Guerrero-Nancuante, and Carla Taramasco. "Protection strategy against an epidemic disease on edge-weighted graphs applied to a COVID-19 case". In: *Biology* 10.7 (2021), p. 667.

[196]   Haggai Maron et al. "Convolutional neural networks on surfaces via seamless toric covers." In: *ACM Trans. Graph.* 36.4 (2017), pp. 71–1.

[197]   Haggai Maron et al. "Provably powerful graph networks". In: *arXiv preprint arXiv:1905.11136* (2019).

[198]   Jonathan Masci et al. "Geodesic convolutional neural networks on Riemannian manifolds". In: *IEEE Conf. Comput. Vis. Pattern Recog.* 2015, pp. 37–45.

[199]   Daniel Mejia, Oscar Ruiz-Salguero, and Carlos A. Cadavid. "Spectral-based mesh segmentation". In: *International Journal on Interactive Design and Manufacturing (IJIDeM)* 11.3 (2017), pp. 503–514.

[200]   Jerry M. Mendel. "Tutorial on higher-order statistics (spectra) in signal processing and system theory: theoretical results and some applications". In: *Proceedings of the IEEE* 79.3 (1991), pp. 278–305.

[201]   Giulia Menichetti, Luca Dall'Asta, and Ginestra Bianconi. "Control of multilayer networks". In: *Scientific reports* 6.1 (2016), pp. 1–8.

[202]   Diego Mesquita, Amauri Souza, and Samuel Kaski. "Rethinking pooling in graph neural networks". In: *Adv. Neural Inform. Process. Syst.* 33 (2020), pp. 2220–2231.

[203]   Francesco Milano et al. "Primal-dual mesh convolutional neural networks". In: *Adv. Neural Inform. Process. Syst.* 33 (2020), pp. 952–963.

[204]   Edward C. Mitchell et al. "A topological deep learning framework for neural spike decoding". In: *arXiv preprint arXiv:2212.05037* (2022).

[205]   Tom M. Mitchell. *The need for biases in learning generalizations*. Citeseer, 1980.

[206]   Volodymyr Mnih, Nicolas Heess, Alex Graves, et al. "Recurrent models of visual attention". In: *Advances in neural information processing systems* 27 (2014).

[207]   Federico Monti et al. "Geometric deep learning on graphs and manifolds using mixture model CNNs". In: *IEEE Conf. Comput. Vis. Pattern Recog.* 2017, pp. 5115–5124.

[208]   Michael Moor et al. "Topological autoencoders". In: *International conference on machine learning*. PMLR. 2020, pp. 7045–7054.

[209]   Christopher Morris et al. "Weisfeiler and Leman go neural: higher-order graph neural networks". In: *Proceedings of the AAAI Conference on Artificial Intelligence* 33.01 (2019), pp. 4602–4609.

[210]   James R. Munkres. *Elements of algebraic topology*. CRC press, 2018.

[211] James R. Munkres. *Topology; a first course.* Prentice-Hall, 1974.

[212] Kevin A. Murgas, Emil Saucan, and Romeil Sandhu. "Hypergraph geometry reflects higher-order dynamics in protein interaction networks". In: *Scientific Reports* 12.1 (2022), p. 20879.

[213] Behnam Neyshabur et al. "The role of over-parametrization in generalization of neural networks". In: *7th International Conference on Learning Representations, ICLR 2019.* 2019.

[214] Monica Nicolau, Arnold J. Levine, and Gunnar Carlsson. "Topology based data analysis identifies a subgroup of breast cancers with a unique mutational profile and excellent survival". In: *Proceedings of the National Academy of Sciences* 108.17 (2011), pp. 7265–7270.

[215] Christopher Oballe et al. "Bayesian topological signal processing". In: *Discrete & Continuous Dynamical Systems-S* (2021).

[216] Antonio Ortega et al. "Graph signal processing: overview, challenges, and applications". In: *Proceedings of the IEEE* 106.5 (2018), pp. 808–828.

[217] Yunsheng Pang, Yunxiang Zhao, and Dongsheng Li. "Graph pooling via coarsened graph infomax". In: *Proceedings of the 44th International ACM SIGIR Conference on Research and Development in Information Retrieval.* 2021, pp. 2177–2181.

[218] Mathilde Papillon et al. "Architectures of topological deep learning: a survey on topological neural networks". In: *arXiv preprint arXiv:2304.10031* (2023).

[219] Adam Paszke et al. "Automatic differentiation in PyTorch". In: *NIPS Workshop.* 2017.

[220] F. Pedregosa et al. "Scikit-learn: machine learning in Python". In: *J. of Mach. Learn Res.* 12 (2011), pp. 2825–2830.

[221] Jose A. Perea et al. "SW1PerS: sliding windows and 1-persistence scoring; discovering periodicity in gene expression time series data". In: *BMC bioinformatics* 16.1 (2015), p. 257.

[222] Giovanni Petri et al. "Networks and cycles: a persistent homology approach to complex networks". In: *Proceedings European Conference on Complex Systems 2012, Springer Proceedings in Complexity* (2013), pp. 93–99.

[223] Giovanni Petri et al. "Topological strata of weighted complex networks". In: *PLoS ONE* 8.6 (2013).

[224] Simone Piaggesi, André Panisson, and Giovanni Petri. "Effective higher-order link prediction and reconstruction from simplicial complex embeddings". In: *Learning on Graphs Conference.* PMLR. 2022, pp. 55–1.

[225] Chiara Plizzari, Marco Cannici, and Matteo Matteucci. "Spatial temporal transformer network for skeleton-based action recognition". In: *Int. Conf. Pattern Recog.* Springer. 2021, pp. 694–701.

[226] Chi Seng Pun, Kelin Xia, and Si Xian Lee. "Persistent-homology-based machine learning and its applications–a survey". In: *arXiv preprint arXiv:1811.00252* (2018).

[227] Charles R. Qi et al. "PointNet: deep learning on point sets for 3D classification and segmentation". In: *IEEE Conf. Comput. Vis. Pattern Recog.* 2017, pp. 652–660.

[228] Thummaluru Siddartha Reddy, Sundeep Prabhakar Chepuri, and Pierre Borgnat. "Clustering with simplicial complexes". In: *arXiv preprint arXiv:2303.07646* (2023).

[229] Davis Rempe et al. "CASPR: learning canonical spatiotemporal point cloud representations". In: *Adv. Neural Inform. Process. Syst.* 33 (2020), pp. 13688–13701.

[230] Bastian Rieck, Christian Bock, and Karsten Borgwardt. "A persistent Weisfeiler-Lehman procedure for graph classification". In: *International Conference on Machine Learning.* PMLR. 2019, pp. 5448–5458.

[231] Bastian Rieck and Heike Leitte. "Persistent homology for the evaluation of dimensionality reduction schemes". In: *Computer Graphics Forum* 34.3 (2015), pp. 431–440.

[232] Bastian Rieck et al. "Uncovering the topology of time-varying fMRI data using cubical persistence". In: *Advances in Neural Information Processing Systems (NeurIPS).* Ed. by H. Larochelle et al. Vol. 33. Curran Associates, Inc., 2020, pp. 6900–6912.

[233] Michael Robinson. *Topological signal processing.* Vol. 81. Springer, 2014.

[234] T Mitchell Roddenberry and Santiago Segarra. "HodgeNet: graph neural networks for edge data". In: *2019 53rd Asilomar Conference on Signals, Systems, and Computers.* IEEE. 2019, pp. 220–224.

[235] T. Mitchell Roddenberry, Nicholas Glaze, and Santiago Segarra. "Principled simplicial neural networks for trajectory prediction". In: *Int. Conf. Mach. Learn.* PMLR. 2021, pp. 9020–9029.

[236] T. Mitchell Roddenberry, Michael T. Schaub, and Mustafa Hajij. "Signal processing on cell complexes". In: *ICASSP* (2022).

[237] Robin Rombach et al. "High-resolution image synthesis with latent diffusion models". In: *IEEE Conf. Comput. Vis. Pattern Recog.* 2022, pp. 10684–10695.

[238] Olaf Ronneberger, Philipp Fischer, and Thomas Brox. "U-Net: convolutional networks for biomedical image segmentation". In: *International Conference on Medical image computing and computer-assisted intervention.* Springer. 2015, pp. 234–241.

[239] Paul Rosen et al. "Using contour trees in the analysis and visualization of radio astronomy data cubes". In: *arXiv preprint arXiv:1704.04561* (2017), pp. 1–7.

[240] Alvaro Sanchez-Gonzalez et al. "Learning to simulate complex physics with graph networks". In: *Int. Conf. Mach. Learn.* PMLR. 2020, pp. 8459–8468.

[241] Adam Santoro et al. "A simple neural network module for relational reasoning". In: *Advances in neural information processing systems.* 2017, pp. 4967–4976.

[242] Andrea Santoro et al. "Higher-order organization of multivariate time series". In: *Nature Physics* (2023), pp. 1–9.

[243] Stefania Sardellitti and Sergio Barbarossa. "Topological signal representation and processing over cell complexes". In: *arXiv preprint arXiv:2201.08993* (2022).

[244] Stefania Sardellitti, Sergio Barbarossa, and Lucia Testa. "Topological signal processing over cell complexes". In: *Proceeding IEEE Asilomar Conference. Signals, Systems and Computers* (2021).

[245] Maxime Savoy. "Combinatorial cell complexes: duality, reconstruction and causal cobordisms". In: *arXiv preprint arXiv:2201.12846* (2022).

[246] Franco Scarselli et al. "The graph neural network model". In: *IEEE transactions on neural networks* 20.1 (2008), pp. 61–80.

[247] Michael T. Schaub and Santiago Segarra. "Flow smoothing and denoising: graph signal processing in the edge-space". In: *2018 IEEE Global Conference on Signal and Information Processing (GlobalSIP).* 2018, pp. 735–739.

[248] Michael T. Schaub et al. "Random walks on simplicial complexes and the normalized Hodge 1-Laplacian". In: *SIAM Review* 62.2 (2020), pp. 353–391.

[249] Michael T. Schaub et al. "Signal processing on higher-order networks: livin'on the edge... and beyond". In: *Signal Processing* 187 (2021), p. 108149.

[250] Michael T. Schaub et al. "Signal processing on simplicial complexes". In: *Higher-Order Systems.* Springer, 2022, pp. 301–328.

[251] Yair Schiff et al. "Characterizing the latent space of molecular deep generative models with persistent homology metrics". In: *arXiv preprint arXiv:2010.08548* (2020).

[252] Michael Schlichtkrull et al. "Modeling relational data with graph convolutional networks". In: *European Semantic Web Conference.* Springer. 2018, pp. 593–607.

[253] Nicholas Sharp et al. "DiffusionNet: discretization agnostic learning on surfaces". In: *ACM Trans. Graph.* 41.3 (2022), pp. 1–16.

[254] Heyuan Shi et al. "Hypergraph-induced convolutional networks for visual classification". In: *IEEE transactions on neural networks and learning systems* 30.10 (2018), pp. 2963–2972.

[255] Jonathan Shlomi, Peter Battaglia, and Jean-Roch Vlimant. "Graph neural networks in particle physics". In: *Machine Learning: Science and Technology* 2.2 (2020), p. 021001.

[256] David I. Shuman, Benjamin Ricaud, and Pierre Vandergheynst. "Vertex-frequency analysis on graphs". In: *Applied and Computational Harmonic Analysis* 40.2 (2016), pp. 260–291.

[257] Karen Simonyan and Andrew Zisserman. "Very deep convolutional networks for large-scale image recognition". In: *arXiv preprint arXiv:1409.1556* (2014).

[258] Gurjeet Singh, Facundo Mémoli, Gunnar E Carlsson, et al. "Topological methods for the analysis of high dimensional data sets and 3d object recognition." In: *PBG@ Eurographics* 2 (2007), pp. 091–100.

[259] Per Sebastian Skardal et al. "Higher-order interactions improve optimal collective dynamics on networks". In: *arXiv preprint arXiv:2108.08190* (2021).

[260]   Dmitriy Smirnov and Justin Solomon. "HodgeNet: learning spectral geometry on triangle meshes". In: *ACM Trans. Graph.* 40.4 (2021), pp. 1–11.

[261]   Zidong Su, Zehui Hu, and Yangding Li. "Hierarchical graph representation learning with local capsule pooling". In: *ACM Multimedia Asia.* Association for Computing Machinery, 2021, pp. 1–7.

[262]   Yizhou Sun et al. "RankClus: integrating clustering with ranking for heterogeneous information network analysis". In: *Proceedings of the 12th international conference on extending database technology: advances in database technology.* 2009, pp. 565–576.

[263]   Ilya Sutskever, Oriol Vinyals, and Quoc V. Le. "Sequence to sequence learning with neural networks". In: *Advances in neural information processing systems.* 2014, pp. 3104–3112.

[264]   Shazia Tabassum et al. "Social network analysis: an overview". In: *Wiley Interdisciplinary Reviews: Data Mining and Knowledge Discovery* 8.5 (2018), e1256.

[265]   Dane Taylor et al. "Topological data analysis of contagion maps for examining spreading processes on networks". In: *Nature communications* 6 (2015), p. 7723.

[266]   Chad M Topaz, Lori Ziegelmeier, and Tom Halverson. "Topological data analysis of biological aggregation models". In: *PloS one* 10.5 (2015), e0126383.

[267]   Leo Torres et al. "The why, how, and when of representations for complex systems". In: *SIAM Review* 63.3 (2021), pp. 435–485.

[268]   Nathaniel Trask, Andy Huang, and Xiaozhe Hu. "Enforcing exact physics in scientific machine learning: a data-driven exterior calculus on graphs". In: *Journal of Computational Physics* (2022), p. 110969.

[269]   Vladimir G. Turaev. *Quantum invariants of knots and 3-manifolds.* Vol. 18. Walter de Gruyter GmbH & Co KG, 2016.

[270]   Yuhei Umeda. "Time series classification via topological data analysis". In: *Information and Media Technologies* 12 (2017), pp. 228–239.

[271]   Ashish Vaswani et al. "Attention is all you need". In: *Advances in neural information processing systems* 30 (2017).

[272]   Petar Veličković. "Message passing all the way up". In: *ICLR 2022 Workshop on Geometrical and Topological Representation Learning* (2022).

[273]   Petar Veličković et al. "Graph attention networks". In: *International Conference on Learning Representations.* 2018.

[274]   Michelle L. Wachs. "Poset topology: tools and applications". In: *arXiv preprint math/0602226* (2006).

[275]   Dominik J. E. Waibel et al. "Capturing Shape Information with Multi-Scale Topological Loss Terms for 3D Reconstruction". en. In: *Medical Image Computing and Computer Assisted Intervention – MICCAI 2022.* Ed. by Linwei Wang et al. Lecture Notes in Computer Science. Cham: Springer Nature Switzerland, 2022, pp. 150–159.

[276]   Cheng Wang et al. "Survey of hypergraph neural networks and its application to action recognition". In: *Artificial Intelligence: Second CAAI International Conference, CICAI 2022, Beijing, China, August 27–28, 2022, Revised Selected Papers, Part II.* Springer. 2023, pp. 387–398.

[277]   Fan Wang et al. "Topogan: A topology-aware generative adversarial network". In: *Eur. Conf. Comput. Vis.* Springer. 2020, pp. 118–136.

[278]   Yunhai Wang et al. "Active co-analysis of a set of shapes". In: *ACM Trans. Graph.* 31.6 (2012), pp. 1–10.

[279]   E. Weinan, Luan Jianfeng, and Yao Yuan. "The landscape of complex networks: critical nodes and a hierarchical decomposition". In: *Methods and applications of analysis* 20 (2013), pp. 383–404.

[280]   Boris Weisfeiler and Andrei Leman. "The reduction of a graph to canonical form and the algebra which appears therein". In: *NTI, Series* 2.9 (1968), pp. 12–16.

[281]   Francis Williams. *Point Cloud Utils.* 2022.

[282]   Hanrui Wu and Michael K. Ng. "Hypergraph convolution on nodes-hyperedges network for semi-supervised node classification". In: *ACM Transactions on Knowledge Discovery from Data (TKDD)* 16.4 (2022), pp. 1–19.

[283]   Zhirong Wu et al. "3D ShapeNets: a deep representation for volumetric shapes". In: *IEEE Conf. Comput. Vis. Pattern Recog.* 2015, pp. 1912–1920.

[284] Zonghan Wu et al. "A comprehensive survey on graph neural networks". In: *IEEE transactions on neural networks and learning systems* 32.1 (2020), pp. 4–24.

[285] Chenxin Xu et al. "GroupNet: multiscale hypergraph neural networks for trajectory prediction with relational reasoning". In: *IEEE Conf. Comput. Vis. Pattern Recog.* 2022, pp. 6498–6507.

[286] Keyulu Xu et al. "How powerful are graph neural networks?" In: *arXiv preprint arXiv:1810.00826* (2018).

[287] Sijie Yan, Yuanjun Xiong, and Dahua Lin. "Spatial temporal graph convolutional networks for skeleton-based action recognition". In: *Thirty-second AAAI conference on artificial intelligence.* 2018.

[288] Maosheng Yang and Elvin Isufi. "Convolutional learning on simplicial complexes". In: *arXiv preprint arXiv:2301.11163* (2023).

[289] Maosheng Yang et al. "Finite impulse response filters for simplicial complexes". In: *2021 29th European Signal Processing Conference (EUSIPCO).* IEEE. 2021, pp. 2005–2009.

[290] Nan Yin et al. "Dynamic hypergraph convolutional network". In: *2022 IEEE 38th International Conference on Data Engineering (ICDE).* IEEE. 2022, pp. 1621–1634.

[291] Zhitao Ying et al. "Hierarchical graph representation learning with differentiable pooling". In: *Adv. Neural Inform. Process. Syst.* 31 (2018).

[292] Manzil Zaheer et al. "Deep sets". In: *arXiv preprint arXiv:1703.06114* (2017).

[293] Sebastian Zeng et al. "Topological attention for time series forecasting". In: *Advances in Neural Information Processing Systems.* Vol. 34. Curran Associates, Inc., 2021, pp. 24871–24882. (Visited on 04/24/2023).

[294] Qi Zhang et al. "Kernel-weighted graph convolutional network: a deep learning approach for traffic forecasting". In: *2018 24th International Conference on Pattern Recognition (ICPR).* IEEE. 2018, pp. 1018–1023.

[295] Shi-Xue Zhang et al. "Deep relational reasoning graph network for arbitrary shape text detection". In: *IEEE Conf. Comput. Vis. Pattern Recog.* 2020, pp. 9699–9708.

[296] Weifeng Zhang et al. "Multiplex graph neural networks for multi-behavior recommendation". In: *Proceedings of the 29th ACM International Conference on Information & Knowledge Management.* 2020, pp. 2313–2316.

[297] Zhen Zhang et al. "Hierarchical graph pooling with structure learning". In: *arXiv preprint arXiv:1911.05954* (2019).

[298] Zhen Zhang et al. "Hierarchical multi-view graph pooling with structure learning". In: *IEEE Transactions on Knowledge and Data Engineering* 35.1 (2021), pp. 545–559.

[299] Lingxiao Zhao et al. "From stars to subgraphs: uplifting any GNN with local structure awareness". In: *arXiv preprint arXiv:2110.03753* (2021).

[300] Yongheng Zhao et al. "3DPointCaps++: learning 3D representations with capsule networks". In: *Int. J. Comput. Vis.* 130.9 (2022), pp. 2321–2336.

[301] Jie Zhou et al. "Graph neural networks: a review of methods and applications". In: *AI Open* 1 (2020), pp. 57–81.

[302] Jianming Zhu et al. "Social influence maximization in hypergraph in social networks". In: *IEEE Transactions on Network Science and Engineering* 6.4 (2018), pp. 801–811.

A   Glossary

Tables 5 and 6 summarize the paper's notations and acronyms, respectively.

Table 5: Tabulation of the notations used in this paper.

Notation	Description
Set notations	
S	Non-empty finite set of abstract entities
P_S	Index set
$\mathcal{P}(S)$	Power set of a set S
$(S, \mathcal{N})$	Topological space of a nonempty set S and a neighborhood topology $\mathcal{N}$
$\mathcal{N}_a(x)$	Adjacency set of a cell x
$\mathcal{N}_{co}(x)$	Coadjacency set of a cell x
$\mathcal{N}_{\{G_1,\ldots,G_n\}}(x)$	Neighbors of x specified by the neighborhood matrices $\{G_1,\ldots,G_n\}$
$\mathcal{N}_{\searrow}(x)$	Set of down-incidence of a cell x
$\mathcal{N}_{\nearrow}(x)$	Set of up-incidence of a cell x
$\mathcal{N}_{\searrow,k}(x)$	Set of k-down incidence of a cell x
$\mathcal{N}_{\nearrow,k}(x)$	Set of k-up incidence of a cell x
$\mathbb{N}$ and $\mathbb{Z}_{\geq 0}$	Set of positive integers and non-negative integers, respectively
Domains	
$\mathcal{G}$	Graph
x^k	Cell x of rank k
rk	Rank function
$(S, \mathcal{X}, \mathrm{rk})$	CC, consisting of a set S, a subset $\mathcal{X}$ of $\mathcal{P}(S) \setminus \{\emptyset\}$, and a rank function rk
$\dim(\mathcal{X})$	Dimension of a CC $\mathcal{X}$
$\{c_\alpha\}_{\alpha \in I}$	Partition into subspaces (cells) indexed by an index set I
$\mathrm{int}(x)$	Interior of a cell x in a regular cell complex
$n_\alpha \in \mathbb{N}$	Dimension of a cell in a regular cell complex
0-cells	Vertices of a CC
1-cells	Edges of a CC
k-*cells*	Cells with rank k
$\mathcal{X}^{(k)}$	k-skeleton of $\mathcal{X}$, formed by i-cells in $\mathcal{X}$ with $i \leq k$
$\mathcal{X}^k$	Set of k-cells of $\mathcal{X}$
$|\mathcal{X}^k|$	Cardinality of $\mathcal{X}^k$, that is number of k-cells of $\mathcal{X}$
$\mathrm{CC}_{n-hop}(G)$	n-hop CC of a graph G
$\mathrm{CC}_p(G)$	Path-based CC of a graph G
$\mathrm{CC}_{loop}(G)$	Loop-based CC of a graph G
$\mathrm{CC}_{SC}(\mathcal{Y})$	Coface CC of a simplicial complex/CC $\mathcal{Y}$
Matrix notations	
$B_{r,k}$	Incidence matrices between r-cells and k-cells
$A_{r,k}$	Adjacency matrices among the cells of $\mathcal{X}^r$ with respect to the cells of $\mathcal{X}^k$
$coA_{r,k}$	Coadjacency matrices among the cells of $\mathcal{X}^r$ with respect to the cells of $\mathcal{X}^k$
CCNNs	
$\mathbf{W}$	Trainable parameter
$\mathcal{C}^k(\mathcal{X}, \mathbb{R}^d)$	k-cochain space with features in $\mathbb{R}^d$
$\mathcal{C}^k$	k-cochain space with features in some Euclidean space
$\mathbf{G} = \{G_1,\ldots,G_m\}$	Set of cochain maps G_i defined on defined on a complex
$\mathcal{M}_{\mathbf{G};\mathbf{W}}$	Merge node
$G : C^s(\mathcal{X}) \to C^t(\mathcal{X})$	Cochain map
$(\mathbf{x}_{i_1},\ldots,\mathbf{x}_{i_m})$	Vector of cochains
$att^l : C^s(\mathcal{X}) \to C^s(\mathcal{X})$	Higher-order attention matrix
$\mathcal{N}_{\mathcal{Y}_0} = \{\mathcal{Y}_1,\ldots,\sigma_{|\mathcal{N}_{\mathcal{Y}_0}|}\}$	Set of a complex object in the vicinity of $\mathcal{Y}_0$
$a : \mathcal{Y}_0 \times \mathcal{N}_{\mathcal{Y}_0} \to [0,1]$	Higher-order attention function
$\mathrm{CCNN}_{\mathbf{G};\mathbf{W}}$	CCNN or its tensor diagram representation
$\mathcal{H}_{\mathcal{X}} = (V(\mathcal{H}_{\mathcal{X}}), E(\mathcal{H}_{\mathcal{X}}))$	Hasse graph with vertices $V(\mathcal{H}_{\mathcal{X}})$ and edges $E(\mathcal{H}_{\mathcal{X}})$; see Definition 43

Table 6: Tabulation of the acronyms used in this paper.

Acronym	Description
AGD	Average geodesic distance
CC	Combinatorial complex
CCANN	Combinatorial complex attention neural network
CCCNN	Combinatorial complex convolutional neural network
CCNN	Combinatorial complex neural network
CNN	Convolutional neural network
DEC	Discrete exterior calculus
GDL	Geometric deep learning
GNN	Graph neural network
MOG	Mapper on graphs
RNN	Recurrent neural network
SCoNe	Simplicial complex network
sub-CC	sub-combinatorial complex
TDA	Topological data analysis
TDL	Topological deep learning
TQFT	Topological quantum field theory

B   Lifting maps

Lifting refers to the process of mapping a featured domain to another featured domain via a well-defined procedure. This section shows how we can lift a given domain to a CC or cell complex. Such lifting is useful as it allows CCNNs to be applied to common topological domains, including graphs and cell/simplicial complexes. This section only scratches the surface, as there remain many lifting constructions to be explored. We refer the reader to [103] for examples of lifting graphs to simplicial complexes.

B.1   n-hop CC of a graph

Let $\mathcal{G} = (V(\mathcal{G}), E(\mathcal{G}))$ be a graph and $n \geq 2$ an integer. The *n-hop CC* of $\mathcal{G}$, denoted by $\mathrm{CC}_{n\text{-hop}}(\mathcal{G})$, is the CC whose 0-cells, 1-cells, and n-cells are the nodes of $\mathcal{G}$, edges of $\mathcal{G}$, and set nodes in n-hop neighborhoods of the nodes in $\mathcal{G}$, respectively. It is easy to verify that $\mathrm{CC}_{n\text{-hop}}(\mathcal{G})$ is a CC of dimension n. Figure 37(a) visualizes the 1-hop CC of a graph.

B.2   Path-based and subgraph-based CC of a graph

Let $\mathcal{G} = (V(\mathcal{G}), E(\mathcal{G}))$ be a graph. A natural CC structure on $\mathcal{G}$ considers paths of $\mathcal{G}$. We define a *path-based CC* of $\mathcal{G}$, denoted by $\mathrm{CC}_p(\mathcal{G})$, to be a CC consisting of 0-cells, 1-cells and 2-cells specified as follows. First, $\mathcal{X}^0$ and $\mathcal{X}^1$ in $\mathrm{CC}_p(\mathcal{G})$ are the sets of nodes and edges of $\mathcal{G}$, respectively. We now explain how to construct a 2-cell in $\mathrm{CC}_p(\mathcal{G})$. Let P be a path in $\mathcal{G}$ with length larger than or equal to two (i.e., with two or more edges). An element x_P in $\mathcal{X}^2$ induced by P is defined to be $x_P = \cup_{v \in P}\{v\}$. The set $\mathcal{X}^2$ in $\mathrm{CC}_p(\mathcal{G})$ is a non-empty collection of elements x_P. It is easy to verify that $\mathrm{CC}_p(\mathcal{G})$ is a CC with $\dim(\mathrm{CC}_p(\mathcal{G})) = 2$. Note that we may replace the path P by a tree/subgraph of graph $\mathcal{G}$ and obtain a similar CC structure induced by the tree/subgraph of $\mathcal{G}$. Figure 37(b) shows an example of a path-based CC of a graph.

B.3   Loop-based CC of a graph

Let $\mathcal{G} = (V(\mathcal{G}), E(\mathcal{G}))$ be a graph. We associate a CC structure with $\mathcal{G}$ that considers loops in $\mathcal{G}$. We define a *loop-based CC* of $\mathcal{G}$, denoted by $\mathrm{CC}_{loop}(\mathcal{G})$, to be a CC consisting of 0-cells, 1-cells and 2-cells specified as follows. First, we set $\mathcal{X}^0$ and $\mathcal{X}^1$ in $\mathrm{CC}_{loop}(\mathcal{G})$ to be the nodes and edges of $\mathcal{G}$, respectively. We now explain how to construct a 2-cell in $\mathrm{CC}_{loop}(\mathcal{G})$. A 2-cell in $\mathrm{CC}_{loop}(\mathcal{G})$ is a set $C = \{x_1^0, \ldots, x_k^0\} \subset \mathcal{X}^0$ such that $\{x_i^0, x_{i+1}^0\}$, $1 \leq i \leq k-1$, and $\{x_k^0, x_1^0\}$ are the only edges in $\mathcal{X}^1 \cap C$. The set $\mathcal{X}^2$ in $\mathrm{CC}_{loop}(\mathcal{G})$ is a nonempty collection of elements C. It is easy to verify that $\mathrm{CC}_{loop}(\mathcal{G})$ is a CC with $\dim(\mathrm{CC}_{loop}(\mathcal{G})) = 2$. Note that the sequence $(x_1^0, \ldots, x_k^0)$ defines a loop in $\mathcal{G}$. This loop is called the loop that characterizes the
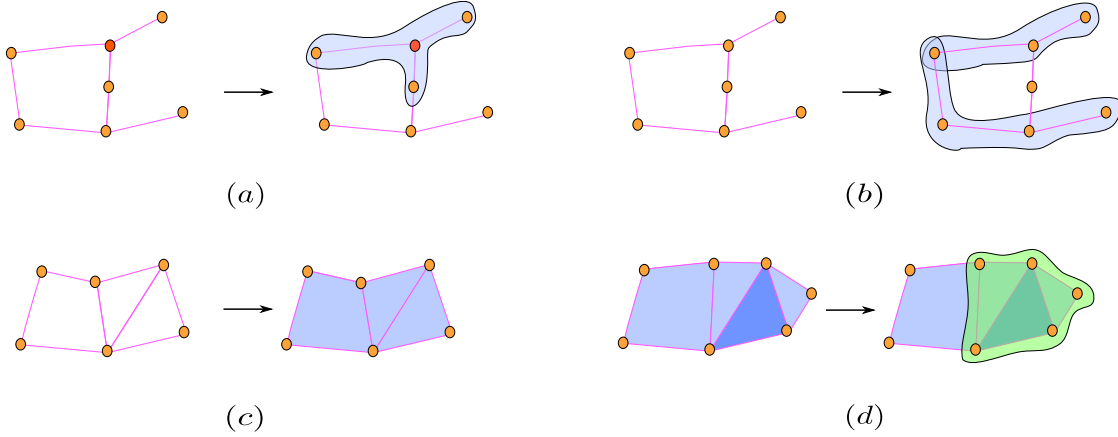
Figure 37: Examples of lifting domains to CCs and cell complexes. (a): The 1-hop neighborhood of the red node can be considered as a 2-cell that we can augment to the graph. Adding such 2-cells to a graph yields a CC called the 1-hop neighborhood of the graph (see Section B.1). (b): A path on a graph of length more than two can be considered as a 2-cell that we can augment to the graph. Adding such 2-cells to a graph yields a CC called a path-based CC of the graph (see Section B.2). (c): A loop in a graph (i.e., a closed path with no repeating edges) can be considered as a 2-cell that we can augment to the graph. Adding such 2-cells to a graph yields a CC called a loop-based CC of the graph (see Section B.3). (d): For every blue 2-cell of a simplicial complex, we introduce a green 3-cell obtained by considering the 1-coface of the 2-cell. Adding such 3-cells to a simplicial complex yields a CC of dimension three called the coface CC of the simplicial complex (see Section B.4).

2-cell $C = \{x_1^0, \ldots, x_k^0\}$. Similar constructions are suggested in [9, 26, 245, 236]. In fact, it is easy to confirm that every 2-dimensional regular cell complex can be constructed in this manner [236]. Figure 37(c) shows an example of a loop-based CC of a graph.

B.4   Coface CC of a simplicial complex/CC

Here, we describe a method to lift a simplicial complex of dimension two to a CC of dimension three. This method can be easily generalized to other dimensions. For a simplicial complex $\mathcal{Y}$ of dimension two, the *coface CC* of $\mathcal{Y}$, denoted by $\mathrm{CC}_{SC}(\mathcal{Y})$, is defined as follows. $\mathcal{Y}^0$, $\mathcal{Y}^1$, and $\mathcal{Y}^2$ in $\mathrm{CC}_{SC}(\mathcal{Y})$ are the nodes, the edges, and the triangles in $\mathcal{Y}$, respectively. We now explain how to construct a 3-cell in $\mathrm{CC}_{SC}(\mathcal{Y})$. Let x^2 be a 2-cell in $\mathcal{Y}$. The 3-cell in $\mathrm{CC}_{SC}(\mathcal{Y})$ associated with x^2 is the union of all 0-cells in $\mathcal{N}_{co,1}(x^2) \cup x^2$. The set $\mathcal{Y}^3$ in $\mathrm{CC}_{SC}(\mathcal{Y})$ is defined as the set of all 3-cells associated with all 2-cells x^2 in $\mathcal{Y}$. It is easy to verify that $\mathrm{CC}_{SC}(\mathcal{Y})$ is a CC with $\dim(\mathrm{CC}_{SC}(\mathcal{Y})) = 3$. A similar lifting construction can be defined to augment any CC of dimension n with $(n+1)$-cells in order to obtain a CC of dimension $n+1$.

B.5   Augmentation of CCs by higher-rank cells

The lifting methods proposed in Sections B.2, B.3, and B.4 can be described abstractly under a single general lifting construction. Specifically, the essence of all these lifting methods is to *augment the underlying CC $\mathcal{X}$ with new cells that have a rank of* $\dim(\mathcal{X}) + 1$. Proposition B.1 formalizes the general lifting construction.

Proposition B.1. *Let S be a nonempty set and $(S, \mathcal{X}, \mathrm{rk})$ a CC of dimension n defined on S. Consider a set $\mathcal{X}^{n+1} \subset \mathcal{P}(S)$ such that if $x \in \mathcal{X}$ and $y \in \mathcal{X}^{n+1}$ with $x \subseteq y$, then $x \subsetneq y$. Further, consider a map $\hat{\mathrm{rk}} \colon \mathcal{X} \cup \mathcal{X}^{n+1} \to \mathbb{Z}_{\geq 0}$ that satisfies $\hat{\mathrm{rk}}(x) = \mathrm{rk}(x)$ for all $x \in \mathcal{X}$ and $\hat{\mathrm{rk}}(x) = n+1$ for all $x \in \mathcal{X}^{n+1}$. For $\mathcal{X}^{n+1}$ and $\hat{\mathrm{rk}}$ satisfying such conditions, $(S, \mathcal{X} \cup \mathcal{X}^{n+1}, \hat{\mathrm{rk}})$ is a CC of dimension $n+1$.*

Proof. The proof follows directly from Definition 9.   □
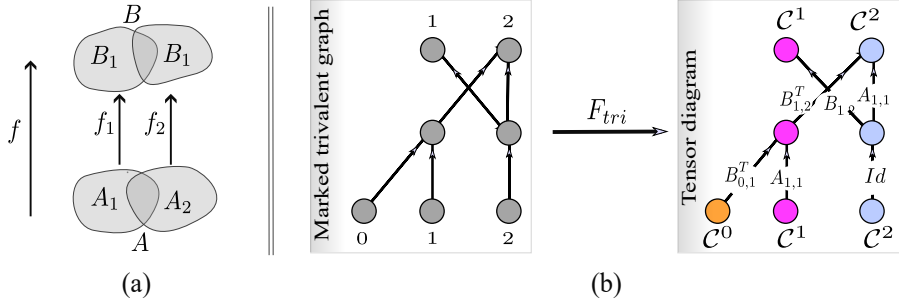
Figure 38: A sketch of the main idea of a TQFT construction in (a) and a functor F_{tri} for constructing tensor diagrams in (b). (a): In the depicted example, the goal is to construct a map $f\colon A \to B$ between two topological spaces A and B. We first decompose A and B into simpler sub-spaces, say $A = A_1 \cup A_2$ and $B = B_1 \cup B_2$, so that A_1, A_2 and B_1, B_2 are 'more elementary spaces' than A and B, respectively. We then construct two maps $f_1\colon A_1 \to B_1$ and $f_2\colon A_2 \to B_2$, and use them to construct f. (b): A visual example of a functor F_{tri} that pairs each marked trivalent graph with a corresponding tensor diagram. This example sends a marked trivalent graph with marked points $\{0, 1, 2\}$ at the bottom and marked points $\{1, 2\}$ at the top to a tensor diagram with domain $\mathcal{C}^0 \times \mathcal{C}^1 \times \mathcal{C}^2$ and codomain $\mathcal{C}^1 \times \mathcal{C}^2$. Once the push-forward, the merge and the split nodes are defined, the functor F_{tri} attaches a well-defined tensor diagram to each trivalent graph. A CCNN can be then constructed from the tensor diagram.

Given a CC $\mathcal{X}$, we call a CC of the form $(S, \mathcal{X} \cup \mathcal{X}^{n+1}, \hat{\mathrm{rk}})$, as constructed in Proposition B.1, a *highest-rank augmented CC of $\mathcal{X}$*. Note that Proposition B.1 provides a constructive and iterative method to build a CC of arbitrary dimension from a nonempty set S of abstract points.

C   CCNN architecture search and topological quantum field theories

The problem of CCNN architecture search for a given TDL task can be cast as a hyperparameter optimization problem over the space of CCNNs. More precisely, consider the query of searching for an optimal CCNN between two fixed Cartesian products $\mathcal{C}^{i_1} \times \mathcal{C}^{i_2} \times \cdots \times \mathcal{C}^{i_m}$ and $\mathcal{C}^{j_1} \times \mathcal{C}^{j_2} \times \cdots \times \mathcal{C}^{j_n}$ of cochain spaces. In practice, this query poses a challenging problem. Rather than performing a computationally expensive CCNN search directly, an alternative approach is to conduct a search in the simpler space of *marked trivalent graphs* between marked points $\{i_1, \ldots, i_m\}$ and $\{j_1, \ldots, j_n\}$, and then map the resulting marked trivalent graph to a corresponding CCNN architecture. In the present section, we briefly sketch such a graph-based search method using tools from *topological quantum field theory (TQFT)* [269], and accordingly we assume some familiarity with the basics of *category theory*.

Tensor diagrams draw their inspiration from TQFT, in which arbitrary maps between topological spaces are constructed from simpler and more manageable building blocks. The main workflow in TQFT constructions involves breaking down the topological spaces under consideration into simpler subspaces, and subsequently utilizing maps between the subspaces to construct maps between the initial topological spaces; see Figure 38(a). Thus, the topological properties of maps between topological spaces are better understood via the topological properties of simpler constituent maps between respective subspaces. This can be especially useful in applications such as knot theory or the study of three-dimensional manifolds, where understanding the topological properties of involved maps is the main interest [269].

Before we introduce the relation between tensor diagrams and TQFTs, we sketch two required preliminaries, namely marked trivalent graphs and TQFTs. First, we define the objects and morphisms of the category of *marked trivalent graphs Tri*. A marked trivalent graph is intuitively described via its layout. Consider the 2d-disk $[0, 1] \times [0, 1]$ with a collection of marked points $\{i_1, \ldots, i_m\}$ at the bottom and a collection of marked points $\{j_1, \ldots, j_n\}$ at the top. A marked trivalent graph is a graph that is drawn inside the disk in such a way that all edges flow within the disk, connecting the marked points at the top with the marked points at the bottom, and meeting at each vertex with exactly three edges. In the category Tri, a trivalent graph with

marked points $\{i_1, \ldots, i_m\}$ and $\{j_1, \ldots, j_n\}$ at the bottom and top, respectively, plays the role of a morphism between the object $\{i_1, \ldots, i_m\}$ and the object $\{j_1, \ldots, j_n\}$. The composition of two such morphisms, when admissible, is defined to be the vertical concatenation of their corresponding marked trivalent graphs. The vertical concatenation of marked trivalent graphs yields a marked trivalent graph. Finally, any trivalent graph can be built by concatenating horizontally and vertically three elementary trivalent graphs similar to the graph shown in Figure 38(b), ignoring the labels in the figure.

At a high level, a TQFT is a functor $F \colon Bord_n \to Vec_K$ that assigns a K-vector space $F(x) \in Vec_K$ to each n-manifold $x \in Bord_n$, and a linear map $F(f)$ to each $(n+1)$-cobordism $f \in Bord_n$. It is noted that a $(n+1)$-cobordism is an $(n+1)$-manifold representing a morphism between two n-manifolds. The functor F is typically defined on a few elementary morphisms in $Bord_n$, but can be extended to arbitrary morphisms in $Bord_n$ by preserving the structure of the elementary maps when mapped via F. Such a functor enables the study of n-manifolds and $(n+1)$-cobordisms defined between them by mapping n-manifolds to their corresponding simpler vector spaces in Vec_K and by mapping $(n+1)$-cobordisms to linear maps between the corresponding vector spaces.

To establish the relation between marked trivalent graphs and tensor diagrams, we introduce a new TQFT F_{tri} that sends each morphism (marked trivalent graph) in Tri to a corresponding tensor diagram by labeling marked trivalent graphs with appropriate cochain maps. Figure 38(b) shows an illustration of such a functor F_{tri}. Through the lens of F_{tri}, the relation between tensor diagrams and marked trivalent graphs becomes clear; a tensor diagram is a marked trivalent graph whose edges are labeled via cochain maps. The functor F_{tri} allows us to search the space of marked trivalent graphs as an equivalent way of conducting CCNN architecture search, since CCNNs are represented by tensor diagrams.

D   Learning discrete exterior calculus operators with CCANNs

The operator $G_{tr} = G \odot att$ of Equations 8 and 11 has an advantageous cross-cutting interpretation. First, recall that G_{tr} has the same shape as the original operator G. More importantly, G_{tr} can be viewed as a learnt version of G. For instance, if G is the k-Hodge Laplacian $\mathbf{L}_k$, then the learnt attention version G_{tr} of it represents a k-Hodge Laplacian that is adapted to the domain $\mathcal{X}$ for the learning task at hand. This perspective converts our attention framework to a tool for learning *discrete exterior calculus (DEC) operators* [88]. We refer the interested reader to recent works along these lines [260, 268], where neural networks are used to learn Laplacian operators in various shape analysis tasks.

Concretely, one of the main building blocks of DEC is a collection of linear operators of the form $\mathcal{A} \colon \mathcal{C}^i(\mathcal{X}) \to \mathcal{C}^j(\mathcal{X})$ that act on a cochain $\mathbf{H}$ to produce another cochain $\mathcal{A}(\mathbf{H})$. An example of an operator $\mathcal{A}$ is the graph Laplacian. There are seven primitive DEC operators, including the discrete exterior derivative, the hodge star and the wedge product. These seven primitive operators can be combined together to form other operators. In our setting, the discrete exterior derivatives are precisely a signed version of the incidence matrices defined in the context of cell/simplicial complexes. We denote the k-signed incidence matrix defined on a cell/simplicial complex by $\mathbf{B}_k$. It is common in the context of discrete exterior calculus [88] to refer to $\mathbf{B}_k^T$ as the kth *discrete exterior derivative* d^k. So, from a DEC point of view, the matrices $\mathbf{B}_0^T, \mathbf{B}_1^T$ and $\mathbf{B}_2^T$ are regarded as the discrete exterior derivatives $d^0(\mathbf{H})$, $d^1(\mathbf{H})$, and $d^2(\mathbf{H})$ of some 0-, 1-, and 2-cochains defined on $\mathcal{X}$, which in turn are the discrete analogs of the gradient $\nabla \mathbf{H}$, curl $\nabla \times \mathbf{H}$ and divergence $\nabla \cdot \mathbf{H}$ of a smooth function defined on a smooth surface. We refer the reader to [88] for a coherent list of DEC operators and their interpretation. Together, cochains and the operators that act on them provide a concrete framework that facilitates computing a cochain of interest, such as a cochain obtained by solving a partial differential equation on a discrete surface.

Our attention framework can be viewed as a non-linear version of the DEC based on linear operators $\mathcal{A}$, and can be used to learn the DEC operators on a domain $\mathcal{X}$ for a particular learning task. Specifically, a linear operator $\mathcal{A}$, as it appears in classical DEC, can be considered as a special case of Equations 8 and 11. Unlike existing work [260, 268], our DEC learning approach based on CCANNs generalizes and applies to all domains in which DEC is typically applicable; examples of such domains include triangular and polygonal meshes [80]. In contrast, existing operator learning methods are defined only for particular types of DEC operators, and therefore cannot be used to learn arbitrary types of DEC operators.

(a) (b) (c) (d)
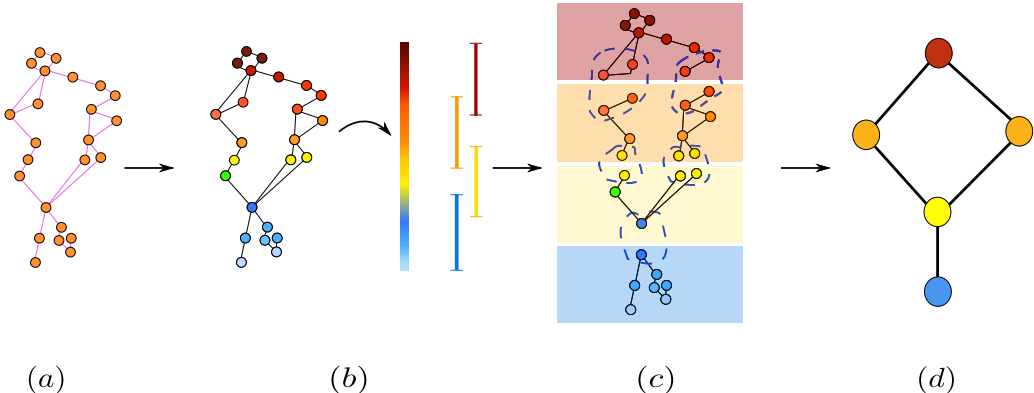
Figure 39: An illustration of the MOG algorithm. The input to the MOG algorithm is a triplet $(\mathcal{X}, g, \mathcal{U})$, where $\mathcal{X}$ is a graph, $g\colon \mathcal{X}^0 \to [0,1]$ is a scalar function defined on the vertex set of $\mathcal{X}$, and $\mathcal{U}$ is a cover of $[0,1]$. (a): An input graph $\mathcal{X}$. (b): The scalar function $g\colon \mathcal{X} \to [0,1]$ is visualized by color-mapping its scalar values according to the displayed color bar. Figure (b) also shows the covering $\mathcal{U} = \{U_1, U_2, U_3, U_4\}$ depicted in red, orange, yellow and blue colors. (c): We pull back via g each cover element U_i in $\mathcal{U}$, and we compute the connected components in $g^{-1}(U_i)$. (d): The vertex set in the graph generated by the MOG algorithm consists of the connected components induced by $g^{-1}(U_i)$, while the edge set is formed by considering the intersection among the connected components. Note that the graph generated by the MOG algorithm approximates the shape of the input graph.

E   A mapper-induced topology-preserving CC-pooling operation

In this section, we give an example of constructing a shape-preserving pooling operation on a CC $\mathcal{X}$. Specifically, we demonstrate the case in which $\mathcal{X}$ is a graph, and utilize the *mapper on graphs (MOG)* construction [130], which is a graph skeletonization algorithm that can be used to augment $\mathcal{X}$ with topology-preserving higher-rank cells, as demonstrated in Figure 4. Although we only demonstrate the shape-preserving pooling construction on graphs, the method suggested herein can be easily extended to CCs.

Let $\mathcal{X}$ be a connected graph and $g\colon \mathcal{X}^0 \to [0,1]$ a scalar function. Let $\mathcal{U} = \{U_\alpha\}_{\alpha \in I}$ be a finite collection of open sets that covers the interval $[0,1]$. The MOG construction of a graph $MOG(V_{MOG}, E_{MOG})$ based on the triplet $(\mathcal{X}, g, \mathcal{U})$ consists of the following steps:

1. We first use the cover $\mathcal{U}$ to construct the pull-back cover $g^\star(\mathcal{U}) = \{g^{-1}(U_\alpha)\}_{\alpha \in I}$.

2. The vertex set V_{MOG} is formed by considering the connected components (i.e., maximal connected subgraphs) induced by $g^{-1}(U_\alpha)$ for each α.

3. The edge set E_{MOG} is formed by considering the intersection among the connected components computed in step 2.

Figure 39 shows an illustrative example of applying the MOG algorithm to a graph. Figure 39(a) shows the graph on which the MOG algorithm is applied, while Figure 39(b) visualizes the scalar function g and the covering $\mathcal{U}$, which consists of four covering elements depicted in red, orange, yellow and blue colors.

The connected components obtained from the MOG algorithm can be used to augment a graph $\mathcal{X}$ with a skeleton $\mathcal{X}^2$ of dimension 2, thus constructing a CC, as described in Proposition B.1. We denote the resulting CC by $\mathcal{X}_{g,\mathcal{U}}$. Figure 40 demonstrates the construction of a CC using this augmentation process based on the MOG algorithm.

MOG is a topology-preserving graph skeletonization algorithm, which can be used to coarsen the size of an input graph $\mathcal{X}$. Such coarsening typically occurs when constructing a pooling layer. So, the skeleton $\mathcal{X}^2$ generated by the MOG algorithm can be utilized to obtain a feature-preserving pooling operation. Figure 41
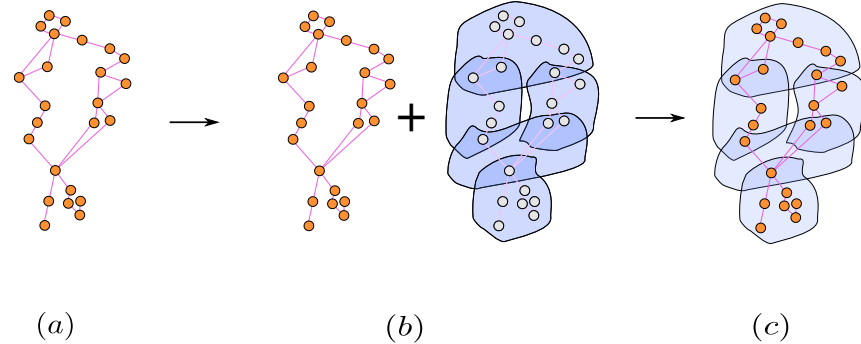
Figure 40: A visual example of obtaining a CC from a graph via the MOG algorithm. (a): An input graph $\mathcal{X}$. (b): The graph $\mathcal{X}$ is augmented by the 2-cells formed via the connected components obtained from applying the MOG algorithm to $\mathcal{X}$, as described in Figure 30. (c): The CC $X_{g,\mathcal{U}}$ obtained by augmenting $\mathcal{X}$ with these 2-cells.
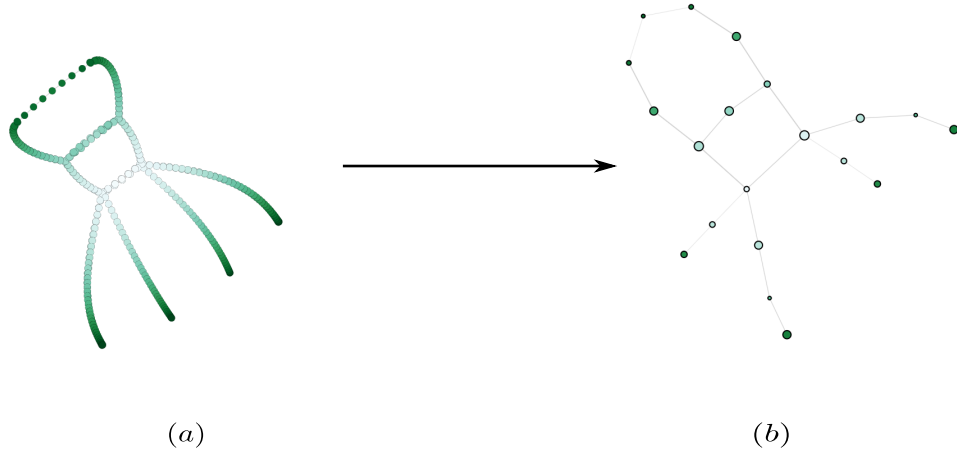

Figure 41: Illustration of coarsening a graph via the MOG algorithm. (a): Visualization of a graph and of a scalar function defined on it, which are used as inputs to the MOG algorithm. The scalar function is visualized by color-mapping its scalar values. (b): The resulting MOG graph. Notice how the MOG construction preserves the overall shape of the original graph.

illustrates that the MOG algorithm coarsens an input graph to produce a graph that preserves topological features of the input graph.

To recap, the MOG algorithm receives an input graph, and outputs a coarsened graph along with connected components. The connected components yield in turn a CC. The coarsened graph and the adjacency relation between the 2-cells of the associated CC are related, as elaborated in Proposition E.1. Figure 42 conveys visually Proposition E.1.

Proposition E.1. *Let* $(\mathcal{X}, g, \mathcal{U})$ *be a triplet consisting of a graph* $\mathcal{X}$, *a scalar function* $g \colon \mathcal{X}^0 \to [0,1]$ *defined on the vertex set of* $\mathcal{X}$, *and a cover* $\mathcal{U}$ *of* $[0,1]$. *Let* $MOG(\mathcal{X}, g, \mathcal{U})$ *be the graph generated by the MOG algorithm upon receiving the triplet* $(\mathcal{X}, g, \mathcal{U})$ *as input. Furthermore, let* $\mathcal{X}_{g,\mathcal{U}}$ *be the CC constructed from the connected components that are generated by the MOG algorithm. The adjacency matrix of the graph* $MOG(\mathcal{X}, g, \mathcal{U})$ *is equivalent to the adjacency matrix* $A_{2,2}$ *of the CC* $\mathcal{X}_{g,\mathcal{U}}$.

Proof. The proof follows by observing that the 2-cells, which are augmented to $\mathcal{X}$ to generate the CC $\mathcal{X}_{g,\mathcal{U}}$, are 2-adjacent if and only if they intersect on a vertex. Moreover, two cells intersect on a vertex if and only if there is an edge between them in the graph $MOG(\mathcal{X}, g, \mathcal{U})$ outputted by the MOG algorithm. □

(a) (b)
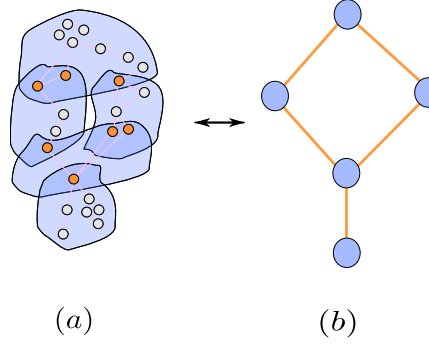
Figure 42: Visual demonstration of Proposition E.1. (a): Visualization of a CC $\mathcal{X}_{g,\mathcal{U}}$, which highlights the intersection between blue 2-cells. (b): The corresponding $MOG(\mathcal{X}, g, \mathcal{U})$ graph. There is a one-to-one correspondence between the blue 2-cells of $\mathcal{X}_{g,\mathcal{U}}$ on the left-hand side and the blue vertices of $MOG(\mathcal{X}, g, \mathcal{U})$ on the right-hand side. Further, two blue 2-cells of $\mathcal{X}_{g,\mathcal{U}}$ (left) intersect on an orange vertex if and only if there is an orange edge (right) that connects the corresponding two vertices of $MOG(\mathcal{X}, g, \mathcal{U})$.

Given a CC $X_{g,\mathcal{U}}$ obtained from a graph $\mathcal{X}$ via the MOG algorithm, the map $B_{0,2}^T \colon \mathcal{C}^0(X_{g,\mathcal{U}}) \to \mathcal{C}^2(X_{g,\mathcal{U}})$ can be used to induce a shape-preserving CC-pooling operation (Definition 37). More specifically, a signal $\mathbf{H}_0$ supported on the vertices of $\mathcal{X}$ can be push-forwarded and pooled to a signal $\mathbf{H}_2$ supported on the 2-cells of $X_{g,\mathcal{U}}$.